Climatic conditions inside nuclear reactor containments

Monitoring campaign

Elforsk rapport 13:83

Mikael Oxfall

Augusti 2013

ELFORSK

CLIMATIC CONDITIONS INSIDE NUCLEAR REACTOR CONTAINMENTS

Monitoring campaign

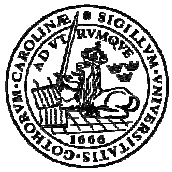

LUND
UNIVERSITY

Mikael Oxfall

Licentiate Dissertation, Report TVBM-3172, Division of Building Materials,
Faculty of Engineering, Lund University, Lund 2013

Lund University, Faculty of Engineering, Division of Building Materials
P.O. Box 118
SE-221 00 Lund, Sweden
www.byggnadsmaterial.lth.se

ISRN LUTVDG/TVBM – 13/3172 – SE(1-100)
ISSN 0348-79-11- TVBM

Printed in Sweden by Media-Tryck, Lund University
Lund 2013

Preface

This Licentiate dissertation is the result of two and a half years of research conducted at Vattenfall Research and Development and at the Division of Building Materials at Lund University. The project was funded by the concrete program at Elforsk Nuclear with the interested parties; Forsmark KG, Oskarshamn KG, TVO Oy, Ringhals AB, SSM and Vattenfall AB.

I would like to thank my supervisors, Professor Lars Wadsö, Assistant Professor Peter Johansson and Adj Professor Manouchehr Hassanzadeh for their support and encouragement throughout this part of the doctoral project.

I would like to thank all personnel at the Nuclear Power Plants for making the monitoring campaigns possible and especially; Jan Gustavsson, Johanna Spåls, Petter Gustavsson, Bengt Adolphsson, Ulf Nilsson and Magnus Kaspersson at Ringhals AB; Andris Zarins, Ulf Modin, Anders Frisk, Lars-Erik Berglund, Marcus Edin, Camilla Skagermark, Johan Eriksson and Andreas Eklund at Forsmark KG.

I would like to thank the personnel at Cementa Research in Slite for assisting me with TG/DSC and TGA measurements.

I would like to thank all colleagues at Vattenfall Research and Development and the colleagues at the Division of Building Materials at Lund University for fruitful discussions and support.

List of appended papers

1. MOISTURE LEVELS AND DRYING POTENTIAL OF THE CONCRETE IN SWEDISH REACTOR CONTAINMENTS

   M, Oxfall. M, Hassanzadeh P, Johansson

   EPJ Web of conferences (Accepted)

2. MOISTURE CONTRIBUTION FROM THE CONCRETE STRUCTURES IN SWEDISH REACTOR CONTAINMENTS

   M, Oxfall. M, Hassanzadeh P, Johansson

   Manuscript, to be submitted

Contribution of co-authors

1. Hassanzadeh and Johansson contributed in planning the paper and assisted in the development of the experiments
2. Hassanzadeh and Johansson contributed in planning the paper and assisted in the development of the experiments

Abstract

The reactor containment is one of the most important buildings at a nuclear power plant. In case of an accident the containment wall is the final protection against radioactive leakage to the surrounding environment. A reactor containment contains different types of concrete structures. They can be grouped as external structures constituting a barrier between the inside of the containment and the outside environment, and internal structures e.g. to sectionalize the internal space of the containment and the biological shield. Concrete structures in reactor containments are e.g. used as load bearing structures, protection of the steel liner from e.g. corrosion and to adsorb radioactive nuclides. During operation the climatic conditions inside the reactor containment can be harsh, with temperatures over 50 °C and low relative humidities (RH). Knowledge about the condition in the containment and in the concrete structures is thereby important in order to evaluate the condition of the reactor containment and possible changes over time.

The objective of this dissertation is to present a measurement setup suitable for long term measurements in concrete and investigate how the climatic conditions inside the reactor containments affect the concrete structures and vice versa. The project is divided into three parts in which the first part contains a material study of concrete from one nuclear reactor containment. The results from the material study showed that no clear variation of moisture transport properties over the depth of a structure could bee observed. The findings will be of great value in the continuation of the PhD project which will follow this Licentiate project, in which a model to predict future and past moisture conditions in the concrete will be developed.

In the second part an accuracy evaluation of a measurement setup is presented. The setup was used to measure the RH and temperature onsite. In the accuracy evaluation the effects of both leakage through the setup and temperature were evaluated. The results showed that measured RH was influenced by the temperature changes as expected. Furthermore, the results indicated leakage through the setup. The leakage may have influenced the measurements of the devices placed closed to the surface of the structure. However, it is concluded that the setup is suitable for long term measurements. An supplementary accuracy evaluation will be presented in the upcoming doctoral thesis

The third part presents result from three monitoring campaigns conducted at different nuclear reactor containments in Sweden. The monitoring campaigns were conducted during one operational year. The campaigns included measurements in different zones of ambient RH and temperature and measurements, on different depth, inside the concrete.

The results showed that measurements on shallow depth were critical but if properly installed there were no indication of leakage. In all zones a clear moisture profile was observed which indicates that the concrete within the reactor containment are still drying after about 30 years of exposure to high temperatures and low RH.

Keywords: Nuclear power plant, concrete, onsite measurements, relative humidity, boiling water reactor, pressurized water reactor, moisture transport coefficient, moisture flux.

Sammanfattning

På ett kärnkraftverk är reaktorinneslutningen en av de viktigaste byggkonstruktionerna. Detta då reaktorinneslutningen är den sista barriären för att förhindra läckage av radioaktivitet till omgivningen i händelse av en olycka. En reaktorinneslutnings innehåller flera olika betongkonstruktioner vilka kan delas in i externa samt interna konstruktioner. Exempel på externa konstruktioner är cylinderväggen, vilken avskärmar inneslutningen och utsidan. Interna konstruktioner är bland annat rumskiljande konstruktioner och den biologsiska skölden. Betongkonstruktionerna i en reaktorinneslutning används bland annat som lastbärande konstruktioner, som skydd av tätplåten mot korrosion och som strålskydd. Under drift kan klimatet inne i en reaktorinneslutning vara krävande för betongen med temperaturer över 50°C och låg relativ fuktighet (RF). Med anledning av detta är kunskap om klimatförhållandena inne i en reaktorinneslutning viktigt för att kunna utvärdera reaktorinneslutningens kondition och eventuella förändringar med tiden.

Målet med denna avhandling är att presentera ett lämpligt mätsystem för registrering av fuktförhållanden i betong över lång tid samt att studera hur klimatförhållandena inne i reaktorinneslutningarna påverkar betongkonstruktionerna och vice versa. Projektet är uppdelat i tre delar i vilken den första innehåller en materialstudie på betong från ett av de Svenska verken. Resultaten från materialstudien visar att det inte var någon signifikant skillnad i fukttransportegenskaper på olika nivåer i betongkonstruktionerna. Denna slutsatts är av stort värde för den nästkommande delen i detta doktorandprojekt där en modell för prediktering av framtida och tidigare fukt och temperaturförhållanden i betongkonstruktionerna kommer att framarbetas.

Den andra delen i avhandlingen inkluderar en precisionsutvärdering av den framtagna mätuppställningen för mätningar av RF och temperaturer i fält. I precisionsutvärderingen studerades förekomsten av läckage samt effekter vid temperaturförändringar. Resultaten visar att mätuppställningen reagerade på temperaturförändringar som väntat men tendenser till läckage över mätuppställningens tätningar kan observeras. Läckaget kan ha påverkat de mätningarna som utförts närmast betongytan men systemet anses fortfarande vara lämpligt för långtidsmätningar. En kompletterande precisionsutvärdering av mätsystemet kommer att genomföras till doktorsavhandlingen.

I den tredje delen presenteras mätresultat från tre olika kärnkraftverk i Sverige. Mätningarna utfördes i olika zoner inne i inneslutningarna och pågick under vardera ett driftår. I varje zon inkluderades mätningar av den omgivande luften samt på olika djup i betongkonstruktioner. Resultaten från mätningarna visar att mätningar på små djup var

kritiska men vid noggrann montering fanns det inga tendenser till läckage. Mätningarna visar även att det var en tydlig fuktprofil i alla zoner, vilket indikerar att betongen i inneslutningarna fortfarande är under uttorkning efter ca 30 år av exponering för höga temperaturer och ett lågt RF.

Nyckelord: Kärnkraftverk, betong, fältmätningar, relativfuktighet, kokvattenreaktor, tryckvattenreaktor, fukttransportkoefficient, fuktflöde.

Table of Contents

1 Introduction

1.1 Background

The reactor containment (RC) is the structure at a nuclear power plant (NPP) where the reactor is located. There are several types of NPP and each may have a different design of the RC and the materials which are constituents of internal and external structures can vary depending on manufacturer. Two Nordic countries, Sweden and Finland, had NPPs in 2012, and there are three types of NPPs used, Boiling Water Reactor (BWR), Pressurised Water Reactor (PWR) and Water Water Power Reactor (VVER). Only the BWRs and PWRs are included in this dissertation.

In the Nordic BWRs and PWRs the RC wall consists of a concrete wall with an embedded steel liner. The steel liner is located in the concrete at a depth of ca 300 mm from the inner surface and is used to ensure leak tightness. Apart from acting as a load carrier the concrete protects the liner from e.g. impacts and corrosion.

The Nordic NPPs were all built during a period from the late 1960s to the mid- 1980s. The climate inside the containments is monitored continuously by the plant owners. The purpose of these measurements is mainly to monitor the temperature in specific zones close to sensitive equipment and may therefore not be suitable for describing the overall climatic conditions. Regardless of NPP the temperature inside the RC can reach up to 50-60°C in some zones. Considering the extreme climate, it is of great importance to evaluate how this affects the concrete and the drying rate that can be expected.

To be able to properly evaluate moisture dependent material properties and evaluate the moisture contribution from the concrete the actual conditions have to be known. To do this, systematic measurements of the moisture conditions have to be made. By measuring the moisture profiles in the concrete during operation and measuring the boundary conditions at the concrete surfaces, the actual moisture conditions in the structures and the drying rate can be determined. This data can thereafter be used to establish a model to determine past and future moisture conditions in the RC concrete. With the actual moisture profiles it is also possible to properly evaluate material properties that are moisture dependent. And with the model it would be possible to evaluate the variations in material properties over time.

Apart from high compressive strength and durability, which may be considered beneficial for a nuclear facility, concrete has several other properties such as thermal diffusivity and

conductivity, heat capacity, moisture transport coefficient, shrinkage, creep and neutron and gamma radiation shielding properties; which must be considered when an RC is designed or assessed. Most of these properties are dependent on the moisture content, water to cement ratio, degree of hydration and cement content. The moisture content also influences other material properties such as gas permeability (Fredlund and Nilsson 2009).

The concrete inside the RCs may act as a moisture source affecting the climatic conditions inside the RC. Fresh concrete contains a large quantity of water. During the hydration phase a certain amount of water will be chemically and physically bound in the cement gel but the remaining, evaporable water, can be dried out over time. The water's effect on the climatic conditions depends on the drying rate which is dependent on the temperature and humidity inside the RCs.

The moisture content in concrete has been studied internationally on several fields, with the focus mainly on drying of concrete slabs and walls in buildings e.g. (Nilsson 1980; Åhs 2011), the influence of moisture content on creep and shrinkage e.g. (Bažant 1970; Song, Kim et al. 2002; Grasley, Lange et al. 2006; Grasley and Lange 2007; Hora and Patzák 2007) and frost related damage e.g. (Fagerlund 1972; Fridh 2005). Most moisture related studies on concrete have been carried out in a laboratory controlled environment or as simulations and only a few studies have been based on environmental effects in the field e.g. (Andrade, Sarrıa et al. 1999; Ryu, Ko et al. 2011). No studies can be found on measurements in a RC but a few studies where the moisture level has been estimated can be found (Hilsdorf 1967; Nilsson 2007). Some measurements have been made on the containment wall outside the liner (Johansson and Nilsson 2007; Nilsson 2007; Nilsson and Johansson 2009). To the author's knowledge there are, however, some measurements on relative humidity in concrete that have been conducted on some reactor containments, but not published in any international journals. The Finnish NPP owner Teollisuuden Voima Oy (TVO) has measured the relative humidity at one of the reactors at Olkilouto during the last ten years. Some of the results from these measurements will be presented, with permission from TVO, in the forthcoming doctoral thesis. Apart from these measurements the author is not aware of any similar measurements performed at RCs.

1.2 Objectives

Clarify the temperature and humidity conditions in containments, by explaining and quantifying them.

Determine the moisture flux inside, and through, parts of concrete structures.

Suggest and develop surveillance methods – i.e. measurement devices, measurement locations, data acquisition systems, etc. – in order to determine the exposure conditions around the structural elements and the impacts of the exposure conditions on the structural elements.

Compare the as-designed climatic conditions around the structural elements with the actual conditions. Explain the differences between them. If necessary, suggest remedial actions to re-establish the as-designed conditions.

Determine whether there are any differences between two containments of the same type with regard to temperature and moisture conditions, and explain the reason for the differences.

1.3 New research

The climatic conditions inside a nuclear reactor containment are monitored constantly by the plant's owner. The main moisture source is usually assumed to be leakage from pipes but no studies that have evaluated potential moisture contribution from the concrete structures have been made. In several studies the moisture conditions in the concrete are assumed, and/or different conditions or expected levels are calculated, but there are no published studies on the actual conditions.

In this dissertation results from on-site monitoring campaigns on three different nuclear reactor containments are presented together with analysis regarding moisture contribution to the climatic conditions in the containments. Furthermore, results from a material study on concrete from one nuclear reactor are included. In the study the moisture transport properties and cement hydration variations have been evaluated on concrete samples that had been exposed to the containment climate over more than 30 years. In addition the properties are evaluated over the depth of a structural component to evaluate if there are any differences.

2 Nuclear power plant

A nuclear power plant (NPP) is here referred to as an NPP that produces electric energy, i.e. research facilities and plants designed for district heating are not included.

There are several types of NPP and variations occur within each type. In this dissertation only the pressurised water reactors (PWR) and boiling water reactors (BWR) present in the Nordic countries will be considered. World wide, the most commonly used reactor type is PWR followed by BWR (Picaut, Chataigner et al. 2001).

The electrical power that is produced at an NPP depends on the temperature and the amount of steam that are produced and also on the turbines and the generators that transform the thermal energy to electricity. Further on the electric power of the different plants will be described by reference unit power and design net capacity. Reference unit power (RUP) is the maximum electrical power that can be maintained by a plant over a prolonged period of time (IAEA 2012). The design net capacity is the RUP as specified in the original unit design.

Differences between the design net capacity and the updated RUP are usually due to upgrades of different components at the NPPs. The upgrades can be on the turbines, generators, or other components within the containment such as steam generators and pressuriser on a PWR. Usually these upgrades do not affect the temperature in the core, primary circuit or in the containment.

2.1 Reactor safety

In general, an NPP consists of a reactor building, a turbine hall and an intake and outlet of cooling water. The reactor vessel is located inside the reactor building within the reactor containment (RC). According to the IAEA NS-G1.10 (IAEA 1998) the main purpose of the RC is to:

- Isolate radioactive substances during operation and in the event of an internal and/or external accident
- Protect the NPP from natural and human induced events
- Radiation shielding during operation and in accidental conditions

The strategy for safety in an NPP is called defence in depth. The strategy consists of five levels with the principle that if one fails the next will take over. The main objective is to prevent accidents, but if the prevention fails it is designed to limit the potential consequences and prevent any evolution to more serious conditions.

The levels of defence in depth is presented in table 1 as in the IAEA report -Defence in depth in nuclear safety- (IAEA 1996)

Table 1. Defence in depth strategy for reactor safety according to IAEA document INSAG-10 (IAEA 1996)

Levels of defence in depth	Objective	Essential means
Level 1	Prevention of abnormal operation and failures	Conservative design and high quality in construction and operation
Level 2	Control of abnormal operation and detection of failure	Control limiting and protection systems and other surveillance features
Level 3	Control of accidents within the design basis	Engineered safety features and accident procedures
Level 4	Control of severe plant conditions, including prevention of accident progression and mitigation of the consequences of severe accidents	Complementary measures and accident management
Level 5	Mitigation of radiological consequences of significant releases of radioactive materials	Off-site emergency response

The main aspect when designing and constructing an RC is therefore aimed to safety and the ability of the structure to withstand different types of accidents. The ultimate goal of the containment is to prevent radioactive substances or radiation to escape out from the RC to the surroundings.

In general there are four main barriers to prevent the radiation release.

- The fuel, e.g. Uranium oxide
- Fuel cladding, e.g. Zirconium
- Primary circuit, including the reactor vessel and the steam pipes
- Containment

The fuel and the fuel cladding are the first two barriers due to the fuel's high melting point and the cladding's tightness. The third barrier is the primary circuit. In a PWR the entire

primary circuit is located inside the containment and a secondary circuit is used to propel the turbines. The water in the primary circuit is in a liquid state during the whole cycle and the vapour is produced in the steam generators. Because of this, the pressure in a PWR reactor has to be higher than in a BWR, ca 15.5 MPa. In the secondary circuit the pressure is held around 6 MPa. In a BWR there is no secondary circuit, instead the steam generated in the reactor is used in the turbines, with a pressure around 7 MPa. Before and after the containment wall there are security vents that prevent a leakage in case of a pipe breakage on either side.

The containment is the last barrier and has to shield the radiation, if the other barriers fail. This is mainly the case if an accident occurs. Possible accidents can be divided into two main groups, internal and external accidents. The external accidents are e.g. earthquakes, flooding, tsunamis, extreme cold or heat, tornadoes (with flying debris), airplane crash, etc. In these cases it has to be ensured that the leak tightness of the containment is not jeopardised. The external accidents may also be a factor that induces an internal accident, e.g. due to a station black out.

The main internal accidents, or events, can be subdivided into five categories (IAEA 2004):

- Break in high energy systems
- Break in systems containing radioactive material
- System transients causing representative limiting loads (e.g. pressure, temperature or dynamic loads)
- Containment bypass events such as loss of cooling accidents (LOCA) in interfacing systems or steam generator tube rupture
- Internal hazards

Loss of cooling accident (LOCA) is classified as a Level 3 event according to the defence in depth strategy, table 1. A LOCA is considered as a basic accident load (Picaut, Chataigner et al. 2001) for the reactor containment. One possible scenario when a LOCA can occur is if one of the pipes in the primary circuit breaks. At this scenario the pressure and temperature inside the containment are rapidly increased affecting the reactor containment with a high internal pressure. The water level inside the reactor vessel drops and if the safety systems which shall maintain the cooling of the core fail there is a risk of core meltdown making the event a serious accident.

If the containment is not leaktight, a LOCA-scenario could result in a leakage of radioactive material to the surroundings. To ensure that the containment can prevent the leakage during a LOCA the tightness is tested before the reactor is started. During these tests the pressure inside the containment is raised to a slightly higher pressure, 1.15 times the design load (Picaut, Chataigner et al. 2001; IAEA 2004), but without the temperature increase. In a PWR a LOCA in general, depending on the containment design, generates a pressure around 0.5 MPa and a peak temperature of ca 150 °C. For a BWR the corresponding pressure is 0.6 MPa and temperature 170 °C (Picaut, Chataigner et al.

2001). After the first start-up the containment's leaktightness in Swedish RCs is tested three times during every ten year period.

The strategies to manage the pressure increase vary depending on the reactor design. The PWRs used in Sweden have the design concept that is called full pressure dry containment. To withstand the increased temperature and steam build-up the containment has a large volume and in this way the pressure is limited without jeopardising the leaktightness.

The BWRs in Sweden and Finland use a pressure suppression containment system. The containments are divided into two main compartments, dry-well and wet-well, connected with several downcomers. In the wet-well there is a suppression pool in which the downcomers are submerged. In case of a steam leakage in the dry-well, the steam will be forced down by the downcomers to condense. By condensing the steam a significant reduction of the pressure will be achieved.

In the event that the fuel cladding melts, in case of a core melt down, hydrogen is produced. To avoid the risk of oxy-hydrogen gas, the air in the BWRs is replaced by nitrogen during operation. In a PWR the total space of the RC is big enough so that dangerous concentrations can not occur. In addition to this the Swedish and Finnish reactors have an emergency ventilation system that can filter the gas of radiation and thereby lower the risk of oxy-hydrogen gas.

2.2 Nordic Nuclear Power

Sweden and Finland are the only two Nordic countries that have nuclear power as an electric power source, as of 2012. In total there are 14 NPPs under operation, one under construction and two that have been decommissioned. In Sweden there are ten NPPs in operation distributed over tree nuclear power sites. Ringhals, which is the biggest site, has four reactors and a total RUP of 3535 megawatt electrical (MW_e), as of 2011. On Ringhals there are one BWR and three PWRs. The other two sites in Sweden are Forsmark and Oskarshamn (Simpevarp), both consist of three BWRs. Apart from the ten plants in operation there are two BWR located in Barsebäck which were shut down in 1999 (Barsebäck 1) and in 2005 (Barsebäck 2).

Finland has two nuclear power sites, Olkiluoto and Loviisa. In Olkiluoto there are two BWR under operation and one additional European Pressurised Water Reactor (EPR) under construction, with a planned start up during the mid 2010s. At Loviisa there are two Water-Water Power Reactors (VVER), these two reactors are not included in this study. In the Nordic countries the total RUP as of 2011 was 12131 MW_e (IAEA 2012).

The Swedish reactors were constructed during the 60s and 80s. The first one for commercial use was Oskarshamn 1 which was constructed during 1966-1968 and put into operation in 1972. The last two constructed were Forsmark 3 and Oskarshamn 3, both put

into operation in 1985. The Finnish plants were constructed during the 70s and 80s; Olkiluoto 1 was put into operation in 1979 and the second in 1982.

Most of the plants in Sweden and Finland have one, or more, similar plants on site or at another location in Sweden and/or Finland. Figure 1 shows a family tree of the NPPs at Ringhals, Forsmark, Oskarshamn, Olkiluoto and the two shutdown reactors at Barsebäck.

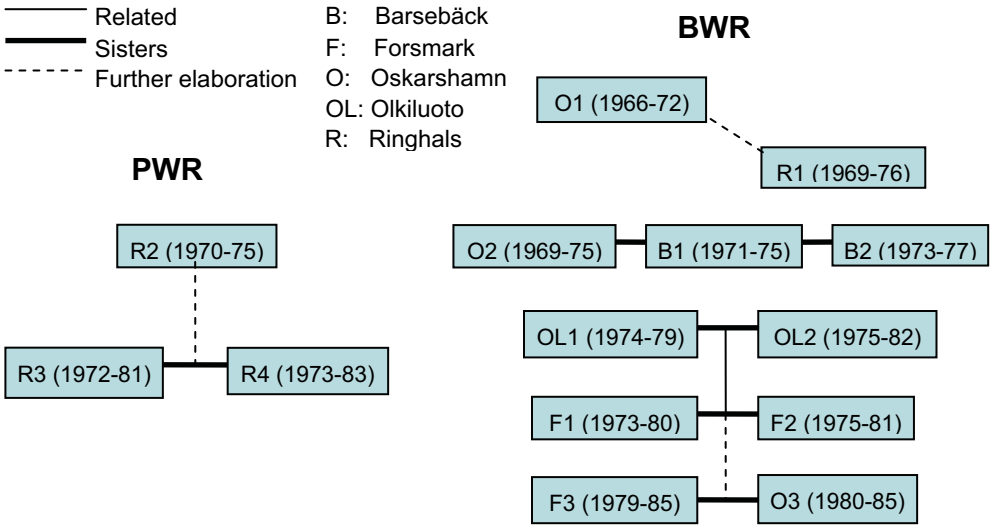

Figure 1 Family tree of the Swedish and Finnish BWR and PWR with the construction start and commercial operation start year within parentheses

The PWRs at Ringhals have all a similar design and will be seen as one group. Ringhals 2 which is the first constructed is slightly different, both considering the containment and reactor design. Ringhals 3 and 4 are sister reactors and a further elaboration of the R2. There are only small differences between the two. All three plants were designed by Westinghouse Electric Corporation.

The Nordic BWRs can be divided into four groups:

- Group 1: Oskarshamn 1 and Ringhals 1
- Group 2: Oskarshamn 2 Barsebäck 1&2
- Group 3: Forsmark 1&2, Olkilouto 1&2
- Group 4: Oskarshamn 3 and Forsmark 3

Group 1 represents the first BWRs for commercial use in Sweden, they have different reactor design but their containment design is similar. Group 2 are all, more or less, identical but Barsebäck 1&2 were shut down in 1999 and 2005. Group 3 have all a similar design but the two plants at Olkiluoto are smaller than their Swedish siblings. Group 4 is

the latest constructed, in operation, and they are a further elaboration from group 3. They are also the biggest NPPs regarding RUP. All Nordic BWRs were designed by ASEA-ATOM. ASEA-ATOM was a part of the General Swedish Electric Company, ASEA.

Four of the five groups presented previously will be used to compare and evaluate the different containment designs, mainly regarding the climatic conditions. One NPP from each group, except BWR group 2, will be evaluated regarding design, material composition and possible heat and moisture sources. Differences within each group regarding the concrete composition may occur; however, this will not be handled in this dissertation.

3 Reactor containments design and materials

One of the most used materials in an NPP structure is concrete. This is especially the case regarding the RCs. Close to 95 % of the NPPs constructed between 1971 and 1999, world wide, have some type of concrete containment (Picaut, Chataigner et al. 2001). Most of the containments are; single wall structures with prestressed concrete; single wall structures with reinforced concrete; double walls of reinforced concrete and/or prestressed concrete (Picaut, Chataigner et al. 2001).

Usually when the containment wall consists of a single concrete wall there is an additional steel liner, either embedded in the concrete or at the inner surface. The steel liner acts as the tight shell and is the main component to ensure leaktightness of the structure. In the RCs with double walled concrete and no liner, the space between the two walls is sealed from the surroundings. In the event that the inner wall leaks, the radiation can be contained and collected preventing any external releases.

Apart from the containment's boundary structure there are vast amounts of concrete used in the internal structures within the RC. The biological shield is one internal structure that can be found in most containment designs. The structure acts as a radiation shield and protects the containment from radiation during operation. The biological shield is also the structure that usually caries the weight of the reactor vessel.

Due to the nuclear reactions within the reactor core, different kinds of radiation are produced. Different materials have different abilities to shield this radiation. Apart from e.g. lead and steel, concrete is a suitable material due to its high density and due to the internal water.

The neutron and gamma radiation shielding properties have been studied in several studies (Thorne 1961; Hilsdorf 1967; Chang-Min, Yoon Hee et al. ; Kharita, Takeyeddin et al. 2008; Alhajali, Naoom et al. 2009; Akkurt, Akyildirim et al. ; Kharita, AlNassar et al. 2010; Kharita, Yousef et al. ; Korkut, Korkut et al. 2011; Vodák, Vydra et al. 2011) and are not seldom focused on usage in nuclear facilities. The major form of radiation that escapes the reactor core is high energy gamma ray and neutron radiation. The reactor vessel absorbs most of the energy from the radiation. Most of the remaining radiation is thereafter absorbed in the biological shield. This absorption of energies results thereby in a temperature rise in the concrete.

The neutron attenuation in concrete is due to the chemical consistence of the cement, and mainly the amount of hydrogen Because of this the attenuation is strongly dependent on the moisture content in the concrete, the main source of hydrogen in concrete. Thorn states that a lowering of moisture content in the concrete by five percentage points increases the relaxation length by about 30 % (Thorne 1961).

Gamma ray shielding does not depend on the moisture content in the same way as the neutron radiation. The shielding properties that affect the gamma ray radiation attenuation are instead the density of the material. Test results with a radiation at 3 MeV (mega-electron volt) show that the gamma ray relaxation length increases by the same magnitude as the inverted moisture loss due to drying (Thorne 1961).

The most important parameter of concrete is however the water to cement ratio, W/C-ratio. This relation describes the amount of water that is added in relation to the amount of cement. With a low W/C-ratio the cement gets denser and thereby acquires a higher compressive and tensile strength. Furthermore, the structure of the hydrated cement becomes tighter which leads to decreased diffusivity and conductivity with regard to the gas and fluid transport, etc. Because of this the W/C-ratio is the single most important parameter regarding durability and strength of the concrete.

Almost all concrete surfaces inside a Nordic RC are coated with an epoxy coating. The main purpose of this coating is to make it easier to clean, if necessary, contaminated surfaces. One crucial effect regarding drying of the concrete is that the coating reduces the moisture transport out of the structures. The effect of the moisture transport due to the epoxy coating will be handled in section 5.2.1.

The main differences between the RCs are the layout and design, especially when BWRs and PWRs are compared. Regardless of which Nordic NPP is studied there are however several similarities. All Nordic RCs consist of a cylindrical containment wall which is divided into outer and inner cylinder walls. The walls are separated by a steel liner which acts as the main component that ensures leaktightness of the containment.

The containment wall is made of concrete and is usually ca 1.1 meter thick and the steel liner is located ca 300 mm from the inner surface. The walls act as protection of the liner both concerning corrosion, due to the concrete’s passivation of steel, and as missile shields. Figure 2 illustrates a typical containment wall for BWRs or PWRs in the Nordic countries.

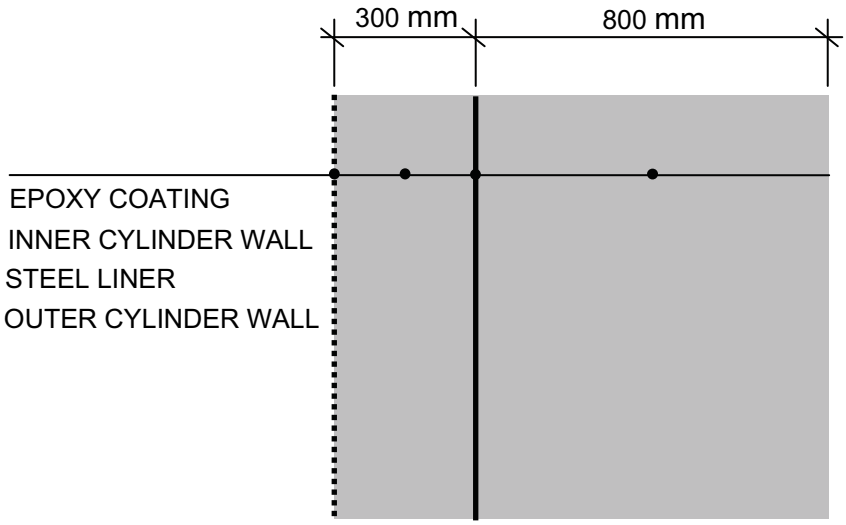

Figure 2. Schematic composition of a containment wall with the inner cylinder wall at the left side

Possible missiles within a RC can be pieces of pipes in case of a pipe breakage. Missiles that may affect the containment from the outside can be flying debris during e.g. a tornado or storm. At the BWRs outer missiles are not likely to affect the containment wall due to an external reactor building, at a PWR the containment is the outer reactor building.

The thickness of steel liner varies between the RCs, there are no clear relations regarding design types, but based on data from (Roth, Silfwerbrand et al. 2002) there are however tendencies of thinner liners with age.

Apart from the design similarities regarding the containment wall, the concrete composition is usually quite similar. In general the concrete has a W/C-ratio of 0.42–0.46 and a cement content around 350–370 kg/m^3. The cement that has been used however varies depending on NPP. Standard Portland cement and low heat Portland cement is the most common but e.g. slag cement (CEM III) has been used at one of the NPPs.

3.1 Pressurised water reactor (PWR)

The full pressure dry containment design strategy, as mentioned in section 2.1, requires a large RC. Usually there is no external building housing the containment, instead the containment wall is exposed to the outdoor climate. The Nordic PWRs have a single prestressed concrete containment wall with an embedded steel liner ca 300 mm from the inner surface. The wall is in total around 1.1 metres thick. The outer part of the wall, outer

cylinder wall, is both horizontally and vertically prestressed. The inner cylinder wall is made of reinforced concrete. It is only the dome at the top of the containment that does not have an inner concrete shield.

Apart from the inner cylinder wall and the bottom slab there are a vast amount of internal concrete structures, including the fuel pool and structures holding the internal components, e.g. steam generators and the pressurizer. Around the reactor vessel, which is located in the lower part of the containment, there is a biological shield. The thickness of the shield can vary between different reactors but for the Swedish RCs they are around 2 m thick. Figure 3 illustrates a section of a PWR, similar to the ones used in Sweden.

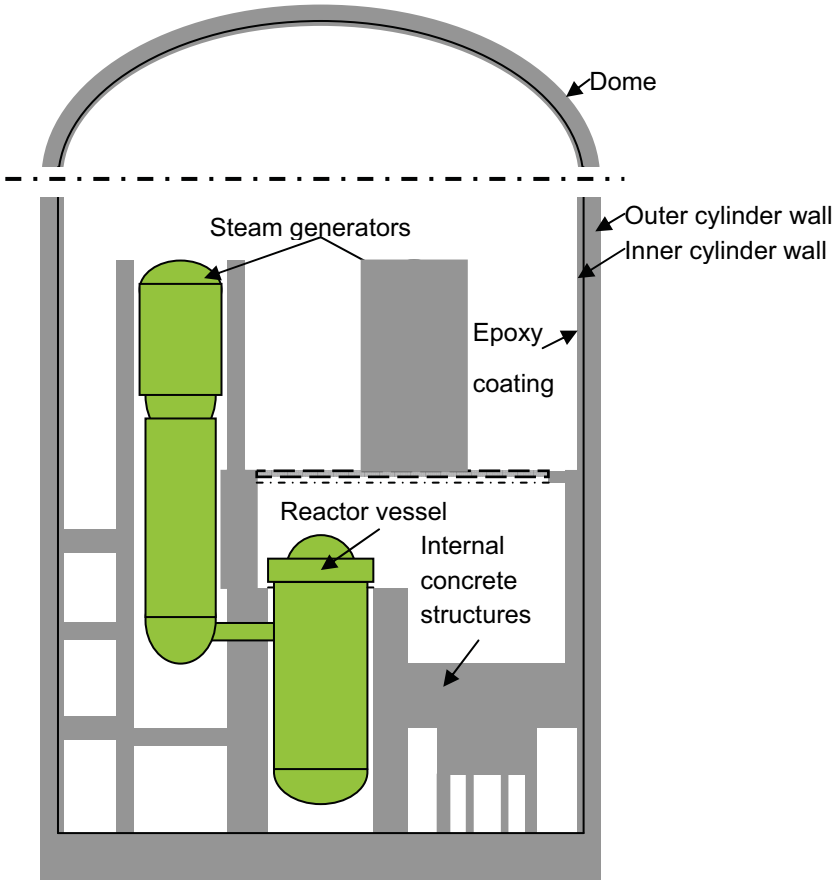

Figure 3. Schematic section of a PWR similar to those used in Sweden.

The three PWRs in Sweden are fairly similar concerning the concrete and structural design whereas Ringhals 2 is the one that differ the most. Ringhals 3 and 4 are close to identical with only small differences. In this dissertation only Ringhals 4 will be described in more detail.

Information regarding the composition of concrete and specific structural dimensions was collected from construction drawing and (Roth, Silfwerbrand et al. 2002) from the Swedish Nuclear Power Inspectorate (SKI). SKI is since 2008 included in the Swedish Radiation Safety Authority (SSM). The concrete quality in the outside cylinder wall has not been considered within this work.

3.1.1 Ringhals 4

The construction of Ringhals 4 started in November 1973 and the reactor was put into commercial operation in November 1983. The reactor was designed by Westinghouse with a design net capacity on 915 MW_e and in 2011 the RUP was 945 MW_e (IAEA 2012).

The steel liner in the bottom slab is 8 mm thick and covered with a ca 200 mm thick concrete layer. The concrete is a K50, or approximately a C 45/55 in accordance with the EN206-1. The concrete consists of CEM I with the Swedish LH (Slow reacting)-cement from Limhamn. The W/C-ratio is 0.49, the maximum aggregate size is 32 mm and the cement content is 320 kg/m^3.

The inner cylinder wall is a 330 mm thick K50 concrete and consists of a CEM I LH-cement from Limhamn with a W/C-ratio of 0.42. The maximum grain size is 32 mm and a cement content of 365 kg/m^3. For the lower parts, up to 18 m above the bottom slab, the steel liner has a thickness of 10 mm and thereafter 8 mm. No information has been found regarding the concrete in the internal structure.

The inner diameter of the containment is 35.4 m and it is ca 52 m high. The total amount of concrete inside the steel liner has been calculated from construction drawings to about 8000 m^3. The total space inside the steel liner, both concrete and space, is around 55000 m^3. This gives a concrete to space volume ratio of ca 1:6. Internal components such as piping, the reactor vessel, the steam generators and pressurizer have not been considered.

3.2 Boiling water reactor

The RC at a BWR is located within the reactor building. Due to the pressure suppression design, as described in section 2.1, the BWR containment can be significantly smaller than a large dry containment such as the Swedish PWRs. A typical BWR containment has a volume of about 12000 m^3 (Picaut, Chataigner et al. 2001) in comparison with ca 55000 m^3 for the PWRs in Sweden. The BWRs in Sweden and Finland have prestressed single concrete containment wall with embedded steel liner. The wall is usually around 1.1 m thick and the steel liner is located around 300 mm from the inner surface. The steel liner is used to ensure leaktightness of the containment and the thickness varies between 3 to 10 mm depending on NPP.

The RC is cylindrical and the inside is divided into two main compartments, dry-well and wet-well. The dry-well is the main compartment housing the reactor vessel and main components. Around the reactor vessel there is a biological shield, made out of prestressed or reinforced concrete. The thickness of the biological shield varies between the different reactors but is usually around 1–2 m. The compartment below the reactor vessel is considered to be a part of the dry-well and is usually called lower dry-well.

The upper dry-well is separated from the wet-well by an intermediate floor. The suppression pool is located in the wet-well. The pool consists of deionised water and the pool walls are coated with stainless steel sheets. The upper parts of the wet-well, above the water line, do not have a steel coating. The inner wall, that separates the wet-well and lower dry-well, consists of reinforced concrete with a thickness around 800 mm. Figure 4 presents an illustration of a BWR containment design.

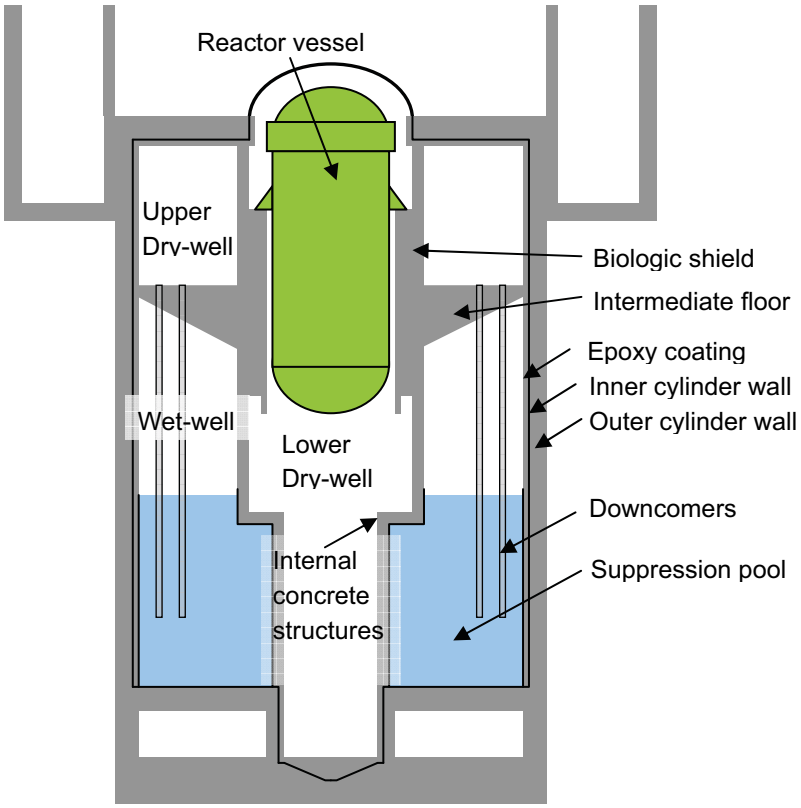

Figure 4. Illustration of a BWR section similar to the BWRs used in the Nordic countries.

As described in section 2.2 the BWRs in the Nordic countries can be divided into four sub groups concerning their structure and reactor design. Only three of these groups will be presented in this dissertation: and for each group one of the containments, Ringhals 1, Forsmark 2 and Forsmark 3 will be described.

For these reactors, information regarding the concrete composition and specific structure dimensions was collected from construction drawings and (Roth, Silfwerbrand et al. 2002). Only concrete within the steel liner is presented.

3.2.1 Ringhals 1

Construction of Ringhals 1 started in January 1969 and it was first put into commercial operation in January 1976. The reactor was designed by ASEA-ATOM and the design net capacity was 760 MW_e, in 2011 the RUP was 854 MW_e (IAEA 2012).

The inner cylinder wall consists of a 250 mm thick concrete wall plus an 80 mm thick concrete injected zone. When casting the containment wall, an 80 mm thick cleft was left in which the steel liner was placed, the cleft was thereafter injected with concrete. The concrete walls are a K50 (ca C45/55) concrete and it is made of CEM I standard (STD) Limhamn cement with a cement content of 375 kg/m^3, W/C-ratio of 0.42 and max aggregate size 32 mm.

The intermediate floor and the biological shield are both constructed with a K50 CEM I Limhamn STD cement, no further information regarding concrete composition was found. The intermediate floor is around 1.6 m thick and the wall between wet-well and lower dry-well is 800 mm. The biological shield is 800/1600 mm thick.

A rough estimate, based on construction drawings, gives a total concrete amount of ca 2000 m^3. The inner diameter of the containment is 22 m and the inner cylinder wall is around 32 m high. The inner volume is estimated from construction drawings to about 13000 m^3. This gives a concrete to space volume ratio of ca 1:5.5 m^3/m^3. Internal components, e.g. reactor vessel and piping, have not been considered.

3.2.2 Forsmark 2

Forsmark 2 is more or less identical to Forsmark 1 and has large similarities to Olkiluoto 1 and 2. Construction started in 1975 and it was first put into commercial operation in July 1981. The rector was designed by ASEA-ATOM and the design net capacity was 900 MW_e. The RUP as of 2011 was 990 MW_e (IAEA 2012).

In the bottom slab there is a 6 mm steel liner covered with ca 250 mm concrete. The concrete is a K40 (ca C35/45) and consists of a CEM I LH cement from Limhamn with a W/C ratio of 0.52 and a cement content of 330 kg/m^3.

The inner cylinder wall is 260 mm thick and made of K50 (ca C45/55) concrete. The concrete consists of CEM I Limhamn LH cement with a W/C-ratio of 0.46. The cement content is 370 kg/m^3 and the maximum aggregate size is 32 mm. The thickness of the steel liner is 6 mm.

No information regarding concrete properties of the internal structures has been found. The biological shield is ca 2 m thick and the intermediate floor is 1 to 3 m thick. The wall separating the lower dry-well and wet-well is 700 mm thick.

The inner diameter of the containment is 22 m and the containment is ca 37 meter high. A rough estimate of the concrete within the containment, based on construction drawings, gives a total concrete amount of ca 2500 m^3. The total volume inside the liner is calculated to ca 13300 m^3. The concrete to space volume ratio is thereby ca 1:4.5 m^3/m^3.

3.2.3 Forsmark 3

Forsmark 3 is an ASEA-ATOM BWR 75 and the construction started in 1979. In August 1985 the reactor was put into commercial operation. The reactor had a design net capacity of 1050 MW_e and in 2011 the RUP was 1170 MW_e (IAEA 2012).

In the bottom centre slab there is an 8 mm thick steel liner covered with concrete. The concrete is K50 (ca C45/55) with a CEM I LH cement, W/C-ratio of 0.42/0.43 and a cement amount of ca 370 kg/m^3 (Roth, Silfwerbrand et al. 2002)(Forsmark). The largest aggregate used is 32 mm.

The inner cylinder wall is 300 mm thick and inside it there is an 8 mm thick steel liner. The concrete is a K50 (ca C45/55) and the cement used is a CEM I LH, the W/C-ratio is 0.42/0.43 and the cement content ca 370 kg/m^3 (Forsmark). The biggest aggregate is 16/32 mm. No information regarding the concrete composition in the inner structures has been found.

The Biological shield is 1300 mm thick, the intermediate floor 1000 mm and the wall separating wet-well and lower dry-well 800 mm.

The internal diameter of the inner containment is 25.5 m and the height 30 m. A rough estimate from construction drawings gives the total amount of concrete within the liner to ca 2300 m^3. The total volume within the liner is estimated to 15500 m^3 which gives a concrete to space volume ratio of ca 1:6 m^3/m^3.

3.3 Similarities and differences

In table 2 the inner cylinder walls from four RCs are presented with the data from (Roth, Silfwerbrand et al. 2002), construction drawings and personal communications with personal on Forsmark. In the table a rough estimate of the total volume and concrete amount as well as the concrete to space volume ratio is shown.

Table 2. Comparison of the inner cylinder walls on four RCs regarding start of construction, concrete composition and volume ratios. Information gathered from construction drawings, personal communications and (Roth, Silfwerbrand et al. 2002)

	Construction start	Cement amount [kg/m^3]	W/C-ratio [kg/kg]	Inner Volume [m^3]	Concrete amount [m^3]	Concrete/ space volume ratio [m^3/m^3]
Ringhals 1	1970	365	0.42	13000	2000	1/5.5
Ringhals 4	1974	365	0.42	55000	8000	1/6
Forsmark 2	1973	370	0.46	13300	2500	1/4.5
Forsmark 3	1976	Ca 370	0.42/0.43	15500	2300	1/6

A comparison of the W/C-ratio or the cement amount in the inner cylinder wall in the four containments shows no significant trends over time or between the two sites. The cement amount is fairly similar for all the four, around 365–370 kg/m^3. The W/C ratio is similar for the two reactors at Ringhals and Forsmark 3 but Forsmark 2 has a slightly higher ratio. The amount of concrete is fairly similar for the three BWR systems and as expected the PWR holds a fairly higher amount due to the bigger size. Comparison of the concrete to space volume ratio shows that the result is fairly similar between all four with a ratio around 1:6. Only the concrete to space volume ratio at Forsmark 2 had a significant difference with 1/4.5.

3.4 Climatic conditions

The temperature and humidity within the reactor containments during operation depends on the moisture and heat sources. For all reactors there are two main heat sources, reactor vessel and primary circuit. In a PWR there is one additional heat source due to the secondary circuit. The temperature in the reactor vessels differs between BWRs and PWRs. Typically the operating temperature in a PWR reactor vessel is within the range of 282–288 ºC (IAEA 2005), the corresponding temperature for a PWR is within the range of 280–325 ºC (IAEA 2007).

The main moisture source within both BWRs and PWRs is most likely leakages from joints in the steam pipes. Another moisture source in a BWR may be the suppression pool, located in the wet-well. To what extent this contributes to the climatic conditions in the dry-well is however inconclusive. The only direct connection between wet-well and dry-well is through the downcomers. In appendix 1 some calculations are presented regarding moisture contribution through the downcomers during the outage.

Another possible moisture transports from wet-well occur through the concrete walls over the water line or through the intermediate floor. This possible moisture transport is due to the moisture gradient over the wall or floor. In the wet-well the humidity should probably be quit high, close to 100 %, due to the open water surface and limited ventilation. In the dry-well the climate should be significantly lower. Whether this moisture transport can have an impact on the climatic conditions will be discussed in section 6.5.

It is also a possibility that some leakage can occur from the suppression pool into the concrete. Even though the walls and bottom in the pools are coated with stainless steel sheets, leakage in joints is possible. If there were a contribution of moisture to the concrete from the pool this would result in a higher moisture contribution to the surroundings due to high moisture content within the concrete. There will not be any measurements of leakage from the suppression pool in this study, however, some field measurements may indicate if water is added to the concrete.

Apart form moisture transports from more humid compartments the concrete itself may be a significant moisture source. As presented in section 3.3 the total amount of concrete in relation to the total space volume within the steel liner is in the region of 1:6. In a PWR, the total amount of concrete has been calculated to ca 8000 m^3 and in a BWR ca 2000 m^3. Even when the cement is fully hydrated there are still vast amounts of water within the concrete that can be dried out over time. This possible moisture contribution will be discussed in paper 2 and section 6.5.2

3.5 As designed conditions

The concrete temperature is the only climatic condition found that is regulated in the design codes regarding the RCs and the concrete in NPPs. The standard used in the Nordic countries is the American ACI 349 and 359, Code Requirements for Nuclear Safety-Related Concrete Structures (ACI-ASME 2001; ACI 2001).

Under normal operation the maximum allowed long term concrete temperature is 150 F, ca 66 °C. In local areas e.g. around steam pipe penetrations the temperature is, however, allowed to reach up to 200 F, ca 93 °C. These temperature limitations may even be allowed to be increased if tests show that the strength of the concrete is not lowered under accepted design criteria due to the increased temperature. Tests should also provide evidence that the elevated temperatures do not cause deterioration of the concrete (ACI 2001).

There are also regulations regarding accident inflicted temperatures or short term temperatures. In these cases the surface temperature shall not exceed 350 F, ca 176 °C. In local areas, however, the concrete surface is allowed to reach up to 650 F, ca 343°C, from steam or water jets in case of a steam pipe failure (ACI-ASME 2001).

No recommendations regarding humidity levels have been found concerning the climatic conditions inside nuclear reactor containment. In (IAEA 2004) there are however

recommendations to monitor the humidity levels during operation e.g. to detect leakage from the primary circuit.

The moisture content within the concrete structures in reactor structures is not regulated. However, due to the high temperature in the containment during operation the concrete will dry over time, even with the tight concrete and epoxy coating. Typical effects of drying concrete are shrinkage and increased risk of carbonation. Because of the nitrogen which is used instead of air during operation, carbonation of the concrete in a BWR is, however, not likely to occur. In a PWR there are however a possibility of carbonation.

4 Moisture fixation and transport

4.1 Moisture fixation

The equilibrium relative humidity (RH) in concrete at a certain temperature corresponds to the amount of water vapour in the concrete's pore structure. The relation between the RH and the moisture content in the concrete can be described by the absorption and desorption isotherms (Nilsson 1980). The absorption and desorption isotherms are specific for each concrete and describe the moisture fixation in concrete at a certain RH, temperature and degree of hydration. The absorption isotherm describes conditions during increasing moisture content, whereas the desorption isotherm corresponds to decreasing moisture content.

Desorption and adsorption isotherms are however only truly valid when the material is constantly dried from ca 100 %RH or rewetted from close to 0 %RH. If a drying material has access to water the moisture starts to follow a scanning curve which goes from desorption to the adsorption isotherm curve. The shape of the scanning curve depends mainly on the moisture conditions at the start of rewetting. The same applies if the opposite situation occurs.

Depending on RH the water in concrete is fixed in different forms. Below ca. 45 %RH the water is mainly fixed by adsorption and above that by capillary condensation. Due to the low cohesive force between the water molecules, the capillary condensation is unstable under ca. 45 %RH. In addition menisci do not form during absorption, or break during desorption, below this level (Bažant 1969). Capillary condensations do not occur in the gel pores because the pores are too small to form capillary menisci. The effect of this can be seen e.g. when the sorption isotherms of cement pastes and concrete with different W/C-ratios are compared, Figure 5. A lower W/C-ratio leads to a more dense paste and a bigger part of the porosity consists of gel pores. With a higher W/C-ratio the porosity increases and more capillary and air pores are formed leading to higher moisture content at higher RH.

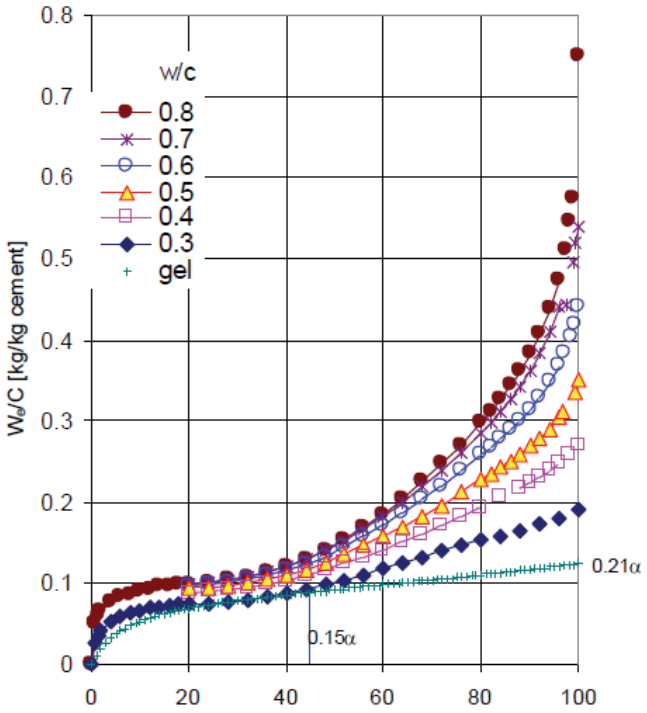

Figure 5. The desorption isotherm for concrete with different W/C-ratios, figure from (Nilsson and Johansson 2009). The degree of hydration varies between the different W/C-ratios. For 0.3 the degree of hydration was 60%, 0.4 70% and the remaining was ca 80 % hydrated (Nilsson 1980)

The degree of hydration is another main parameter that affects the desorption isotherm. As for the W/C-ratio a concrete or cement paste gets denser with a higher degree of hydration. This is due to the pore structure's dependence on the amount of hydrated cement. When fully hydrated the amount of gel pores is the highest and with a lowering of the degree of hydration the amount of capillary pores and air pores rises. This is due to the hydration process and the way the hydration products fill the voids between the cement grains. Figure 6 illustrates the relation between degrees of hydration and desorption isotherm.

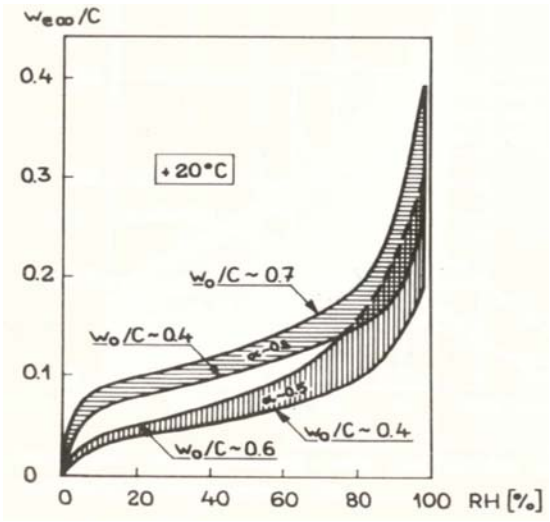

Figure 6. The desorption isotherm for concrete with different W/C-ratios and degrees of hydration. The figure is received from (Nilsson 1980) in which data from (Ahlgren 1972) has been used. In the upper zone the degree of hydration was ca 0.8 and in the lower ca 0.5

In a thick structure it is possible for the degree of hydration to vary over the depth. This can be the case if there is a temperature gradient over the structure, since the hydration is faster at higher temperatures. Differences in moisture levels may also result in differences in hydration. If there is a difference in degree of hydration this leads to differences in the moisture fixation properties.

When the temperature is raised in the concrete the capillary bound water and the adsorbed gel water are redistributed due to a higher chemical potential (Gibbs energy) in the gel water (Sellevold and Bjøntegaard 2006). Some of the adsorbed water molecules are transported to the capillary bound water until a new equilibrium is reached (Sellevold and Bjøntegaard 2006; Grasley and Lange 2007). This water addition leads, according to the Kelvin equation, to an increase of the meniscus radius and thereby an increase in RH, (Sellevold and Bjøntegaard 2006; Grasley and Lange 2007). Furthermore, a higher temperature leads to a lowering of the surface tension and expansion of the water molecules (Powers and Brownyard 1947). This also leads to an increase of RH at constant water content due to an increased meniscus radius in the capillary condensed water (Powers and Brownyard 1947; Sellevold and Bjøntegaard 2006; Grasley and Lange 2007); the opposite applies when the temperature is lowered. However, this phenomenon is only valid when RH is above ca. 45 %RH due to the instability of water meniscus under this level. When heated the RH in concrete increases both under 45 %RH and above due to changes in potential in the adsorbed water both in the gel pores and in bigger pores.

The relation between raised temperature and changes in RH has been investigated in several studies e.g. (Bažant 1969; Bažant 1970; Radjy, Sellevold et al. 2003; Sellevold and

Bjøntegaard 2006; Grasley and Lange 2007). Bažant, (Bažant 1969) calls this relation [%RH/°C] hygrothermic coefficient, this term will be used throughout the dissertation. Figure 7 shows measured hygrothermic coefficients presented in (Radjy, Sellevold et al. 2003). The effects of the capillary condensation determined by means of the Kelvin equation are also included in the figure, legend as capillary theory.

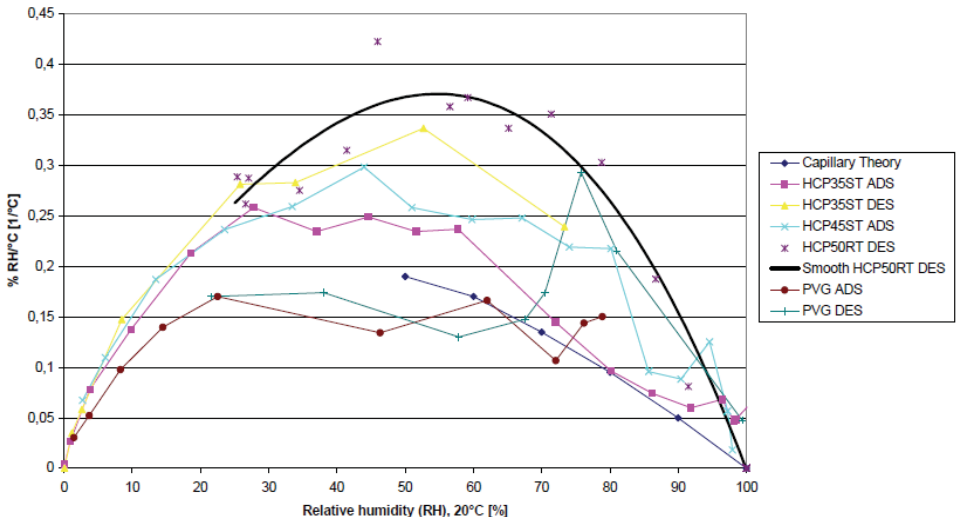

Figure 7. The hygrothermic coefficient at different relative humidities at 20 °C for different concrete compositions and during adsorption (ADS) and desorption (DES), figure from (Radjy, Sellevold et al. 2003)

In most of the studies of hygrothermic coefficient the measurements have been made in temperatures around 20°C. In the referenced studies the hygrothermic coefficient at 50 %RH varies between 0.25 and 0.35 %RH/°C depending on W/C-ratio and whether the specimen was wetting or drying. Only one study has been found on elevated temperatures, (Bažant 1970), in this study the hygrothermic coefficient was 0.5 %RH/°C at 35 °C and 55 %RH. This shows that the hygrothermic coefficient is dependent on both temperature and RH. The temperature dependence can also be seen when measurements of the adsorption or desorption isotherm at different temperatures are studied (Poyet 2009; Poyet and Charles 2009).

4.2 Isothermal moisture transport

Moisture transport in a porous material, such as concrete, is a result of two transport types, vapour transport and liquid transport. In this study moisture transport theory is essential for both the material study and the estimation of the moisture contribution from the concrete to the RCs.

Vapour transport is usually described as diffusion. The diffusion of vapour is isothermal and driven by differences in chemical and physical potential in the material. The driving potential is often described as gradients of vapour pressure, water vapour content, moisture content, moisture ratio, pore water pressure or RH (Claesson 1993).

Diffusion can be described by Fick's first law eq. (1)

$$J = -D\frac{\partial c}{\partial x} \tag{1}$$

Where J is the flux, D is the diffusivity, c is the potential and x is the length.

Flick's first law can then be rewritten to different driving potentials e.g. water vapour content (v) eq. (2)

$$J_v = -\delta_v \frac{\partial v}{\partial x} \tag{2}$$

Where J_v is the water vapour flux, [kg/(m^2×s)], v is the water vapour content [kg/m^3], x is the length (m) and δ_v is the vapour diffusion coefficient (m^2/s).

Two types of liquid transport, viscous saturated flux and capillary transport, are of interest regarding moisture transport in porous materials. The viscous saturated flux is dependent on water pressure gradients and can be described by Darcy's law. However, if there is no pressure gradient, e.g. hydrostatic, over the material this flux potential can be neglected.

The second liquid transport mechanism is capillary transport, in contrast to the diffusion and viscous saturated flux there are no generally accepted models to determine the capillary transport (Janz 2000). However, one approach is to use Darcy's law with the pore water pressure, P_l, as the driving potential, e.q (3) (Janz 2000).

$$J_l = -\frac{k_p}{\eta}\frac{\partial P_l}{\partial x} = -D_l \frac{\partial P_l}{\partial x} \tag{3}$$

Where J_l is the liquid flux [kg/m^2×s], D_l [kg/(m×s×Pa)] is the transport coefficient, P_l the pore water pressure [Pa] and x the length [m].

What transport type is most dominant in a structure at a certain condition is strongly dependent on the pore structure of the material and the moisture condition within the material at the given condition. At lower RH in the concrete the main transport is due to diffusion, either in the adsorbate layers or in the pores. At higher RH, above 45 %RH, the transport due to capillary transport is increasing and finally takes the upper hand. However, if the material structure is too dense and there are only small amounts of

capillary pores the capillary transport is more or less absent. This can be the case in cement paste when the W/C-ratio is low.

When the moisture transport through a porous material is measured a mixture of transport types occurs. The total flux can be described by eq. (4)

$$J_{tot} = J_v + J_l = -\delta_v \frac{\partial v}{\partial x} + \lambda_m \frac{\partial s}{\partial x} \tag{4}$$

Where λ_m [kg/m^2×s] is the transport coefficient and s is the suction [Pa]. Suction is defined as the pore water pressure minus the atmospheric pressure. In general the suction is significantly larger then the atmospheric pressure and thereby almost equal to the pore water pressure in these conditions (Janz 2000).

It is of great advantage to have a model that describes the total moisture flux with only one transport potential and only one moisture transport coefficient. In equilibrium at an isothermal state it is possible to rewrite the total flux equation, equation 4, due to the relation between the pore water pressures, vapour pressure, water vapour content to eq. 5 (Claesson 1993).

$$J = -\delta \frac{\partial v}{\partial x} \tag{5}$$

Where δ [m/s^2] is the moisture transport coefficient, v is the water vapour content [kg/m^3] and x the length [m]. The derivation of equation 5 is presented in appendix 2. However if the system is not isothermal this simplification is not possible and the two fluxes have to be separated.

5 Material study

To establish a good model that describes the drying process in a structure it is essential to have good knowledge of the material properties of the specific concrete. Moisture transport can e.g. be described with the moisture transport equation 5, presented in section 4.2. The main material property to calculate the moisture transport is therefore the moisture transport coefficient. The coefficient is dependent on both the material composition and the moisture condition in the concrete. Because of this the coefficient varies in the material due to the moisture profile but also if there is a variation in degree of hydration.

It is also important to quantify the vapour transport resistance of the epoxy that most concrete surfaces are coated with in the RCs. The vapour resistance, Z [s/m] is a recalculation of the moisture transport coefficient when the thickness is included in the coefficient, see equation 6. With the vapour resistance, equation 5 can be rewritten to equation 7.

$$Z = \frac{dx}{\delta} \tag{6}$$

$$J = \frac{\partial v}{Z} \tag{7}$$

To determine the moisture content in concrete from RH measurements the absorption- and desorption isotherm for that concrete has to be established. Measurements of absorption and desorption isotherms was however not finished at the time for this dissertation hence not presented.

As a part of the material study a preliminary study of the moisture content was also made through measurement of degree of capillary saturation. These results are presented in appendix 3.

Both the moisture transport coefficient and the moisture fixation properties are dependent on the degree of hydration. The concrete in an RC may have different degrees of hydration due to temperature and moisture gradients. It is therefore important to evaluate if variations occur. In this study this was done both with an attempt to measure the calcium hydroxide

(CH) content in the concrete at different depths and by comparing the measured parameters with specimens from different depth.

5.1 Material from Ringhals 4

The material that was used in the material study was collected from a 6×8 m^2 concrete block from the RC wall at Ringhals 4. The concrete block was removed because of a steam generator replacement in 2011. Figure 8 shows the inner side (inner cylinder wall) of the concrete block after the concrete for the material study was extracted. The specimens where extracted about four weeks after that the concrete block had been removed from the cylinder wall. During that period of time the concrete block was stored outdoors. The concrete composition is described in table 3 and the clinker composition of the cement (LH Limhamn) is presented in table 4. The concrete at Ringhals 4 is similar to that used in the other NPPs, see section 3.3.

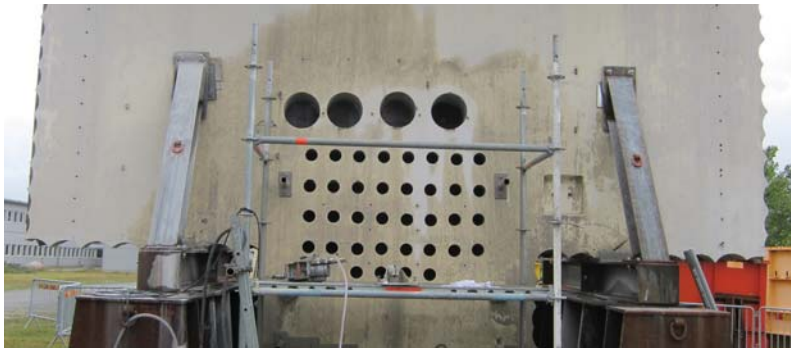

Figure 8. Concrete block from the containment wall at Ringhals 4 with the positions of the concrete cylinders extracted from the inner cylinder wall

Table 3. Concrete composition of the inner cylinder wall at Ringhals 4 (Roth, Silfwerbrand et al. 2002)

Cement type	Cement [kg/m^3]	Water [kg/m^3]	W/C-ratio	Gravel and sand [kg/m^3]	Stone [kg/m^3]
LH Limhamn	365	154	0.42	752	1135

Table 4. Clinker composition of LH Limhamn, data from Cementa AB

Alite (C3 S)	Belite (C2 S)	Aluminate (C3 A)	Ferrite (C4 AF)	Free CaO	Gypsum	Specific surface [m^2/kg]
35	46	-	11	0.3	4.8	366

In total, 36 concrete cylinders with a diameter of 94 mm were collected for determination of the material properties. Six additional cylinders with a diameter of 294 mm were extracted, four from the inner cylinder wall and two from the outer one. These cylinders were used to determine the degree of capillary saturation profile of the structure as a pre study of the moisture profile in the inner and outer cylinder wall, see appendix 3.

The samples were core drilled and water was used for cooling. The positions of the holes were chosen so that the amount of reinforcement in the samples was minimised. After extraction, the concrete samples were wrapped in plastic and transported within one day to the laboratory at Division of Building Materials, Faculty of Engineering, Lund University. The 94 mm cylinders were thereafter stored indoors for ca 5 months before the test specimens for the different tests were prepared.

Each test specimen from the 94 mm cylinders was sawed out from the cylinders using a diamond blade with water cooling. The specimens were taken from different depths and had different thicknesses, see table 5.

Table 5. Description of the test specimens and test conditions for each test setup. The measurements were made in different climates, one at 20 °C (1) and the other at 50 °C (2).

	Core Diameter [mm]	Specimen Thickness [mm]	Specimen Depth [mm]	Temp. [°C] (1)	(2)	RH [%]: Surroundings (1)	(2)	RH [%]: Cup (1)	(2)	Nr.
Epoxy: Vapour resistance	94	10	0–10	20	50	55	10	75 85 97	75 85 97	36
Moisture transport coefficient	94	20	40–60 100–120 230–250	20	50	55	10	33 75 85 97	- 75 85 97	63
Amount of CH	94	10	40–50 150–160 250–260	-		-		-		9

5.2 Moisture transport properties

The moisture transport coefficient of the concrete and the vapour resistance of the epoxy were determined in steady state isothermal conditions, using the cup method. The method has been used in several studies on porous materials such as concrete (Nilsson 1980; Hedenblad 1993; Janz 2000).

The setup consisted of a glass cup with an inner diameter on 94 mm and a height of 65 mm. The specimen was placed on the cup as a lid and the sides were sealed. In the cups different saturated salt solutions were placed and the average distance from the surface and the specimens was 40 mm.

The cylinder surface on the test specimens was sealed with a pre heated bitumen strip with aluminium tape on the outer surface. The strip was heated at 105 ºC for ca 45 s and there after pressed to the concrete surface to ensure that the surface was properly sealed. The specimen was then placed on the glass cup and two layers of aluminium tape were applied. Figure 9 shows a picture of nine of the test specimens used.

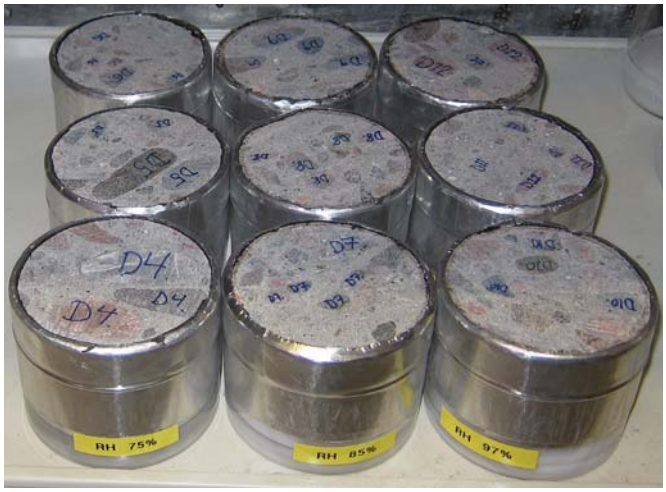

Figure 9. Nine specimens used for determination of moisture transport coefficient by the cup method.

To validate the aluminium and asphalt seals, three additional cups were prepared. The validation specimens were made of 20 mm thick aluminium with a diameter of 94 mm. The seals were applied in the same manner as for the concrete specimens and the bitumen tape covered 10 mm of the aluminium so that the test could be used for validation of the measurement set-up used for the concrete and the epoxy coated specimens. Instead of a saturated salt solution, deionised water was used giving an inner humidity of ca 100 %RH.

The validation specimens were placed in a climate chamber with 55 %RH and 20 ºC. The mass change of the specimens varied some milligrams up and down during the measurement period and after seven month the mass was between five and two milligrams from the starting weight. This strongly indicates that no leakage over the seals had occurred.

The moisture transport coefficient of the concrete was determined by using equation 5 on the steady state condition that was obtained in the cups. By measuring the weight loss of the specimens over a longer period of time it could be recalculated to a moisture flux, J

[kg/m^2×s]. The measurements were made at different RH intervals, which could be translated into different vapour contents (v). Together with the thickness of the specimens this gave the moisture gradient (dv/dx). Division of the moisture flux by the moisture gradient gave the moisture transport coefficient in that specific interval.

To obtain different RH intervals different saturated salt solutions were used. The salts used in these studies are presented in table 6.

Table 6. RH from saturated salt solutions at 20 and 50°C (Greenspan 1977)

	20°C	50°C
$MgCl_2$	33.07 ± 0.18 % RH	
NaCl	75.47 ± 0.14 % RH	74.43 ± 0.19 % RH
KCl	85.11 ± 0.29 % RH	81.20 ± 0.31 % RH
K_2SO_4	97.59 ± 0.53 % RH	95.82 ± 0.45 % RH

The RH presented in table 6 is the RH that was obtained at the surface of the saturated salt solutions. However, the space between the surface of the saturated salt and the concrete specimen reduces, the RH at the specimen surface due to the vapour resistance of air. The vapour resistance is temperature dependent and at 20 °C it is ca 25×10^{-6} m^2/s, the corresponding value at 50 °C is about 30×10^{-6} m^2/s (Hjorslev Hansen 1993).

Because of the steady state conditions the moisture transport from the surface of the saturated salt to the specimen is equal to the moisture flux through the specimen. The ΔRH can thereby be determined by inserting the data in equation 5. Apart from the moisture resistance of the air, there is a surface resistance both at the saturated salt solution surface and the specimen. These surface resistances can however be negligible (Nilsson 1980; Anderberg and Wadsö 2008).

In their paper, Anderberg and Wadsö present (Anderberg and Wadsö 2008) a model for the mathematical calculation of the mean moisture transport coefficients in RH intervals that have not been measured.

In (Anderberg and Wadsö 2008) it is shown that for two measurements with the cup method, measured in the same external climate and different internal climates, the mean moisture transport coefficient in an interval between the two internal ones could be calculated using:

$$\overline{\delta_{12}} = \frac{\overline{\delta_{02}}(v_2 - v_0) - \overline{\delta_{01}}(v_1 - v_0)}{v_2 - v_1} \qquad [8]$$

Where index 0 represents the external vapour condition, and 1 and 2 the two internal ones.

The moisture transport coefficient has previously been determined by e.g. Hedenblad (Hedenblad 1993) for different concrete compositions. The results show that a concrete with a W/C-ratio of 0.4 has a moisture transport coefficient of ca 0.13×10^{-6} m^2/s, in the region 33 to 65 %RH. The corresponding moisture transport coefficient for a concrete with W/C-ratio of 0.5 is ca 0.14×10^{-6} m^2/s. In figure 10 the moisture transport coefficient in relation to the RH of the 0.5 W/C-ratio is presented.

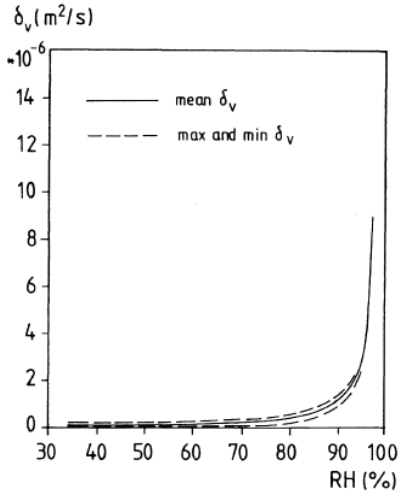

Figure 10. Measured moisture transport coefficient of concrete with W/C-ratio of 0.5, picture taken from (Hedenblad 1993)

5.2.1 Epoxy vapour resistance

The vapour resistance of the epoxy coating that the concrete surfaces in the RCs are coated with has a great impact on the drying of the structures. Specimens from all 36 cylinders were collected to determine the vapour resistance of the epoxy coating. On half of the specimens the epoxy coating was ground off with a diamond saw. These specimens were used to determine the moisture transport properties of the concrete close to the surface. During the cutting and preparation, four of the specimens without the epoxy coating were damaged and removed.

Of the 32 test specimens, 18 had the epoxy coating and 14 were without. Six different climatic conditions were studied, with the specifications as in table 7. Triple samples were used in each climate, except at ca 75 and ca 85 %RH for the specimens without epoxy where only two specimens were used in each climate. 16 specimens were placed in a climate chamber with 55 %RH and 20 °C and the remainder were placed in an oven with 50 °C.

Table 7. Description of the test specimens and the test condition. The measurements where made in different climates, one at 20 °C (1) and the other at 50 °C (2).

	Core Diameter [mm]	Specimen Thickness [mm]	Specimen Depth [mm]	Temp. [°C] (1)	(2)	RH [%]: Surroundings (1)	(2)	RH [%]: Cup (1)	(2)	Nr.
Epoxy:	94	10	0–10	20	50	55	10	75	74	32
Vapour								85	81	
resistance								98	96	

The measurements in the oven were conducted at the Division of Building Materials, Faculty of Engineering, Lund University. Due to the relatively stable moisture content in the air in Lund, Sweden, during winter, ca 4 g/m^3, the RH was ca 10 % in the oven during the measurement period.

Four of the specimens coated with epoxy were displaced from their original position during the initial period in the oven. This was most likely due to the pressure rise in the cup when heated. One specimen with 75 %RH, two with 81 %RH and one with 96 %RH had been affected. When observed, the specimens were pressed back into position. No clear evidence of any effect was however observed during the prolonged measurements. Only one of the affected specimens (75 %RH) had the highest moisture flux compared with the others in the same climatic condition. This indicates that the sealing function of the bitumen and Al-tape was not significantly affected.

The specimens that were placed in the climate chamber were exposed to a constant temperature of 20 °C and 55 %RH.

All specimens without the epoxy coating were capillary-saturated before the cups were assembled, to make sure that all specimens were approaching the steady state of the flux through desorption. This was not done on the specimens with epoxy coating due to the, high vapour resistance of the coatings, in comparison with concrete. It was expected that the epoxy coating will dominate the overall vapour resistance.

To be able to determine the vapour resistance of the epoxy, the RH directly under the coating had to be known. This was however not possible to determine. An alternative method to quantify the influence of the epoxy was instead to consider the epoxy coating and the 10 mm thick concrete layer as a composite material. The outer 10 mm in a structure will act in the same manner as these measurements; hence this approach gives the needed information. As a comparison the vapour resistance of the epoxy-concrete composite was also recalculated to an equivalent concrete thickness.

The water vapour resistance of the composite, epoxy and concrete, was calculated from the steady state moisture flux. In figure 11 and 12 the moisture transport coefficient for both climates is presented.

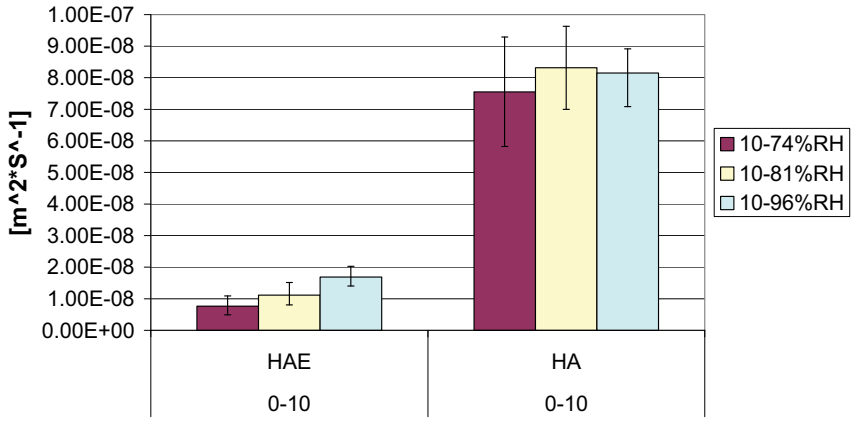

Figure 11. Average moisture transport coefficient measured with cup method on 10 mm thick epoxy-concrete composite (HAE) and concrete (HA) at 50°C in an oven with 10 %RH. Error bars represent max and min value.

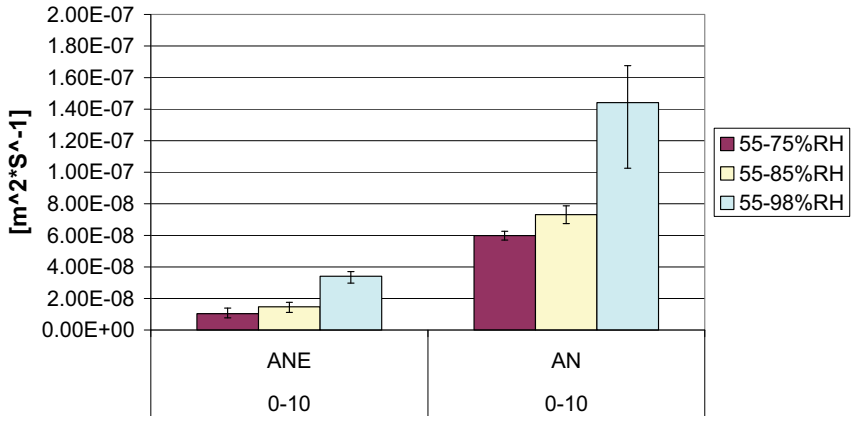

Figure 12. Average moisture transport coefficient measured with cup method on 10 mm thick epoxy-concrete composite (ANE) and concrete (AN) at 20°C in a climate chamber with 55 %RH. Error bars represent max and min value.

The moisture transport coefficient was recalculated to vapour permeation resistance according to equation 6. The moisture transport coefficient, vapour resistance and an equivalent concrete thickness compared to the surface concrete are presented in table 8.

Table 8. The moisture transport coefficients of epoxy coated concrete samples and recalculations to vapour resistance and an equivalent concrete thickness of the specimens in relation to the concrete samples without epoxy.

50 gC	Moisture transport coefficient, δ [m^2/s]	Vapour resistance, Z [s/m]	Equivalent concrete thickness [mm]
10–74 %RH	7.64E-9	1.30.E+6	98
10–81 %RH	1.12E-8	8.84.E+5	74
10–96 %RH	1.68E-8	5.97.E+5	49
20 gC			
55–75 %RH	1.05E-8	9.70E+5	58
55–85 %RH	1.47E-8	6.87E+5	50
55–98 %RH	3.40E-8	3.34E+5	48

When the results presented in table 8 are compared, it is clear that there is a significant difference in resistance at the two temperatures. The difference between the two temperatures can partly be described by the different RH interval. The moisture transport coefficient is strongly moisture dependent. However, the coefficient is quite stable at lower RH, up to ca 75 %RH. Because of this, in the measurements at 50 °C the moisture transport coefficient had a higher influence from low RH than in the measurements at 20 °C. The moisture dependence in concrete is clearly shown in the results presented in (Hedenblad 1993), see figure 10. The measurements between 10 and 75 %RH at 50 °C and 55–75 at 20 °C showed, however, that there is a significant difference and thus there is a clear temperature influence.

In contrast to the measurements at 20 °C the moisture transport coefficient of the specimens without epoxy, at 50 °C, did not show an RH dependence. The reason why there seems to be no big difference may be that there has been crack formation in the specimens due to the increased temperature. Comparison of the error bars also shows that the measurements at 50 °C had a larger uncertainty. The moisture transport coefficient was however in the same region as the measurements at 20 °C which indicates that there are no drastic variations in the material.

The calculated equivalent concrete thickness of the epoxy-concrete composite showed a large scattering tendency. This was a result of the absence of a clear RH dependence from the measurements on the concrete specimens at 50 °C. At 20 °C a smaller divergence was observed. This was to some extent expected due to the moisture dependence at high RH.

Using the model presented in (Anderberg and Wadsö 2008), see equation 8, on the measurements gave the moisture transport coefficient in the additional intervals 75–85 %RH and 85–97 %RH for the measurements at 20 °C and 75–81 %RH and 81–96 %RH at

50 °C. The results are presented in figures 13 and 14 for the measurements at 50 °C and 20 °C.

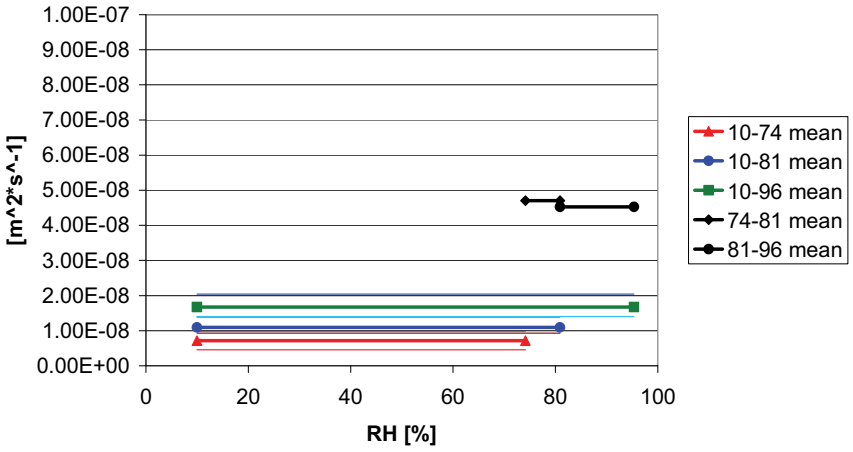

Figure 13. Measured and calculated moisture transport coefficient of epoxy coated specimens at 50 °C in RH intervals according to the legend. Error bars represent max and min measured coefficients. The moisture transport coefficient was only calculated on the mean values.

The calculated moisture transport coefficient in the interval 74–81 %RH seems to be higher then the one in the interval between 81–96 %RH. This is however not likely. The model, see equation 8, depends on the difference between the measured coefficient at the two intervals and the relation of vapour content (or RH) between the measured intervals and their internal difference. In this case, either the measured coefficient in the interval 10–96 %RH was too low, the measured coefficient in the interval 10–81 %RH was too high or the measured coefficient in the interval 10–74 %RH was too low. It was however not possible to determine which of the measurements gave rise to error.

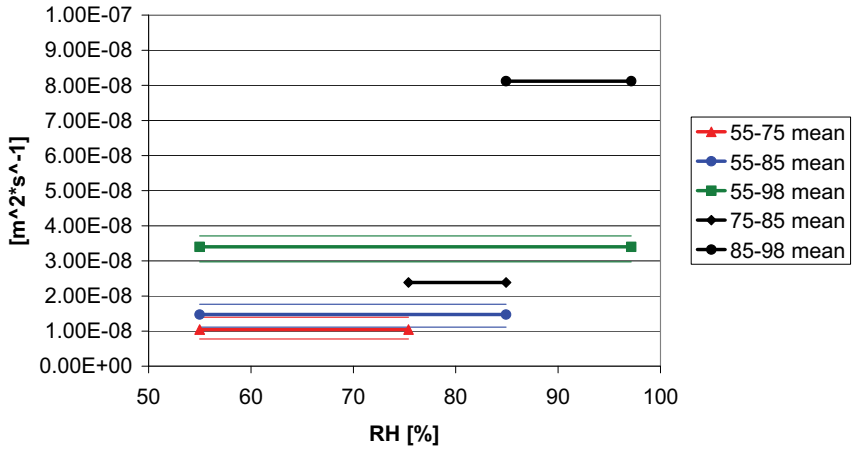

Figure 14. Measured and calculated moisture transport coefficient of epoxy coated specimens at 20 °C in RH intervals according to the legend. Error bars represent max and min measured coefficients. The moisture transport coefficient was only calculated on the mean values.

The collected result shows clear tendencies that the vapour transport resistance of the epoxy coating is significantly higher then that of concrete at both low and high temperatures. The measurements also show that the vapour resistance is both moisture and to some extent temperature dependent. The cause of temperature dependence may be that the epoxy probably swells when heated and thereby closes some of the pores inside.

5.2.2 Moisture transport coefficient

A total of 21 concrete cylinders were used for measuring the moisture transport coefficient of the concrete from the inner cylinder wall at Ringhals 4. From each of the cylinders three concrete specimens, with a thickness of ca 20 mm, were taken at the depths: 40–60 mm, 100–120 mm, 240–260 mm. Some of the concrete cylinders contained pieces of the reinforcement at 40–60 mm depth. On these cylinders the specimens were taken either in front or behind the reinforcement.

The measurements were conducted using the cup method. The moisture transport coefficient was then determined through equation 5. The measurement series consisted of 63 specimens and was performed in seven climatic conditions. 36 specimens were placed in a climate chamber at 20 °C and 55 %RH and 27 specimens were placed in an oven at 50 °C and ca 10 %RH. Three specimens from each depth were studied in both the climate chamber and in the oven. In the oven three saturated salt solutions were used and in the climate chamber all four, see table 9.

Table 9. Description of the test specimens and the test condition. The measurements where made in different climates, one at 20 °C (1) and the other at 50 °C (2).

	Core Diameter [mm]	Specimen Thickness [mm]	Specimen Depth [mm]	Temp. [ºC] (1)	(2)	RH [%]: Surrounding (1)	(2)	RH [%]: Cup (1)	(2)	Nr.
Moisture transport coefficient	94	20	40-60 100-120 230-250	20	50	55	10	33 75 85 98	- 74 81 96	63

The measurements in the oven were conducted at the Division of Building Materials, Faculty of Engineering, Lund University. Due to the relatively stable moisture content in the air in Lund, Sweden, during winter, ca 4 g/m^3, the RH was ca 10 % in the oven during the measuring period.

Prior to the measurements, all specimens were capillary saturated. This was done to ensure that all specimens were drying during the acclimatisation. In the next step the surfaces of the cylinders were sealed with a bitumen tape and Al-tape as described earlier.

The specimen's thickness, 20 mm, was too small to be considered as a representative test specimen, traditionally 3–4 times the maximum grain size. Specimens with aggregates that go all the way through the specimens may have a higher moisture transport due to a higher porosity in the interface zone between the aggregates and the cement paste. These interface zones are usually referred to as the interfacial transition zone (ITZ) (Ollivier, Maso et al. 1995).

The ITZ around big through aggregates may however not have a significant effect on the moisture transport. These zones have an extremely small influence of the total surface, in contrast to other defects in the cement matrix, such as micro cracks, which would probably stand for a higher degree of influence. No studies have, however, been found regarding ITZ on big through grains.

To identify these ITZ zones all specimens were photographed on both sides prior to the assembly of the cups. After the measurement of moisture transports the specimens with values that stood out from the average were studied to determine if any aggregates penetrated the specimens. No such correlation was however found.

The results presented in (Hedenblad 1993) indicate that the moisture transport coefficient is strongly dependent on the thickness of the specimens. The measurements were conducted on specimens that were, 63, 100 and 150 mm thick. A clear correlation was found between a thicker specimen and higher moisture transport coefficient, but no explanation of this phenomenon was given. These results were not any new findings and Hedenblad referred to two other studies that had observed the same phenomenon. In the measurements conducted by Hedenblad it seems, however, that the size effect was larger at high W/C-ratios, this was however not discussed in the thesis. One plausible explanation

for the differences, according to Hedenblad, was that moisture transport in concrete is in fact non-Fickian. The author has however not found any confirmation for this statement.

In figures 15 and 16 the moisture transport coefficients of the concrete specimens from the different depths at the two temperatures are presented. As an addition, the moisture transport coefficient of the plain concrete specimens (HA and AN) in the measurements in section 6.2.1 is included.

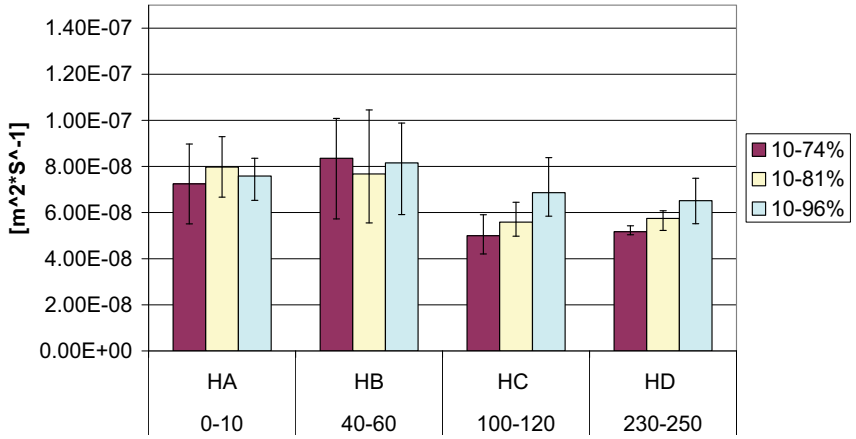

Figure 15. Average moisture transport coefficient measured with cup method on 20 mm thick concrete specimens (HB HC HD) from three different depths and one additional 10 mm thick specimen (HA) at 50 °C in an oven with 10 %RH. Error bars represent max and min value.

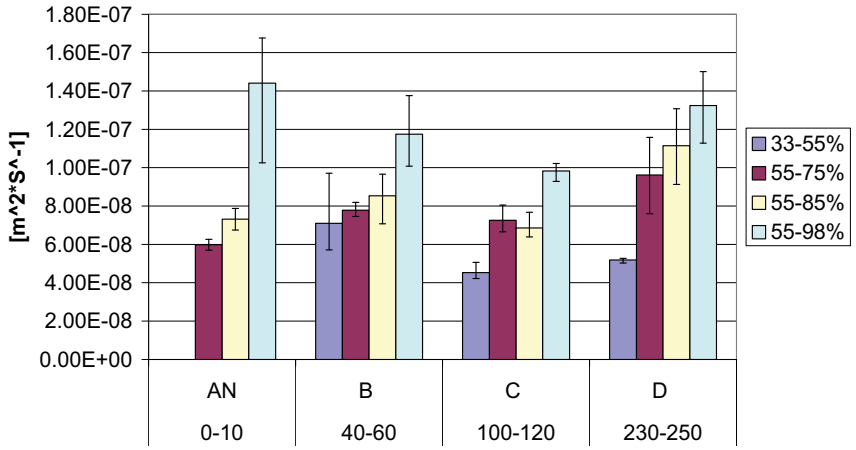

Figure 16. Average moisture transport coefficient measured with cup method on 20 mm thick concrete specimens (B C D) from three different depths and one additional 10 mm

thick specimen (AN) at 20 °C in a climate chamber with 55 %RH. Error bars represent max and min value.

There is some clear evidence that the moisture transport coefficient is lower at higher temperatures, especially at high RH. However, as mentioned in the earlier section, the RH interval in which the coefficient is measured is much bigger for the measurements at 50 ºC. And as can be seen in figure 10 on page 39 the moisture transport coefficient is strongly moisture dependent but only at RH over 65–75 %.

The measurements show that there are no significant differences with regard to the position of the specimens on the core, especially from the measurement at 20 ºC. At 50 ºC it seems, however, that the position of the specimen may have some influence on the moisture transport coefficient. As can be observed the coefficient is somewhat higher at positions close to the surface. The results from the outer 10 mm and from the depth 40–60 are quite similar at 50 ºC and significantly higher than those from a greater depth. However, if there had been any large differences in the material this should also been seen from the measurements at 20 ºC. With the accessible data it is not possible at this stage to determine whether the variation was due to differences in the concrete.

A comparison between the outer 10 mm and the specimens from the depth 40–60 mm regarding the size influence as described by Hedenblad (Hedenblad 1993) shows some differences. However it is not possible at this stage to determine whether this is due to the size differences or due to variations in material composition. The biggest difference is seen at 20 ºC and with an RH in the cup of 75 %. The results in the other conditions overlap hence a significant difference can not be determined.

The model described in (Anderberg and Wadsö 2008), see equation 8, was adapted to the measurement. The results from specimens in HB are however not included due to the fact that they did not follow the RH dependence during measurements that was expected. In the series, one or more of the measurements had a too high or too low moisture transport coefficient in relation to the others. Because of this the calculated moisture transport coefficients give clearly non accurate results and it would be complicated to compare these with the others.

Figures 17–21 present the moisture transport coefficient from the measurement series HC, HD, B, C and D. Apart from the measured values the calculated coefficients in the intervals 74–81 %RH 81–96 %RH for the specimens exposed to 50 ºC and 75–85 %RH and 85–98 %RH at 20 ºC is presented. The error bars of the measured results represent the max and min value. Calculations of the moisture transport coefficient with equation 8 were only performed on the mean values.

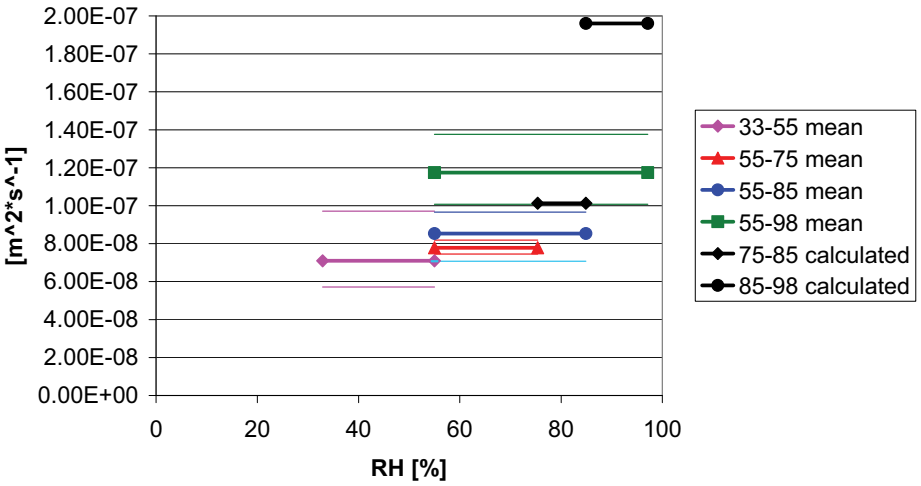

Figure 17. Measured and calculated moisture transport coefficient of concrete specimens from 40–60 mm depth at 20 °C in RH intervals according to the legend. Error bars represents max and min measured coefficients. The moisture transport coefficient was only calculated on the mean values.

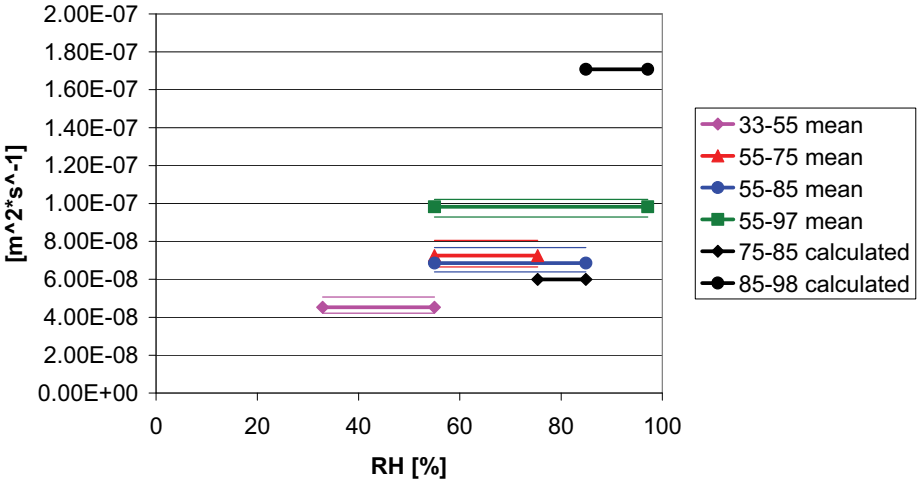

Figure 18. Measured and calculated moisture transport coefficient of concrete specimens from 100–120 mm depth at 20 °C in RH intervals according to the legend. Error bars represent max and min measured coefficients. The moisture transport coefficient was only calculated on the mean values.

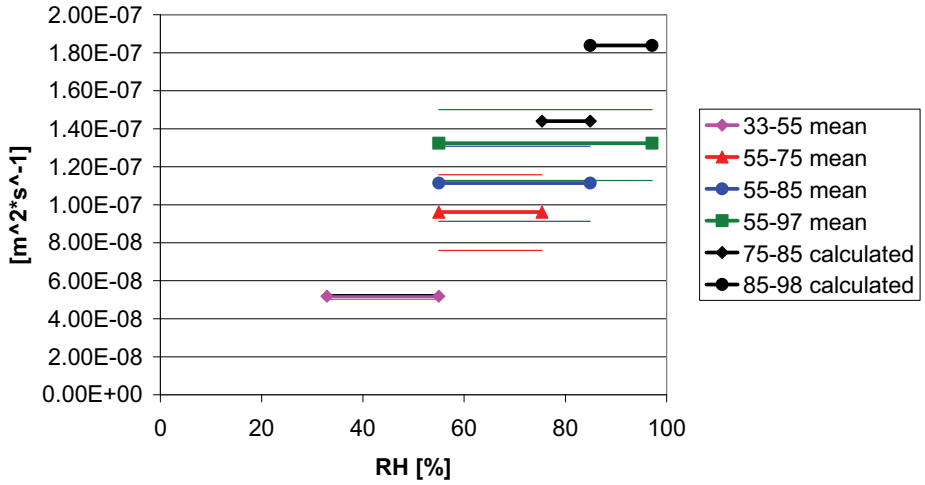

Figure 19. Measured and calculated moisture transport coefficient of concrete specimens from 230–250 mm depth at 20 °C in RH intervals according to the legend. Error bars represent max and min measured coefficients. The moisture transport coefficient was only calculated on the mean values.

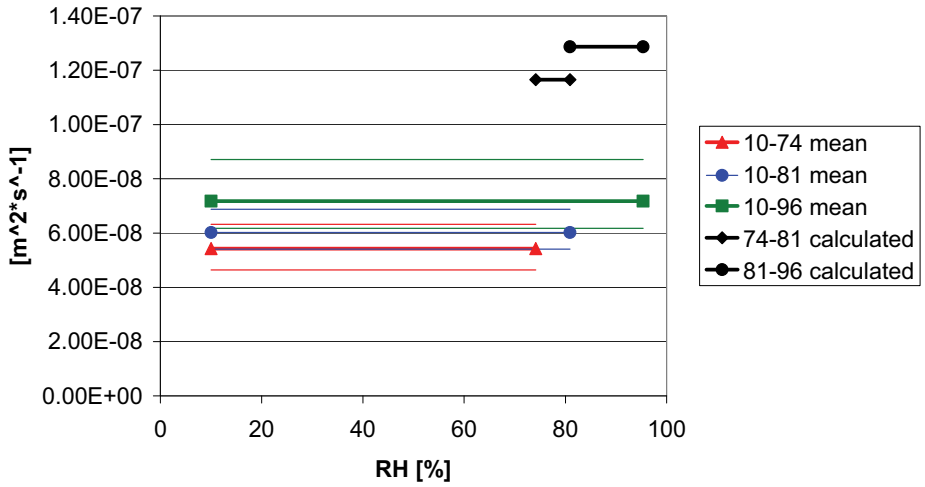

Figure 20. Measured and calculated moisture transport coefficient of concrete specimens from 100–120 mm depth at 50 °C in RH intervals according to the legend. Error bars represents max and min measured coefficients. The moisture transport coefficient was only calculated on the mean values.

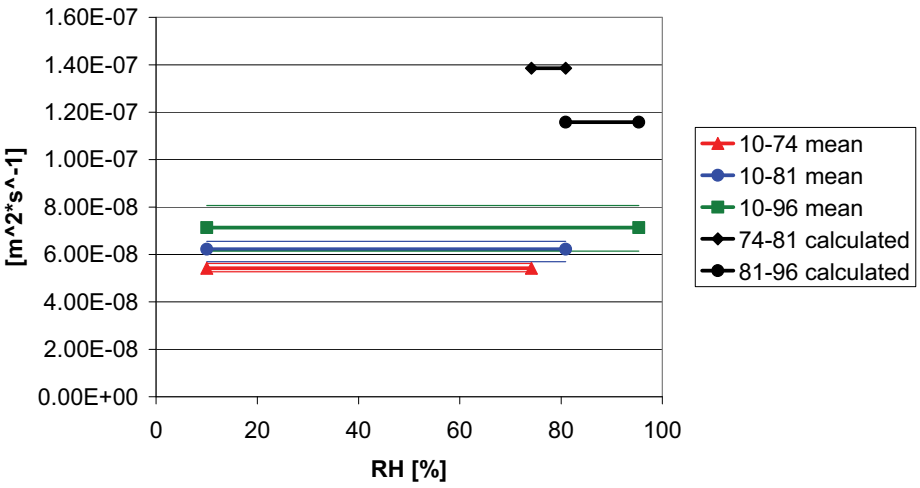

Figure 21. Measured and calculated moisture transport coefficient of concrete specimens from 230–250 mm depth at 50 °C in RH intervals according to the legend. Error bars (parallel lines) represents max and min measured coefficients. The moisture transport coefficient was only calculated on the mean values.

As for the measurements on the epoxy coated specimens some of the calculated coefficients stand out as "not likely". For the measurements on the concrete specimens this is especially the case for the calculated moisture transport coefficient in the interval 74–94 %RH in 50 °C from the depth 230–250 mm, see figure 21. Event though the measured coefficients show an expected moisture dependence, the calculated value between 74–81 %RH was higher than that in the interval 81–96 %RH. The model used, see equation 8, depends on the difference between the measured coefficient at the two intervals and the relation of vapour content (or RH) between them. It was however not possible to determine from these results where the error originated.

The collected results show that the measured moisture transport coefficient was significantly lower than those obtained by Hedenblad (Hedenblad 1993). On average the measured moisture transport coefficient in the low RH intervals was around 0.05×10^{-6} m^2/s at 20 °C. The corresponding moisture transport coefficient measured by Hedenblad (Hedenblad 1993) on a similar concrete (W/C-ratio 0.40) but 100 mm thick was 0.13×10^{-6} m^2/s. The concrete at Ringhals 4 had thus moisture transport coefficients that were between 1/2 and 1/3 of those measured by Hedenblad.

The reason for the difference may be the fact that the specimens form Ringhals 4 had reached a higher degree of hydration and therefore had a more dense cement paste. These results also indicate that ITZ, due to through aggregate grains, might not be a problem. However the size effect of the specimens may be one reason for the difference, it is however not possible to determine whether this would explain the total difference.

5.3 Amount of Calcium hydroxide (Variation of hydration)

Concrete is a composite material that mainly consists of ca 70 % aggregates (sand, gravel and stones), cement, water and often additives (chemical and/or mineral). The cement, when reacted with water, constitutes the matrix which binds the aggregate particles.

In the technical field of cement chemistry the most common chemical components of a Portland cement clinker are usually simplified:

- Calcium oxide (CaO) $\rightarrow$ C
- Silicon dioxide (SiO_2) $\rightarrow$ S
- Water (H_2O) $\rightarrow$ H
- Aluminium oxide (Al_2O_3) $\rightarrow$ A
- Ferric oxide (Fe_2O_3) $\rightarrow$ F

When water is added to the dry concrete mixture a reaction starts between cement and water, i.e. the cement starts to hydrate. Water reacts with the different clinker components and a crystalline matrix is formed. This matrix is often referred as the cement gel. The main hydration products in the cement gel are calcium hydroxide (CH) and calcium silicate hydrate (C-S-H). C-S-H is the main contributor to strength in the cement gel and the CH contributes to the high pH in the pore water.

The C-S-H represents different compositions of the calcium silicate hydrates, hence the dashes. In cement, C-S-H represents a group of crystalline formations and is considered as poorly crystallised and partly amorphous, hence usually referred to as C-S-H gel (Taylor 1997). Apart from CH and C-S-H gel other common components are ettringite monosulfate and CASH. The composition depends on the cement clinker composition and thus the cement type.

During the hydration of cement, water is chemically fixed in the concrete. According to the model that Powers established during the 1940s (Powers and Brownyard 1947), the amount of bound water can be calculated if the clinker composition and degree of hydration are known. The amount of bound water depends on the composition of the specific cement clinker that is used and in general it is assumed that the completely hydrated cement chemically binds water corresponding to ca 25 % of its non-reacted weight. This value can, however, vary depending on the clinker composition.

During the hydration the concrete pore structure is formed. With a low W/C-ratio the pores in the paste are almost exclusively small pores called gel pores. With a higher W/C-ratio more large pores are formed. The larger pores are usually called capillary pores the name is derived from the way the water is fixed. There are also a number of bigger air pores that are of interest, mainly concerning frost damage in concrete.

The hydration process is not a linear process, after 28 days between 40–80 % of the cement may have hydrated but even after several years full hydration may not have been reached. The variations depend mainly on W/C-ratio, curing conditions, access to water and the cement type.

Variations in the degree of hydration in a structure can occur due to sustained temperature gradients or whether the structures had started to dry at an early age. A variation in hydration would lead to variations in material properties such as moisture transport coefficient.

A concrete with a high W/C-ratio has a more rapid hydration process due to an easier access to water at the later stages. With a lower W/C ratio the cement paste gets denser with time and the hydration slows down. When the capillary pores are filled with hydration products further hydration is not possible. The lowest possible W/C-ratio that, with time, results in a full hydration can be calculated to 0.36 with free access to water and 0.42 if only the blending water is present (Hansen 1986).

There are several models that describe the hydration process of cement. The most famous and the one most used is probably the Powers Brownyard model (Powers and Brownyard 1947) in which the volume fractions of the different compositions can be calculated. The model may not be totally accurate, especially when concrete is studied. This is partly because the model was established on cement pastes.

The knowledge from Powers and Brownyard's work has been used in several studies to determine e.g. the degree of hydration or to estimate the amount of different components, e.g. (Midgley 1979; Bhatty and Reid 1985; Wong and Buenfeld 2009). One traditional way to determine the degree of hydration is to compare the total amount of non evaporable water and gel-water in the cement with the theoretical maximum amount of water that the cement binds at full hydration. The method is called loss on ignition (LOI).

One problem with the LOI is that the possible influence of aggregates or other components is hard to identify. For instance, aggregates that contain e.g. $CaCO_3$, limestone, will lose weight during the LOI due to the decarbonisation. If the amount of limestone is not known proper calculations can not be made.

When cement, or concrete, is exposed to elevated temperature the cement structure is decomposed. The decomposition appears in different steps in which different formations lose their gel-water and break. One way to describe the decomposition is to divide it into three steps, as presented in (El-Jazairi and Illston 1977).

- 105 °C to 440 °C. Dehydration of mainly C-S-H gel, among others
- 440 °C to 580 °C. Dehydroxylation of CH
- 580 °C to ca 1000 °C. Decarbonation of CaCo3

The temperature interval for dehydroxylation may vary somewhat, but that the decomposition of CH occurs around 450 °C is stated by several e.g. (El-Jazairi and Illston 1977; Midgley 1979; Bhatty and Reid 1985; Alarcon-Ruiz, Ehrlacher et al. 2005; Pane and Hansen 2005).

When a thermogravimetric analysis (TGA) is performed the temperature is plotted against the weight loss. During the TGA of cement paste or concrete the dehydroxylation can clearly be seen as a rapid increase in weight loss around 450 °C. The phenomenon is also clear when a differential thermal analysis DTA or differential scanning calorimetry DSC is performed. In both techniques it is possible to determine if there is an endodermic or exothermic reaction at different temperature intervals. Decomposition of CH, which is an endothermic reaction (Bhatty and Reid 1985), shows as a peek in the DTA or DSC measurements. This peek is located at the same temperature interval as seen in the TGA.

Using the knowledge from Powers and Brownyard together with TGA, DTA or DSC measurements it is possible to determine the amount of CH that a specific concrete should contain. This is done through recalculations of the weight loss in the dehydroxylation interval. The recalculation is made based on the hydration reactions for the four main clinker compositions. The reaction process may however be more complicated than this generalisation. However, this estimation would give an indication of the CH amount or at least it is possible to compare variations over the depth of a structure.

Simplified, the clinker reactions can be written as:

- $2C_3S + 6H \rightarrow C_3S_2H_3 + 3CH$

Parts: 1 0.24 0.75 0.49

- $2C_2S + 4H \rightarrow C_3S_2H_3 + CH$

Parts: 1 0.21 1 0.21

- $C3A + 6H \rightarrow C_3AH_6$

Parts: 1 0.40 1.40

- $C4AF + 2CH+10H \rightarrow C_3AH_6 + C_3FH_6$

Parts: 1 0.31 0.37 0.78 0.90

where parts stands for the mol of the different components.

From this the water that is bound by the hydration of the different clinker components but also the amount of CH that is formed can be summarised. It is therefore possible to derive the equation that describes the CH formation (kg. CH/kg. cement), see equation 9.

$$CH\ formation = \frac{C_3S}{100} * 0.49 + \frac{C_2S}{100} * 0.21 - \frac{C_4AF}{100} * 0.31 \qquad [9]$$

During the dehydroxation the CH decomposition can be written as:

$$Ca(OH)_2 \rightarrow CaO + H_2O$$

The molar mass of CH is 74.093 g/mole, CaO is 56.077 g/mole and water 18.015 g/mole. This gives a water to CH ratio of, 18.015/74.093 =0.243 kg/kg. By measuring the amount of water that is released during the dehydroxation of a cement paste it is then possible to calculate the amount of CH that it represents. In the next step the maximum amount of CH that can be formed can be calculated according to equation 9. The quotient between the theoretical and the calculated max is thus a value of the degree of hydration.

5.3.1 Measurements

The measurements of the amount of CH were made on nine test specimens. The specimens were taken from four depths, 40–50, 150–160 and 250–260 mm and sawed out from three concrete cylinders. All specimens were then placed in an oven at 105 °C for ca 4 hours. Usually the specimens should be left in the oven until steady state but due to the tight time schedule this was not possible. In an LOI measurement this would lead to an error due to an incorrect starting weight. However, because only the weight loss around 450 °C was measured in this setup the evaporable water that existed at the beginning had evaporated before the measurements.

Each specimen was crushed and graded, down to a size of ca 200 µm. The powder from each specimen was then placed in a diffusion tight plastic cup to limit the carbonisation process.

About 2 grams from each cup was placed in a TGA, LECO TGA 500. The measurements were made at Cementa Research in Slite, Sweden. One additional TG/DSC measurement was made with a Netzsch STA 449 C w. The sample was ca 40 mg and the TG and DSC measurements were made to verify that the endothermic peak that appears during the dehydroxation corresponds to the results from the TGA measurements, see figure 22.

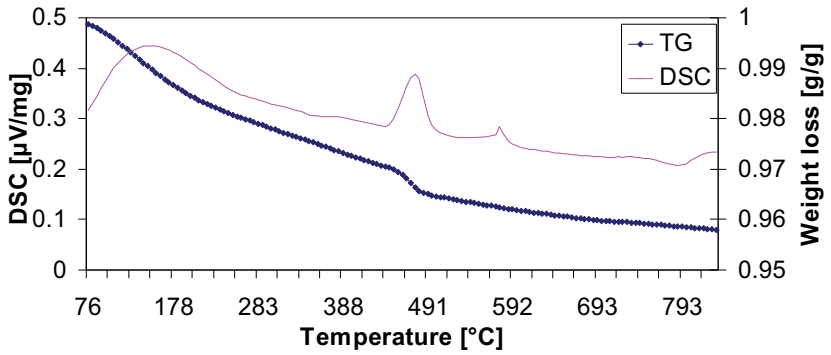

Figure 22. Measurements of TG and DSC of one sample from the inner cylinder wall at Ringhals 4. The X-axis shows the DSC results and the weight as a percentage of the initial

mass of the sample. The location of endothermic peak in the temperature interval 440 to ca 500 °C corresponds to the big drop observed in the TG measurements and is due to the dehydroxylation. The second peak, around 570 °C, is due to α-δ transformation of quartz in the aggregates (Schrefler, Khoury et al. 2002)

When the amount of CH in a concrete is determined the amount of cement that the specimen contains has to be determined. In this study this has been done by personnel at Vattenfall Research and Development AB by determining the amount of CaO by titration. The cement amount was measured on three samples from each plastic cup. The average value of the cement amount was then used to calculate the weight loss of water in relation to the amount of cement in the specimen.

In figure 23 the weight loss from 370 °C to 470 °C, in relation to the cement amount of all nine specimens that were tested in the TGA, is presented. The weight loss is in relation to the sample weight at 105 °C multiplied by the measured cement amount. From figure 23 the weight loss drop was determined for each sample. The interval from which data was gathered was one measuring point prior the drop and one after.

The main purpose of these measurements was to see any variations over the structure and therefore the actual CH amount or degree of hydration is not the primary objective of these measurements. The total dehydroxation occurs in a bigger interval than the sudden drop. However, the biggest and clearest part is represented by the drop. By only including this in the evaluation the total amount of CH is underestimated but at the same time the influence of other decompositions should be minimised.

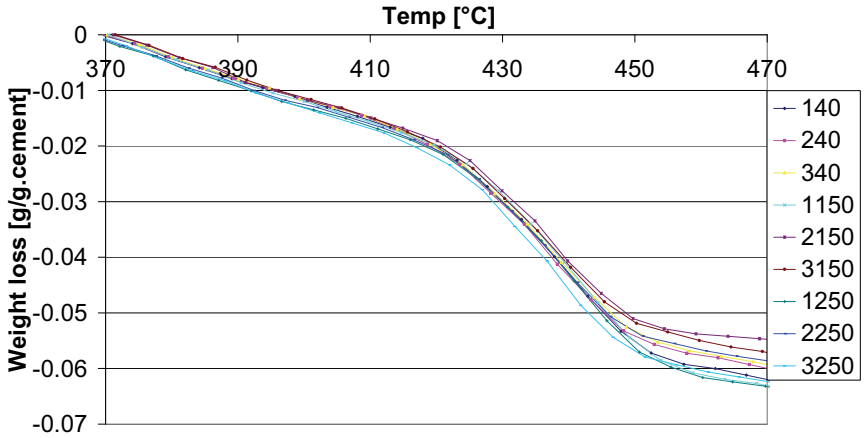

Figure 23. TGA measurement results of nine concrete samples from Ringhals 4. Three samples were taken from each depth and the weight loss is in relation to the cement amount at 105 °C.

In figure 24 the variation of hydration is plotted.

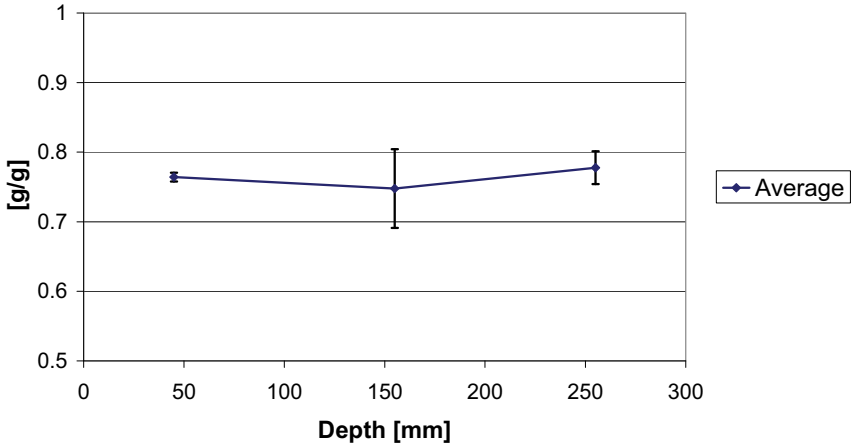

Figure 24. Results of variations in amount of CH in relation to theoretical max amount of CH in fully hydrated concrete specimens. Error bars represent the max and min value.

The results presented in figure 24 show no clear tendencies of variation of hydration over the depth of the inner cylinder wall at Ringhals 4. Assuming that all CH was decomposed in the measured interval gives a degree of hydration of ca 75 %. This value is lower than what can be expected on a 30 years old structure. The reason why the value is lower is due to the fact that the CH decomposes over a bigger temperature interval. According to (Taylor 1997) 98 % of the CH is decomposed in the temperature interval 370–580 °C. But as described earlier the main loss is seen both with the endothermic peak and the sudden drop of weight around 450 °C.

6 Monitoring campaigns

Within the scope of this project a measurement setup for monitoring of moisture and temperature in concrete was designed. The setup was used to study the climatic conditions inside nuclear RC during operation. Three monitoring campaigns were performed on different RCs in Sweden during the operation period 2012–2013. In the monitoring campaigns the actual moisture conditions and temperature within the containments and in the concrete structures were measured. The three reactors included in this first period were, Ringhals 1, Ringhals 4 and Forsmark 2. In a second period 2013–2014 one additional reactor will be monitored, Forsmark 3.

The setup was designed and tested both in an accuracy evaluation and during on site monitoring campaigns. The design of the setup is presented in paper 1, in which data from the first days of measurements at Ringhals 1 is also evaluated regarding tightness of the sealings. The results showed that the setup was valid for long term measurements but that tendencies of suspected leakage could be observed in measurements at shallow depth.

The results from the accuracy evaluation together with measurements from the first 150 days of monitoring at the three RC included in the period are presented in paper 2. In the accuracy evaluation both the tightness of the setup and the effects from temperature variations were considered. The measurements showed tendencies of suspected leakage on some of the test specimens but overall the setup performed with adequate results. The temperature dependence of the measurements followed the assumed theories, both in the accuracy evaluation and in the monitoring campaigns.

In this chapter further discussion regarding the tightness of the setup and stability of the measurement setup is presented. Measurement results from 150 days of the monitoring are presented and the results verify the conclusions made in the two papers.

Some rough estimates regarding moisture contribution due to the drying of the concrete structures are presented in paper 2. The calculations show that a substantial amount of water contributes to the climatic conditions in the RC during operation.

6.1 Method

The equipment used for the accuracy evaluation and monitoring campaigns consisted of RH and temperature measurement probes, HMP 110, from Vaisala OY. The probe measures RH with a Vaisala HUMICAP® 180R sensor and the temperature with Pt1000 RTD, 1/3 Class B IEC 751.

The data was collected with a logger, CR1000, and a multiplexer, AM25T, from Campbell Scientific Inc, for the measurements on Ringhals 1 and Ringhals 4 as well as the accuracy evaluation. For the measurements on Forsmark 2 an in-house system called “datascan” was used.

The control cubicles were located close to the existing through-connection in all RCs. Because of this the length of the cables varied and the longest cables used were ca 50 m. Communication out from the RC was performed with Westermo short distance modems, M14, for the campaigns at Ringhals 1 and 4 and with the in-house system at Forsmark 2.

6.1.1 Measurement setup

Measurements of RH in concrete required several sealings to minimise or eliminate leakage from/to the surroundings. Each measurement setup consisted of a casing pipe with four sets of sealings, see Figure 25.

The casing pipe had a diameter of 16 mm and was made of polypropylene plastic. The inner volume was sealed with a rubber o-ring, which also fixed the probe in the pipe. At the inner end of the casing pipe a rubber plug with a diameter of 17 mm was used to seal off the edges of the bottom and to separate the surface that was measured. The rubber plug was originally included in a measurement setup from Umigard. The sealants used to close the opening gap were SikaFlex AT-Connection for the accuracy evaluation, Ringhals 4 and Forsmark 2, and SikaFlex AT-Façade for Ringhals 1. SikaFlex AT-Connection was also used at all three RCs to seal the outer opening of the casing pipe. In the accuracy evaluation a rubber plug that consisted of two semi cylinders was used. It was replaced in the monitoring campaigns due to a suspected leakage due to the crevice.

A leaktightness test of the inner plug and the o-ring was made with adequate result using a bellow, that created a under pressure in the measuring volume before the accuracy evaluation. The tightness of the opening gap sealer was not tested in this study but SikaFlex AT-Connection has been used in previous studies with good results at Division of Building Materials, Faculty of Engineering, Lund University (Nilsson and Johansson 2009; Johansson). Both sealants, Connection and Façade, were a 1-component silane terminated polymers with similar properties according to the manufacturer.

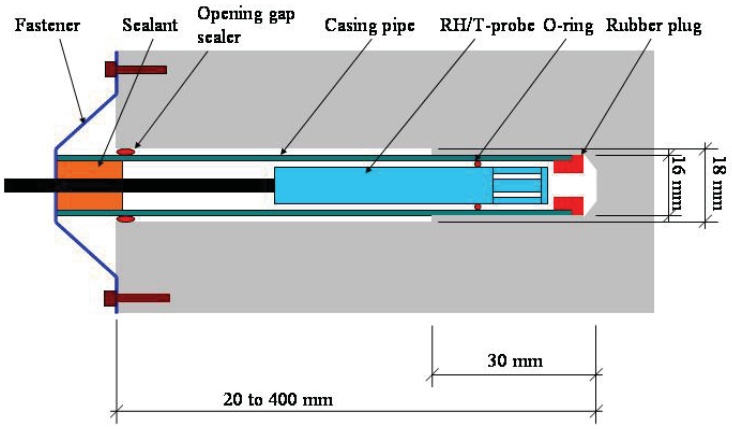

Figure 25. Measurement setup for temperature and RH measurement in concrete adapted for different depth, figure from Article 1. When measuring on a greater depth than 30 mm the outer part of the holes had an increased diameter to reduce the friction between the casing pipe and the concrete surface enabling the disassembly of the setup.

The holes were hammer-drilled and no water cooling was used, to avoid adding moisture to the concrete. The lack of cooling resulted in an increase of temperature in the concrete and possible drying. This is a problem if the measurements were made early after the installation, but in this case the equipment was installed and left in the holes over a long term. A hammer drill was used instead of diamond core drilling to minimise the risk of damaging reinforcement in case of accidental contact.

The holes that were deeper than 30 mm had a diameter of 18 mm on the outer section and the inner 30 mm had a diameter of 16 mm, se Figure 25. This was done to reduce the friction between the casing pipe and concrete. This was essential to allow dismantling after the monitoring campaigns. To eliminate the drill cuttings the holes were cleaned with a vacuum cleaner and a pipe cleaner. Left drill cuttings could affect the moisture fixation and thus the measured RH in the holes.

The measurement setup was installed in the hole and fixed with the opening gap sealant and a corrugated fastener. The fastener was used to press the casing pipe and inner plug against the bottom of the holes. The position of the fastener was fixed by using concrete screws, see Figure 26. The figure shows a picture of the setup when the casing pipe has been split in half.

Figure 26. Photograph of the measurement setup with the casing pipe split in half.

In order to decrease the temperature influence on the casing pipe and the probes, the ends of the casing pipe were insulated with 2 – 3 mm thick EPDM rubber sheeting. Possible effects of the rubber sheeting will be tested in a supplementary accuracy evaluation after the monitoring campaign is completed. The supplementary accuracy evaluation will also include temperature differences between the measured concrete surfaces and the measured temperature with the probes.

6.1.2 Calibration of measuring setups

All probes came with a calibration certificate performed at 20 °C from the manufacturer. The uncertainty of the equipment according to the manufacturer is presented in table 10.

Table 10. Uncertainty according to manufacturer, (VAISALA 2010)

	Range	Uncertainty -40 – 0 °C	Uncertainty 0 – +40 °C	Uncertainty +40 – +80 °C	Stability [2 years]
HUMICAP 180R	0–90 %RH	± 3.0 %RH	± 1.7 %RH	± 3.0 %RH	± 2.0 %RH
	90–100 %RH	± 4.0 %RH	± 2.5 %RH	± 4.0 %RH	± 2.0 %RH
Pt1000 1/3 Class B	-40–+80 °C	± 0.4 °C	± 0.2 °C	± 0.4 °C	

The probes were calibrated at Division of Building Materials, Faculty of Engineering, Lund University, with the calibration equipment, Thunder scientific corporation – 2500 Humidity generator. The calibration was made with the same cables and loggers that were used in the monitoring campaigns and the accuracy evaluation, except for the setup designed for Forsmark 2 where the probes and ca 2 m cable were calibrated together with the logger and multiplexer used for Ringhals 4.

The data from the probes to the logger were transmitted by analogue signals. The resistance of the cables to electric current may influence the results of measurements, especially when long cables are used. The data that was sent from the logger to the PC was digital and therefore these signals do not affect the measured results. Because of this only the cables from the probes to the logger and the logger itself were included in the calibration. The effects of cable length on the measurements will be further analysed at a later stage.

The calibration of the equipment that was used for the monitoring campaigns at Ringhals 1 and Forsmark 2 was made at two temperatures, 20 and 50 °C. At each temperature the RH was set to 50, 75, 85 and 95 %. The calibration for Ringhals 4 had one additional RH point at 30 %.

All probes will be calibrated after the measurements to detect whether the probes have drifted during the measuring period. If the measurements have drifted, a linear correction of the measurement will be made on the measurements. However, if the divergence can be identified as a distinct drop or increase during the measurements a correction from that event will be made.

With the probes both temperature and RH were measured in mV in the interval of 0–2500 mV. The temperature measuring range of the probes was -40 °C to +80 °C and the RH, 0–100 %. In tables and graphs the data has been converted into °C and %RH according to the calibrations. The temperature conversion was assumed to be linear to the measurement interval of the probes.

The conversion was done in two steps:

1. The measured RH, in mV, from one probe was first inserted in a second degree polynomial equation describing the calibration curve for RH at 20 °C. Thereafter the same value was inserted in the corresponding equation that describes the calibration at 50 °C.
2. A linear equation describing the temperature dependence of the RH was established from the calculations presented in the first point. The measured temperature from the probe was thereafter inserted in that equation which gave the RH at that temperature in accordance with the calibrations.

The main error from the conversion was that the temperature relation of the RH measurements was assumed linear. The effect was evaluated through the calibrations before the accuracy evaluation which was made at three temperatures, 20 °C, 35 °C and 50 °C, Figure 27.

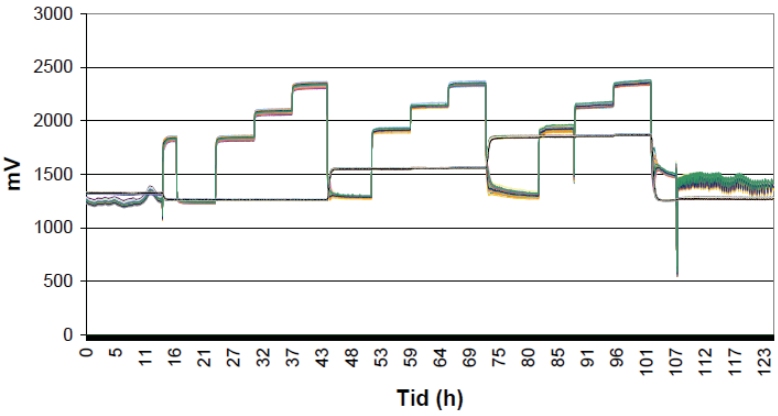

Figure 27. Calibration curve with the results in mV conducted at three temperatures, 20, 35 and 50 °C and at four RH, 50, 75, 85 and 95 %RH.

In figure 28 the arithmetic mean from all probes at the different temperatures and relative humidities is plotted as well as the linear relation between the measurements at 20 and 50 °C.

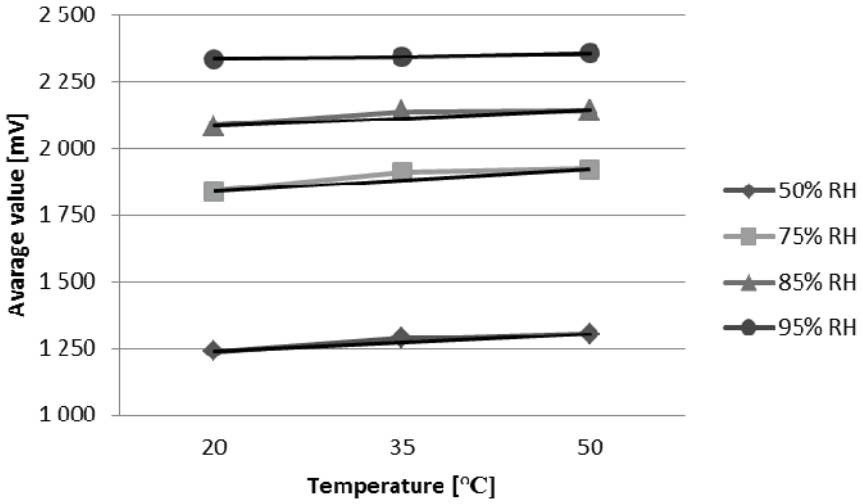

Figure 28. Measured temperature dependence of RH in relation to a linear relation between 20 and 50 °C, as used in the conversion.

The temperature relation is not linear, as seen in figure 28. It is however not possible to determine the biggest difference with only three temperatures because the exact shape of the dependence is not certain. Instead a comparison of the measured value at 35 °C and the calculated value using the linear function is shown in table 11. The temperature dependence is also compared with the standard deviation of the probes at the three temperatures.

In table 11 the standard deviation from the calibration on the probes used for the accuracy evaluation is shown. At each RH and temperature level the standard deviation of the average values from the last three hours during the calibrations is used. The results are not recalculated to RH, instead the variation in mV is compared with the measuring range given by the manufacturer, 0–2500 mV. However, one %-point in the measuring range corresponds to one %RH.

Table 11. Standard deviation from 25 probes at different temperatures and RH and the error from assuming linear temperature dependence in comparison with measured results at 35 °C

Temperature	50 %RH	75 %RH	85 %RH	95 %RH
20 °C	0.32 %-points	0.51 %-points	0.57 %-points	0.66 %-points
35 °C	0.33 %-points	0.50 %-points	0.40 %-points	0.45 %-points
50 °C	0.67 %-points	0.66 %-points	0.57 %-points	0.46 %-points
Diff. 35 °C	0.61 %-points	1.17 %-points	0.93 %-points	-0.15 %-points

The total scatters of the probes vary depending on RH and temperature. A clear correlation between increased temperature and RH with an increased scatter could be seen, except at high RH and temperatures where an increase lowers the scatter. The approximation that the temperature dependence is linear is fairly good; it will however increase the uncertainty at temperatures around 35 °C. Compared with the uncertainty given by the manufacturer, see table 10, the measured scatter is within the range of the probes.

6.2 Measurements Ringhals 1

The measurements at Ringhals 1 started in July 2012. The measurements were performed in six different zones within the containment, five of which in the upper dry-well and the last in the lower dry-well. The measurements were divided into four primary and two secondary measurements. In the primary measurements the RH was determined at four depths, and one additional probe was used to measure the boundary condition at the concrete surface. The secondary measurements were made at two depths in the concrete and one at the surface.

In table 12 the positions of the measurement zones are presented. +100 correspond to sea level and the angle is in relation to the primary steam pipe exit of the containment. The personnel sluice is located at ca 90 degrees. Furthermore, figure 29 presents a section of the containment with the vertical locations of the zones.

Table 12. Horizontal and vertical position of each zone at Ringhals 1. Four primary (P) and two secondary (S) measurements

Zone	Depth [mm]	+ Heights [m]	Distance from center [m]	Angle [°]
1P	Air: 20: 50: 150: 250	112	11.00	120
2P	Air: 20: 50: 150: 250	103	11.00	195
3P	20: 50: 150: 400	103	10.00	195
4P	Air: 20: 50: 150: 400	96	5.80	40
S1	Air: 50: 150	115	11.00	240
S2	Air: 50: 150	106	11.00	30

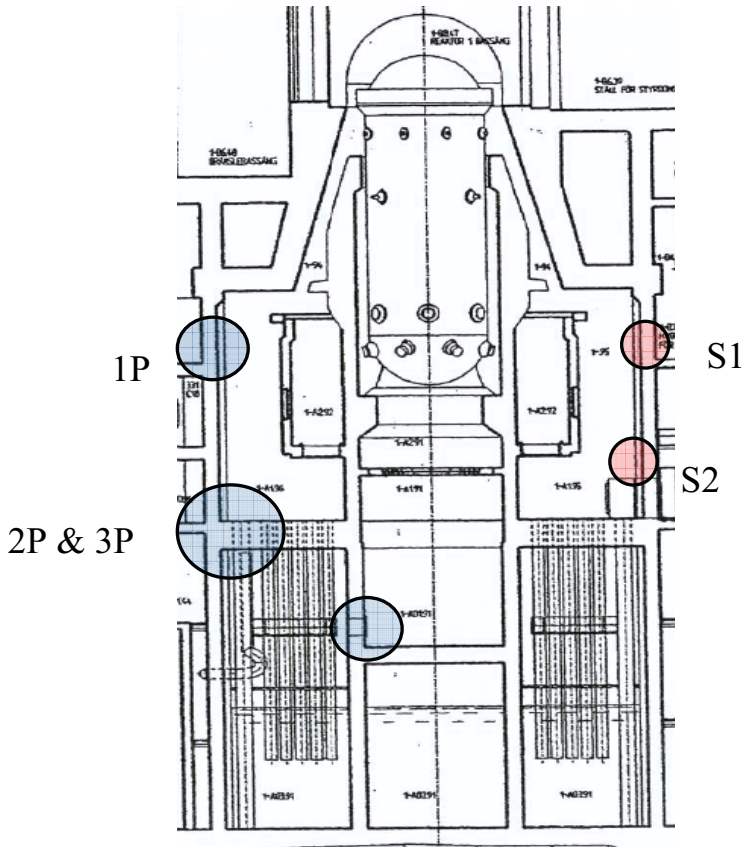

Figure 29. Section of Ringhals 1 with a schematic location of measurement zones. Zones 1P, 2P, S1 and S2 were located in the inner cylinder wall. 3P was located in the intermediate floor and 4P in the wall separating the lower dry-well and wet-well.

In total 25 RH/Temperature probes were used and 20 of these were mounted in the concrete. Two primary measurements 1P and 2P, and the two secondary measurements were made in the inner cylinder wall. Primary zone 3 was made in the intermediate floor between the wet-well and upper dry-well. Primary zone 4 was in the concrete wall separating the lower dry-well and wet-well.

The data was collected with the logger and Multiplexer from Campbell scientific. The Equipment was placed in an existing control cubicle in direct connection to the main personnel sluice. Data was collected every 20th minute and a mean value every second hour. Communication between the logger and a PC was established through existing cables using a short distance modem, Westermo 14M, with the PC placed outside of the containment.

6.3 Measurements Forsmark 2

Measurements at Forsmark 2 started in June 2012. As for the measurements on Ringhals 1 the monitoring campaign was divided into four primary and two secondary measurements. The secondary measurements were made at two depths in the concrete and one measuring the climate at the concrete surface. The primary measurements were made at three or four depths in the concrete and one additional measuring point at the concrete surface for the boundary conditions. The steam pipes were located at 0 degrees in the upper dry-well and the personnel sluice at 90 degrees.

In table 13 the positions of the zones is presented, the table also shows the measuring depth.

Table 13. Horizontal and vertical position of each zone at Forsmark 2. Four primary (P) and two secondary (S) measurements

Zone	Depth [mm]	+ Heights [m]	Distance from centre [m]	Angle [°]
1P	Air: 20: 50: 120: 190	131	11.00	270
2P	Air: 20: 50: 120: 190	124.5	11.00	60
3P	Air: 20: 50: 120: 250	114	5.20	260
4P	Air: 20: 50: 120	102	5.20	10
S1	Air: 50: 120	131	11.00	110
S2	Air: 50: 120	124.5	11.00	190

Two of the zones were located in the inner cylinder wall in the upper dry-well, the other two were located in the cylinder wall that separates the lower dry-well and wet-well. The

two secondary zones were both located in the upper dry-well. In figure 30 a schematic illustration of the zones and their locations in height is presented. In total 25 probes were installed and 19 of these were mounted in the concrete.

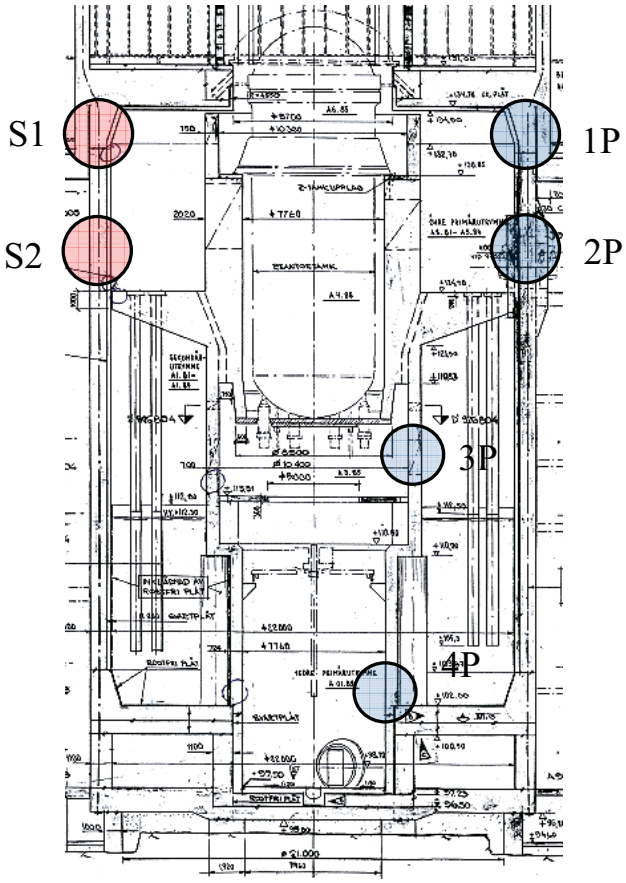

Figure 30. Section of Forsmark 2 with a schematic location of measurement zones. Zone 1P, 2P, S1 and S2 was located in the inner cylinder wall, 3P and 4P in the wall separating the lower dry-well and wet-well.

The data on Forsmark 2 was not collected with the same equipment as for Ringhals 1 and 4. Instead a built-in system, datascan, was used. Because of this the entire measurement system was not calibrated prior to the measurements, instead the measurement probes and ca two meters of wiring were calibrated together with the logger and multiplexer used in Ringhals 1. The data was collected every 20 minutes.

6.4 Measurements Ringhals 4

The measurements on Ringhals 4 started in August 2012. During the first 14 days the reactor was shut down and first started in September. On Ringhals 4 no secondary measurements were made due to the symmetry and size of the containment. The primary measurements were made in five zones. All five zones were within the same quadrant between 90 and 180 degrees. The personnel sluice is located at zero degree and the steam pipes at ca 270 degrees. The primary measurements were made at three or four depths in the concrete and one additional measuring point at the concrete surface measuring the boundary conditions.

In table 14 the positions of the zones are presented and figure 31 shows a section of the containment where the position in height of the zones is illustrated.

Table. 14. Horizontal and vertical position of each zone at Ringhals 4. Five primary (P) measurements

Zone	Depth [mm]	+ Heights [m]	Distance from centre [m]	Angle [°]
1P	Air: 20: 50: 150: 240	134.5	11.00	90
2P	Air: 20: 50: 150: 240	115	11.00	130
3P	Air: 20: 50: 150: 240	95	10.00	140
4P	Air: 20: 50: 150	107	5.80	180
5P	Air: 20: 50: 150: 400	93	11.00	150

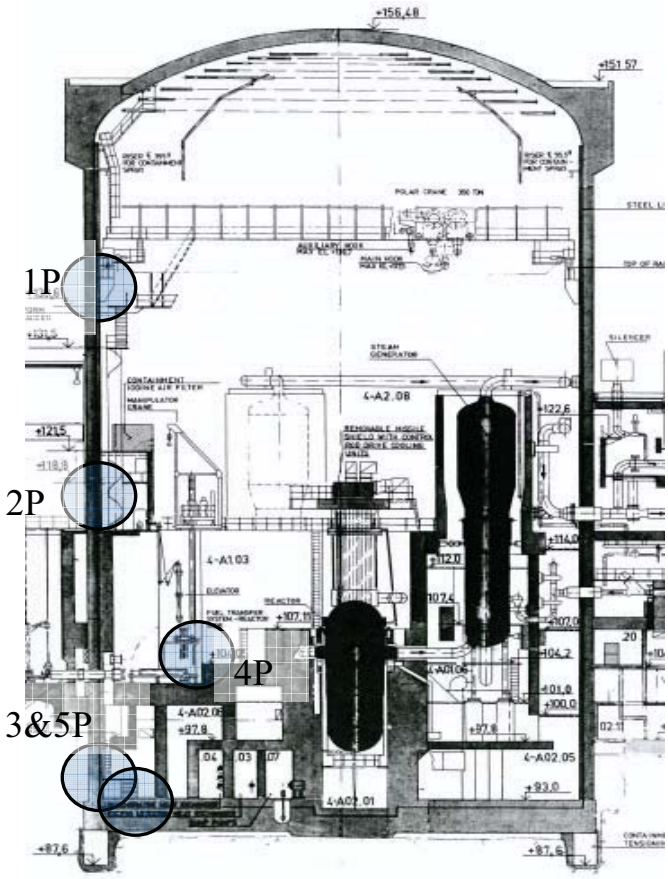

Figure 31. Section of Ringhals 4 with a schematic location of measurement zones. Zones 1P, 2P and 3P were located in the inner cylinder wall, 4P in the basin wall and 5P in the bottom slab.

In total 24 measuring probes were used, 19 of these were mounted in the concrete and the remainder measured the boundary condition at the concrete surface. Zones one, two and three were in the inner cylinder wall. Zone four was located at the fuel-pool wall and zone five in the bottom slab.

The data was collected with a logger and multiplexer from Campbell and mounted in a control cubicle that was mounted at +115 120°. Data was collected every 20 minutes and as a mean value of every second hour. From the logger data was sent to the control room using existing cables. However, after installation a communication problem occurred between the logger and PC preventing the data to be collected as scheduled.

6.5 Results

The results from the monitoring campaigns and the accuracy evaluation of the setup are presented in papers 1 and 2. Some of the concluding remarks together with further discussions are presented in this dissertation.

6.5.1 Accuracy evaluation

In paper 2 an accuracy evaluation of the measurement setup is presented. In the accuracy evaluation the test specimens were exposed to varying temperature and RH. The evaluation was dividend into two parts where the first had a cyclic RH and the second a cyclic temperature.

The accuracy evaluation was made on ten concrete specimens with different, not specified, compositions. All surfaces, except the surface on which the setups were mounted, were sealed with aluminium tape. The measurements were made at 20 and 50 mm depth, with five setups on each depth.

The first part of the evaluation showed that with a constant temperature, 20 °C, and a varying RH the internal RH in the concrete at 20 mm depth varied due to changes in the surroundings. These variations were, however, delayed by several hours. After completed cycles, the specimens were exposed to a constant low RH for another 600 h. During this period the RH in the concrete decreased steadily.

The measurements at 50 mm depth showed only small variations of RH during the first ca 600 h, when the specimens were exposed to cyclical RH. When the RH was kept on a constant low level, only a small tendency of decreasing RH was observed.

The variations and the decreasing trend observed at 20 mm depth may be leakage over the sealings but it may also be moisture transport through e.g. cracks in the concrete. This will be furthered analysed in an upcoming complementary accuracy evaluation.

The second part of the accuracy evaluation consisted of exposure to cyclic temperature at a constant vapour content. The results of the measurements at 50 mm depth showed clear evidence that the RH increased when the temperature was raised and decreased when the temperature was lowered. This result was expected due to the temperature dependence of RH as presented in section 4.1.

At 50 mm depth the cyclic temperature was repeated twice with similar results, indicating the repeatability of the measurements. At 20 mm the measurements had a down going trend during the whole test. This was, however, expected due to the observed decrease during the test at constant temperature.

The overall conclusion from the accuracy evaluation was that the setup was stable when measuring at 50 mm depth but not at 20 mm depth. When these results were compared with the monitoring campaign at e.g. Ringhals 1 it was seen that some of the measurements at 20 mm depth were stable and followed the theory regarding temperature influence. These results indicated that the setup was also valid at 20 mm depth but that extra attention has to be considered when installing the setup.

Two main reasons why the measurements in the accuracy evaluation at 20 mm depth did not correspond to the results observed in the monitoring campaign might be the influence of the epoxy coating in the RC and the concrete qualities. The epoxy coating and a tighter concrete lowers the possible moisture flux from the holes through the concrete.

6.5.2 Monitoring campaigns

The measurements in the three monitoring campaigns have been conducted for different lengths of time. The measurements at Ringhals 1 and Forsmark 2 both started during June 2012 and Ringhals 4 in August 2012.

In December 2012 the power to the logger at Ringhals 1 was lost. The logger was restarted in January 2013. Data presented here is between the 8th of June and the 15th of December 2012.

The data presented from Forsmark 2 is from the 7th of June to the 13th of February 2013. The monitoring campaign at Ringhals 4 started on the 31st of August 2012 and data was collected until the 31st of January 2013.

These measuring intervals gave 144 days of data from Ringhals 4, 188 from Ringhals 1 and 250 from Forsmark 2. The equipment was installed during the outages of the plants and the reactor was started after 14 days at Ringhals 1, 12 days at Forsmark 2 and 15 days at Ringhals 4. Measurements will proceed to the outages in 2013.

In figures 32 to 48 the results from the three campaigns are presented. P stands for primary measurements and S for Secondary. The data presented from Ringhals 1 and 4 was the mean value from every second hour. The data presented from Forsmark 2 was the value from every 20 minutes.

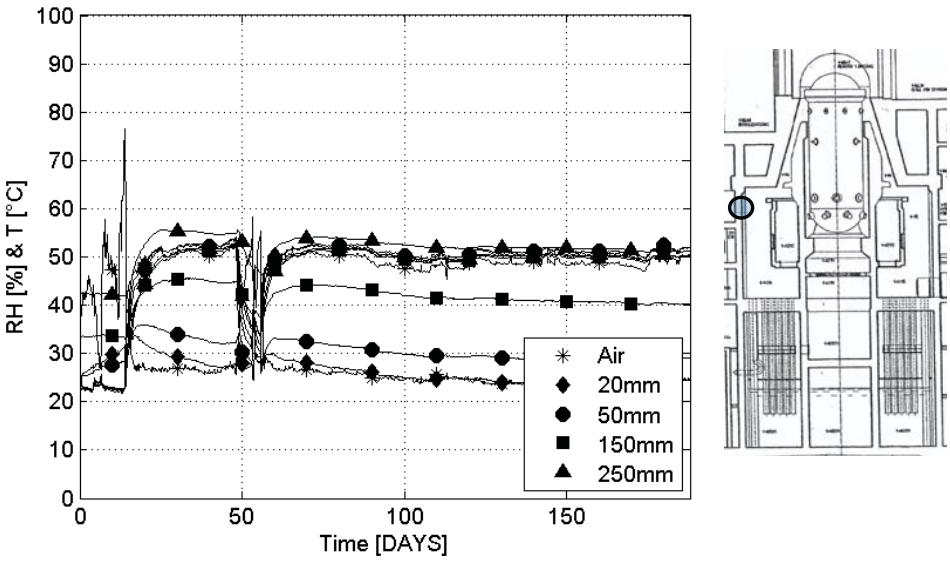

Figure 32. Measured RH and temperature in the inner cylinder wall (1P) at Ringhals 1, +112 120°. Measurements were conducted at four depths in the concrete and one additional measuring point (Air) ca 5 cm from the concrete surface. Symbols at 10, 30, 50 etc. represent RH and 20, 40, 60 etc. temperature

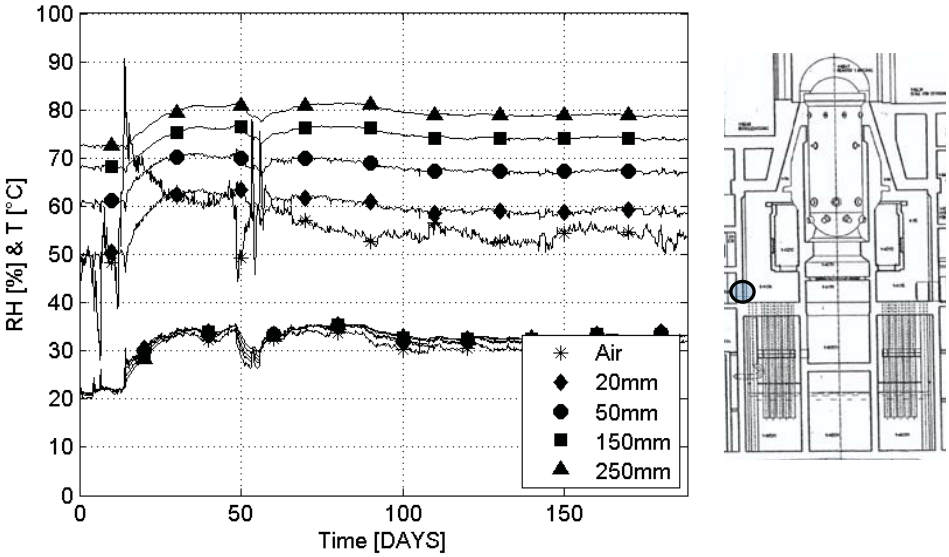

Figure 33. Measured RH and temperature in the inner cylinder wall (2P) at Ringhals 1, +103 195°. Measurements were conducted at four depths in the concrete and one additional measuring point (Air) ca 5 cm from the concrete surface. Symbols at 10, 30, 50 etc. represent RH and 20, 40, 60 etc. temperature

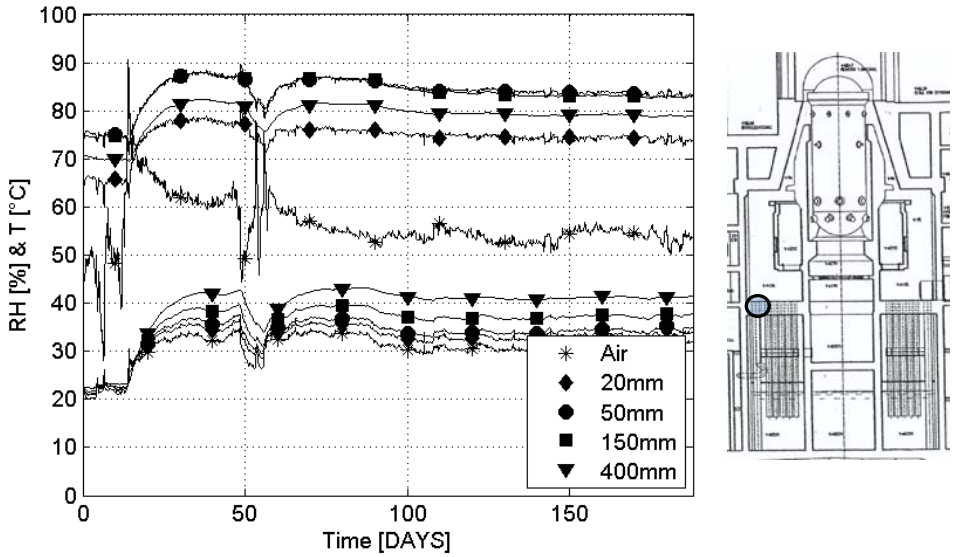

Figure 34. Measured RH and temperature in the intermediate floor (3P) at Ringhals 1, +103 195°. Measurements were conducted at four depths in the concrete and the same measurement from the concrete surface in 2P (Air) was used as boundary condition. Symbols at 10, 30, 50 etc. represent RH and 20, 40, 60 etc. temperature

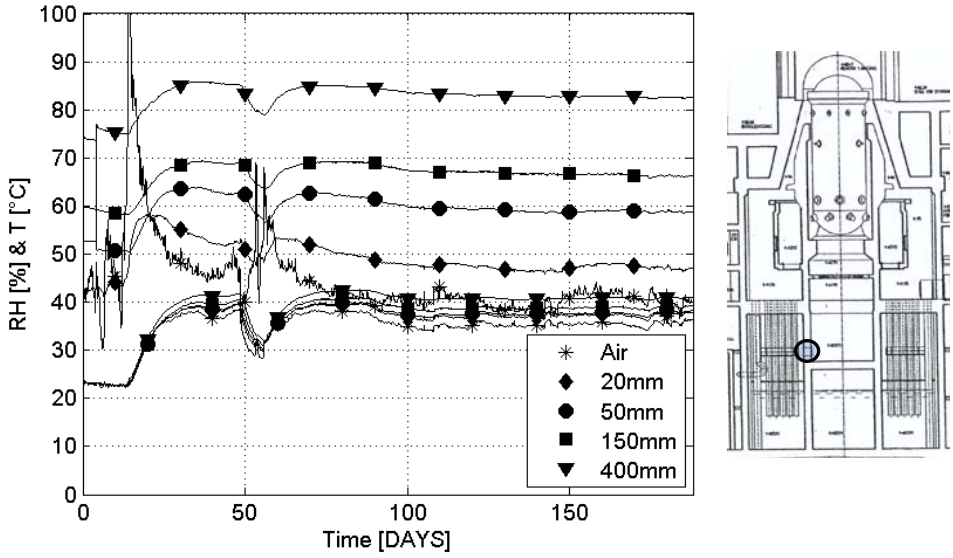

Figure 35. Measured RH and temperature in an internal wall (4P) at Ringhals 1, +96 40°. Measurements were conducted at four depths in the concrete and one additional measuring point (Air) ca 5 cm from the concrete surface. Symbols at 10, 30, 50 etc. represent RH and 20, 40, 60 etc. temperature

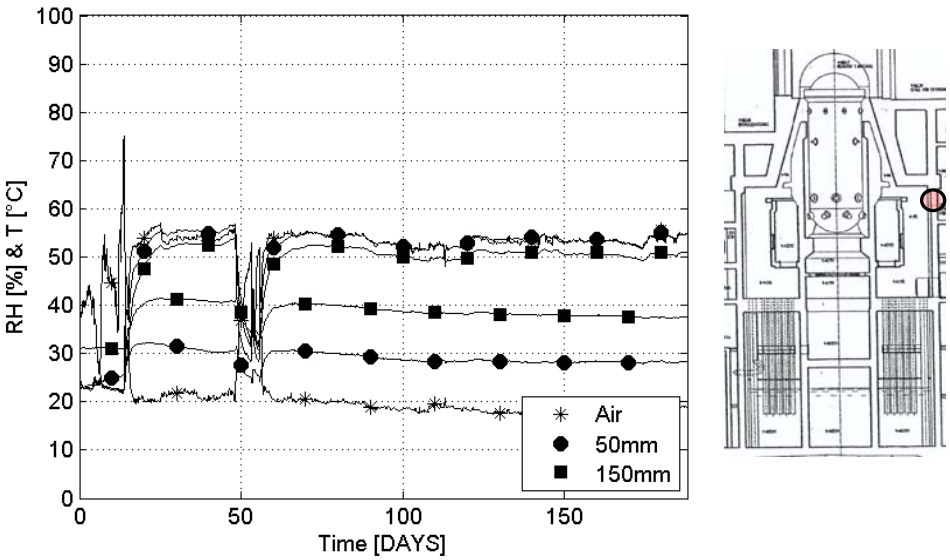

Figure 36. Measured RH and temperature in the inner cylinder wall (S1) at Ringhals 1, +115 240°. Measurements were conducted at two depths in the concrete and one additional measuring point (Air) ca 5 cm from the concrete surface. Symbols at 10, 30, 50 etc. represent RH and 20, 40, 60 etc. temperature

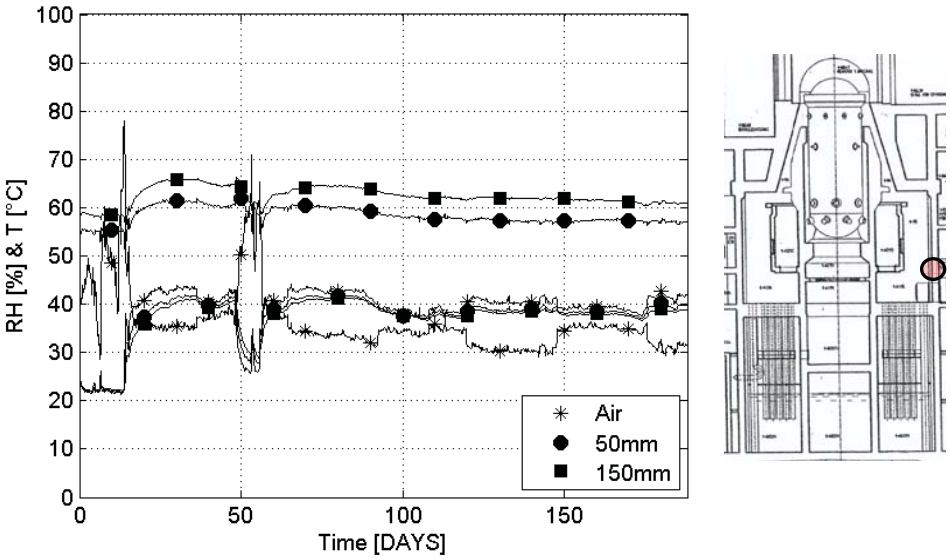

Figure 37. Measured RH and temperature in the inner cylinder wall (S2) at Ringhals 1, +106 30°. Measurements were conducted at two depths in the concrete and one additional measuring point (Air) ca 5 cm from the concrete surface. Symbols at 10, 30, 50 etc. represent RH and 20, 40, 60 etc. temperature

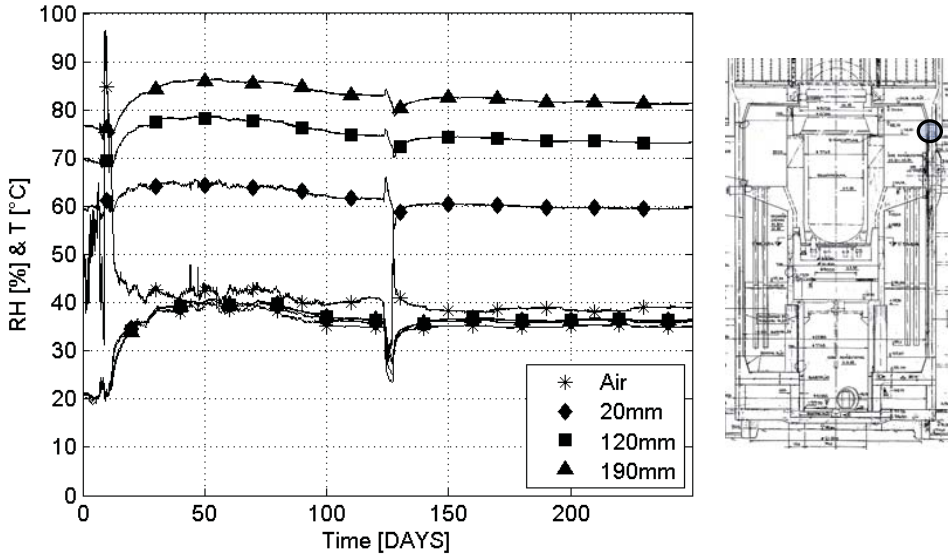

Figure 38. Measured RH and temperature in the inner cylinder wall (1P) at Forsmark 2, +131 270°. Measurements were conducted at three depths in the concrete and one additional measuring point (Air) ca 5 cm from the concrete surface. Symbols at 10, 30, 50 etc. represent RH and 20, 40, 60 etc. temperature

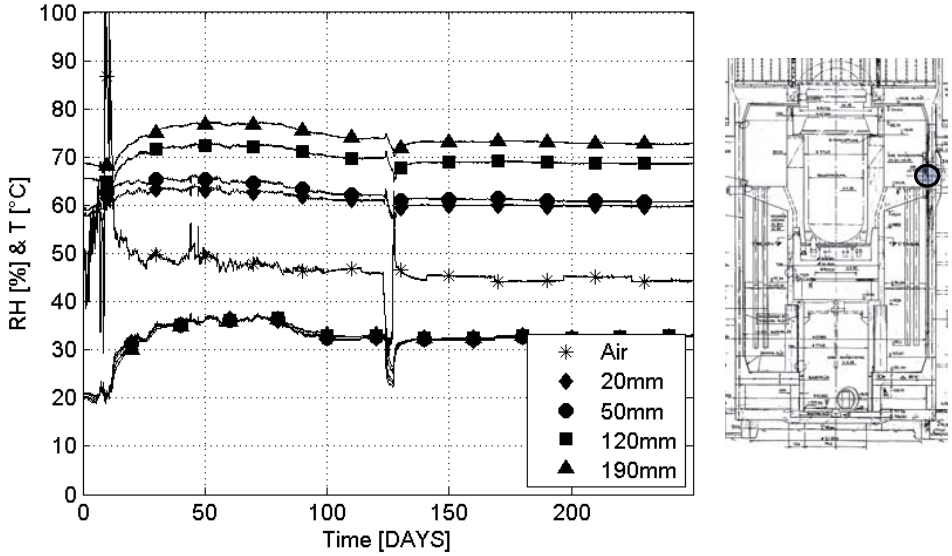

Figure 39. Measured RH and temperature in the inner cylinder wall (2P) at Forsmark 2, +124.5 60°. Measurements were conducted at four depths in the concrete and one additional measuring point (Air) ca 5 cm from the concrete surface. Symbols at 10, 30, 50 etc. represent RH and 20, 40, 60 etc. temperature

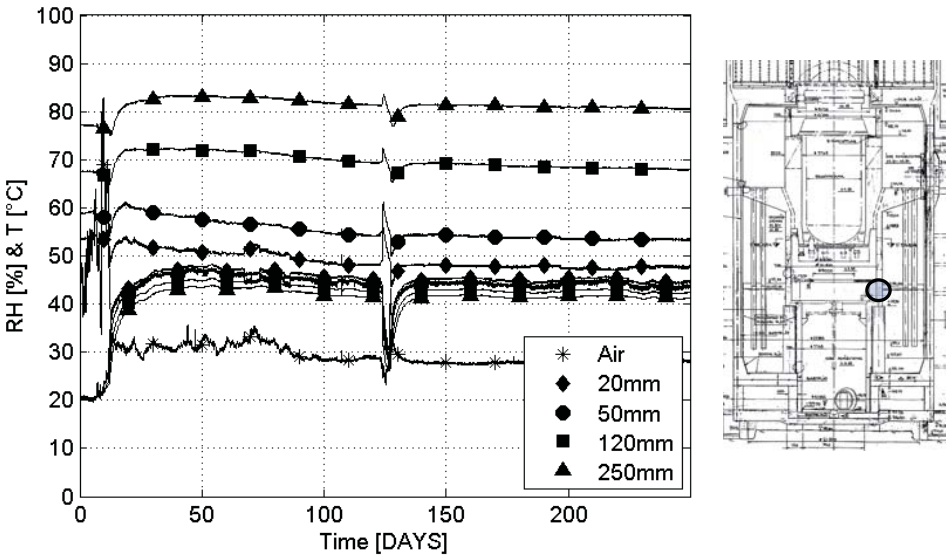

Figure 40. Measured RH and temperature in an inner wall (3P) at Forsmark 2, +114 260°. Measurements were conducted at four depths in the concrete and one additional measuring point (Air) ca 5 cm from the concrete surface. Symbols at 10, 30, 50 etc. represent RH and 20, 40, 60 etc. temperature

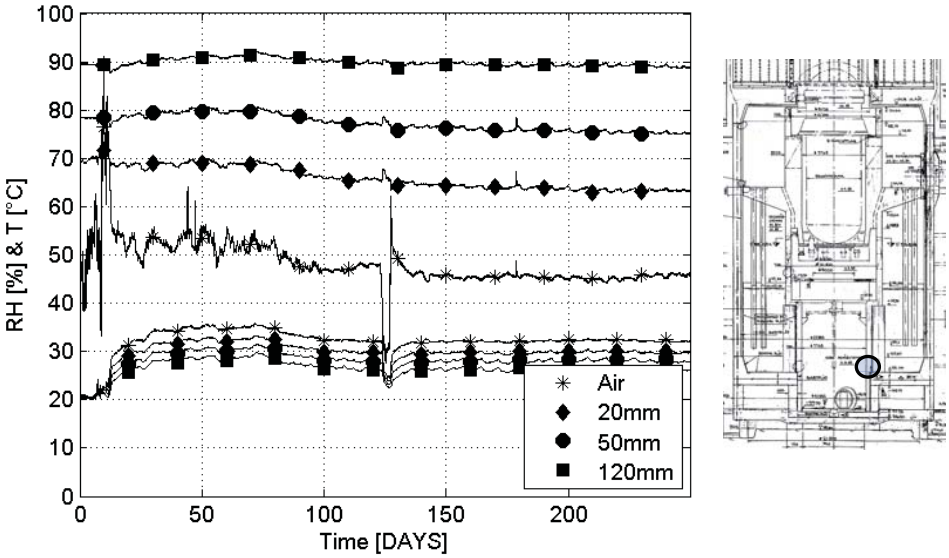

Figure 41. Measured RH and temperature in an inner wall (4P) at Forsmark 2 +102 10°. Measurements were conducted at three depths in the concrete and one additional measuring point (Air) ca 5 cm from the concrete surface. Symbols at 10, 30, 50 etc. represent RH and 20, 40, 60 etc. temperature

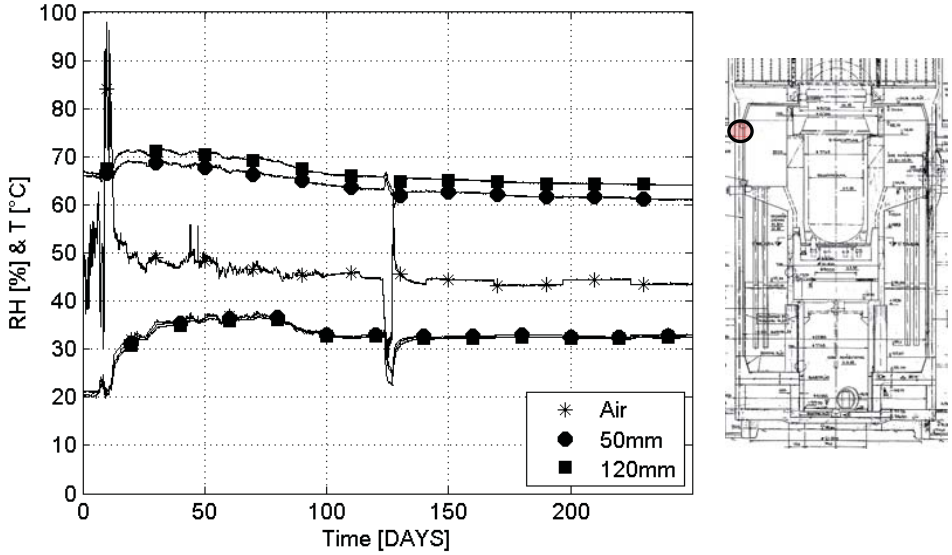

Figure 42. Measured RH and temperature in the inner cylinder wall (S1) at Forsmark 2, +131 10°. Measurements were conducted at two depths in the concrete and one additional measuring point (Air) ca 5 cm from the concrete surface. Symbols at 10, 30, 50 etc. represent RH and 20, 40, 60 etc. temperature

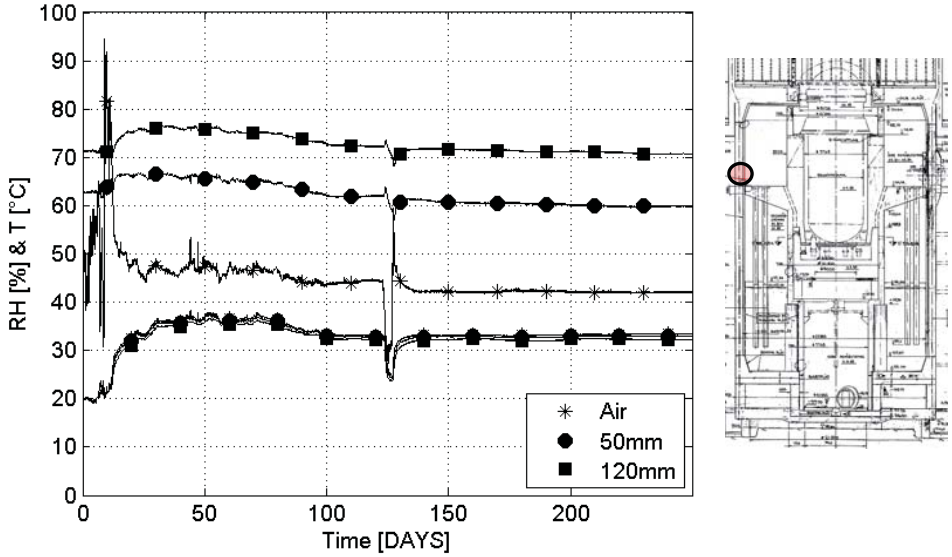

Figure 43. Measured RH and temperature in the inner cylinder wall (S2) at Forsmark 2, +124.5 190°. Measurements were conducted at two depths in the concrete and one additional measuring point (Air) ca 5 cm from the concrete surface. Symbols at 10, 30, 50 etc. represent RH and 20, 40, 60 etc. temperature

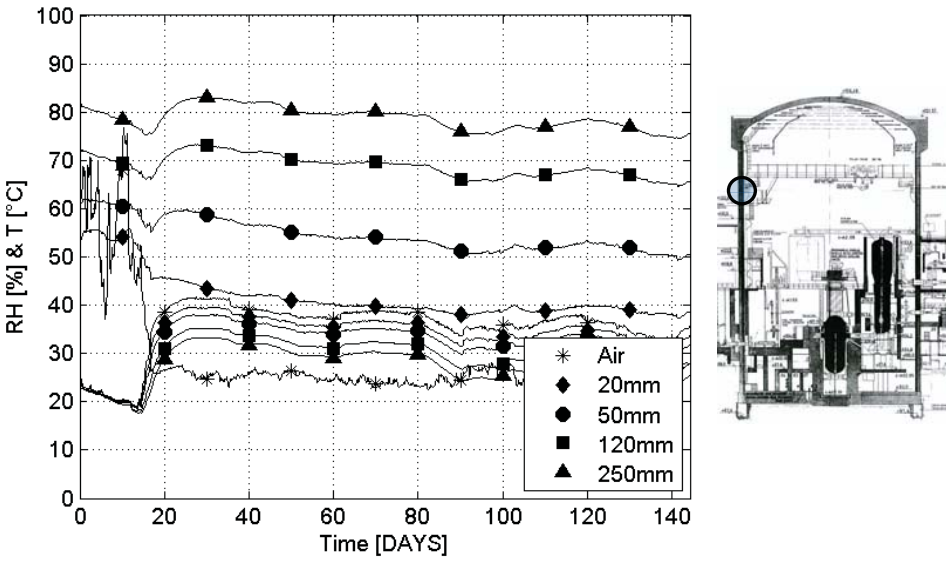

Figure 44. Measured RH and temperature in the inner cylinder wall (1P) at Ringhals 4 +134.5 90°. Measurements were conducted at four depths in the concrete and one additional measuring point (Air) ca 5 cm from the concrete surface. Symbols at 10, 30, 50 etc. represent RH and 20, 40, 60 etc. temperature

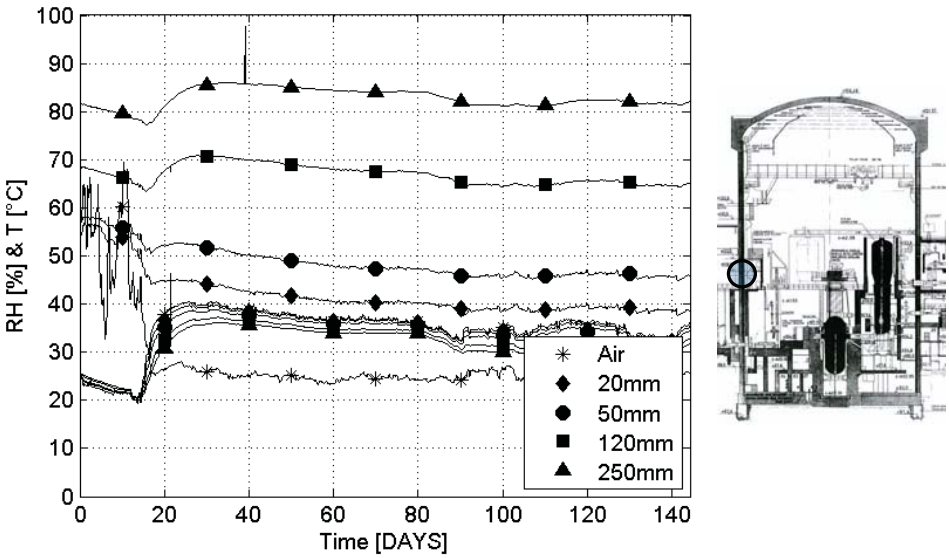

Figure 45. Measured RH and temperature in the inner cylinder wall (2P) at Ringhals 4, +115 130°. Measurements were conducted at four depths in the concrete and one additional measuring point (Air) ca 5 cm from the concrete surface. Symbols at 10, 30, 50 etc. represent RH and 20, 40, 60 etc. temperature

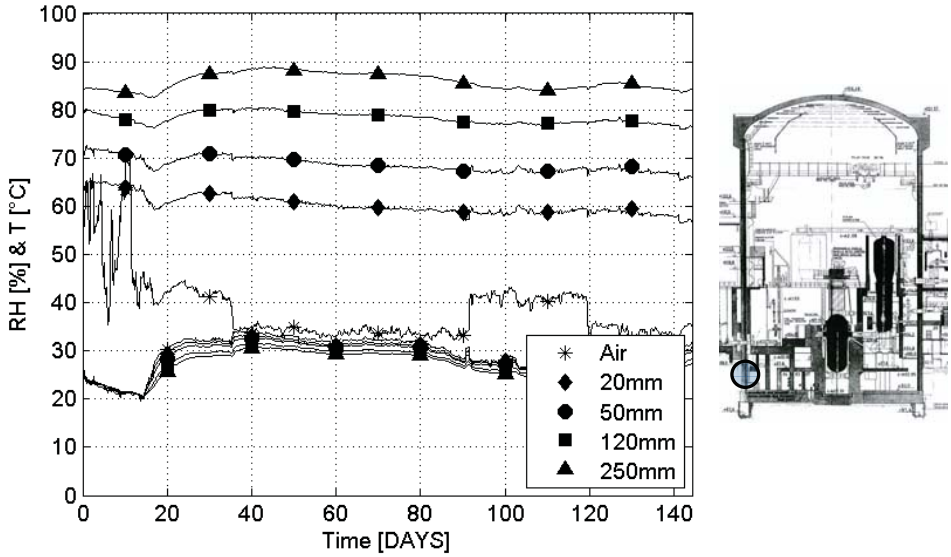

Figure 46. Measured RH and temperature in the inner cylinder wall (3P) at Ringhals 4, +95 140°. Measurements were conducted at four depths in the concrete and one additional measuring point (Air) ca 5 cm from the concrete surface. Symbols at 10, 30, 50 etc. represent RH and 20, 40, 60 etc. temperature

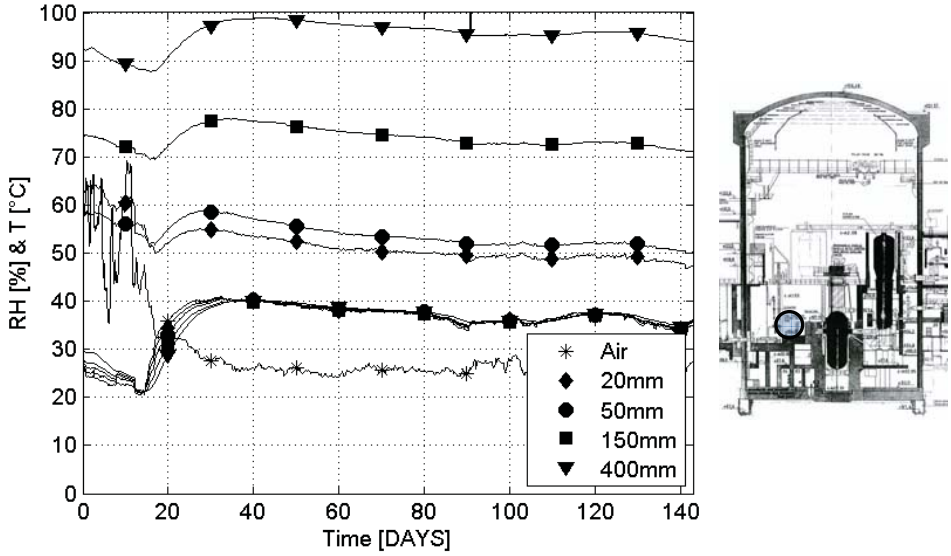

Figure 47. Measured RH and temperature in an internal structure (4P) at Ringhals 4, +107 180°. Measurements were conducted at four depths in the concrete and one additional measuring point (Air) ca 5 cm from the concrete surface. Symbols at 10, 30, 50 etc. represent RH and 20, 40, 60 etc. temperature

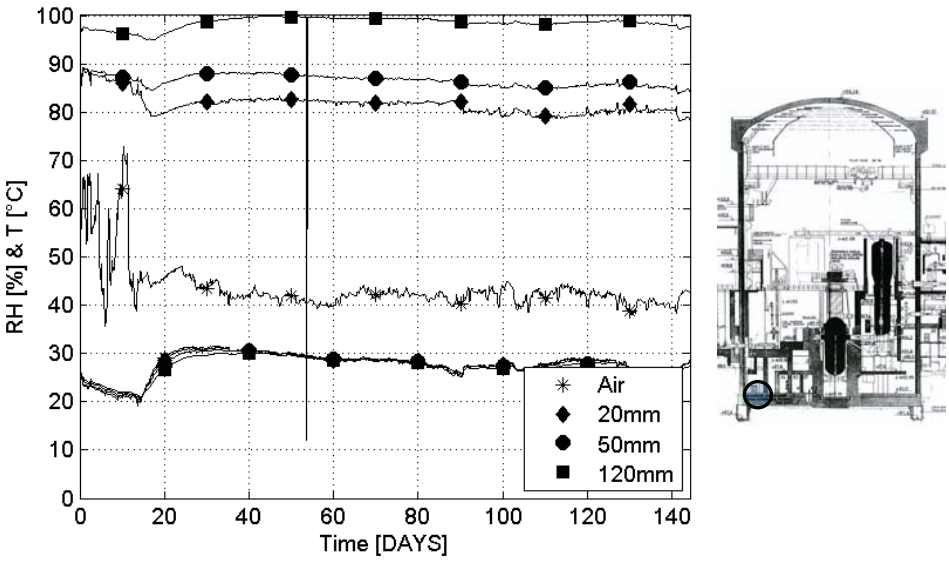

Figure 48. Measured RH and temperature in the bottom slab (5P) at Ringhals 4, +93 150°. Measurements were conducted at three depths in the concrete and one additional measuring point (Air) ca 5 cm from the concrete surface. Symbols at 10, 30, 50 etc. represent RH and 20, 40, 60 etc. temperature

In paper 1 the measurement setup was evaluated based on the first 80 days of measurements at Ringhals 1. It was concluded that the measurements showed clear evidence that the setup worked in long term measurements but that tendencies of what could be leakage was observed in shallow depth measurements.

As stated in the paper, the setups used for measurements at 20 and 50 mm depth were those that showed clearest tendencies of possible leakage. The results from Ringhals 1, Ringhals 4 and Forsmark 2 presented in this dissertation show, however, that after a long term all measurements, except for one, stabilise in a condition different from that in the containment.

The down going trend observed in almost all zones the first ca 100 days can instead be correlated with the temperature decrease. Directly after the reactor restarted the highest temperatures in all the containments were reached and thereafter the temperature was slowly lowered and finally stabilised. The decrease and stabilisation of RH in the concrete corresponds well for all measurement with this temperature variation.

Only one setup showed clear indication of leakage. That setup was mentioned in paper 1, zone 1P 20 mm depth Ringhals 1, as potential leakage see figure 32. Figure 49 shows the measured RH and temperature at 20 mm depth together with the boundary conditions for 1P at Ringhals 1.

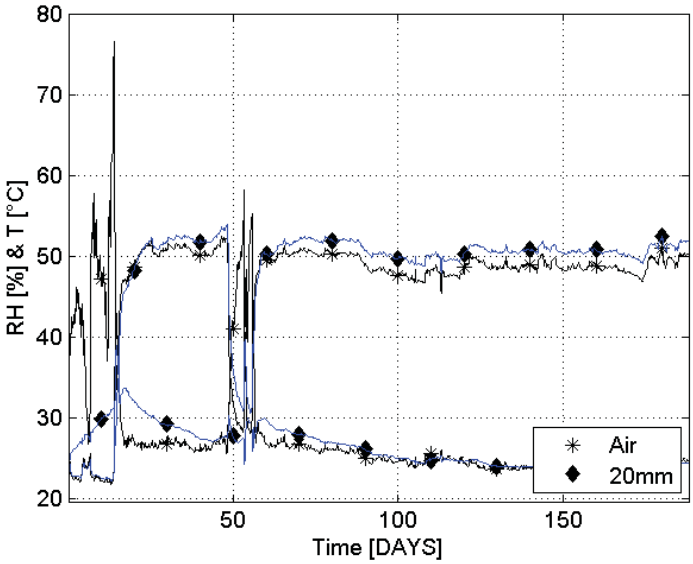

Figure 49. Measured RH and Temperature at 20 mm depth and at the concrete surface in zone 1P at Ringhals 1, +112 120°. The symbols at 20, 40, 60 etc. represent the temperature and at 10, 3o, 50 etc. the RH.

During the first ca 15 days the RH at 20 mm depth drastically increases from ca 25 %RH to a maximum of ca 35 %RH. When the reactor was started the RH in the containment (Air) decreased from 40-50 %RH down to ca 25 %RH and the temperature increased from ca 20 °C to 50 °C. At this stage the RH at 20 mm depth started to decrease and within time it reached the same level as measured outside the concrete. This is a clear indication that leakage can be the reason.

However, the start point of the measurements was within a couple of %-points from the RH obtained after ca 150 days. The first measurements were made within a day after the equipment had been installed. Even though there might have been leakage, the first measurements should not be affected more than a couple of %-points before the first data point was gathered. This indicated that the concrete close to the surface may already have reached equilibrium with the conditions in the RC during operation.

The measurements in the same zone at 50 mm depth showed similar tendency during the first period of time, with an initial increase of RH the first 15 days. However, after the reactor restarted the RH decreased somewhat but as for measurements in other zones the RH was stabilised when the temperature was stabilised.

Similar results as presented previously were obtained at 50 mm depth from the secondary measurements (S1), see figure 36. The zone was located in a similar location as 1P at Ringhals 1. The combined results from both zones strongly indicate that the drying of the concrete surface high up in the inner cylinder wall at Ringhals 1 was close to equilibrium

with the surroundings. During operation at 50 °C the RH was ca 30 % and during the outage ca 25 %RH.

At 150 mm depth and deeper the moisture level was higher but far from the initial conditions. The concrete high up in the upper dry-well at Ringhals 1 was the most dry compared with all other zones in all three monitoring campaigns. This area was also that with the overall highest temperatures, ca 50–55 °C. The temperature was still below the maximum allowed temperature in concrete according to the regulations, 66 °C, but the higher temperature has most likely resulted in the lower moisture content in comparison with the other zones.

The temperatures obtained in the other zones both at Ringhals 1 and from the other monitoring campaigns were usually around 30–40 °C, with some exceptions.

The RH close to the surfaces in the other zones was usually between 40–60 %RH. The measured RHs correspond fairly well with the boundary conditions. A low RH and high temperature usually resulted in a low RH in the concrete due to a bigger moisture transport potential and vice versa.

The temperature measurements in the setup were however one critical area. The temperature that was measured with the probes can be seen as an average temperature in the cavity. The surface temperature of the concrete in the cavity may thus be lower or higher than the measured value.

As presented in (Johansson and Nilsson 2007), the difference between the temperature on the concrete surface and the probe with a similar measuring setup at 30 mm depth was evaluated. In their test setup they mounted one additional thermocouple on the bottom surface of there holes in addition to their RH/Temperature probes. Their results showed that the difference in temperature between the thermocouple and their RH/Temperature probe was around 1–1.5 °C and that the temperature measured by the probe was lower then the thermocouple. A higher temperature in the concrete in relation to the probes would give a lower RH by some %-points.

In their study (Johansson and Nilsson 2007) the outer cylinder wall on Ringhals 4 was studied and their results indicated that the temperature in the concrete was higher then the surroundings. Inside the RCs the relation could however be assumed reversed, with a lower temperature in the concrete. Therefore the measured RH in this study may be slightly higher than measured. This has however not been investigated at this point but will be a part of an additional evaluation study of the test setup.

The setup, itself, may also have an influence on the temperature measurements. Even though the casing pipe was made of plastic with low thermal conductivity, a supplementary insulation and that no air could circulate inside, there might be a temperature exchange between the surroundings and the equipment through the setup. This may especially be a problem with the measurements at 20 and 50 mm depth because most of the casing pipe was outside the hole.

In most of the measurements there were no distinctive temperature gradients over the structure when the measurements had stabilised. However during the first days after the reactors were started a temperature gradient could be observed on several setups. Figure 50 shows the temperature measured in zone 4 during the first 20 days after the reactor in Ringhals 4 restarted.

The measurements show that the temperature increase was significantly slower at greater depth. After ca 20 days the temperature in the whole structure was constant. This indicates that the influence of the surroundings on the setups was fairly small especially at 50 mm or greater depth. As a next step in the evaluation of the measurement setup the temperature influence will be further analysed.

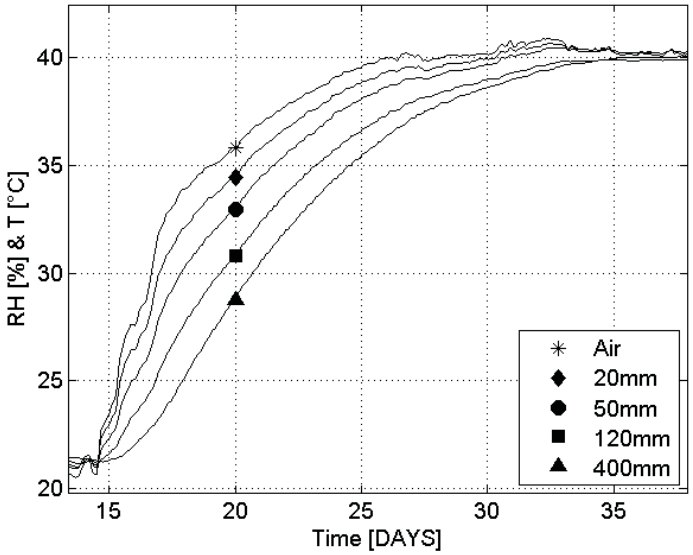

Figure 50. Measured temperature increase at different depths in an internal structure, zone 4P, at Ringhals 4, +107 180°. The plot includes the restart, ca 15 days after the measurements started.

Comparison of the measurements on the three RCs shows both similarities and differences. In general the highest temperatures were observed at Ringhals 1 in the upper dry-well. Temperature gradients in the concrete could be seen in several zones with a highest temperature close to the surface.

Two zones, P3 and P4, see figures 34 and 35, at Ringhals 1 had higher temperature in the concrete than the surroundings. Both zones were on structures that separated the wet-well and dry-well. The deepest measurements were made at 400 mm depth, where both zones had similar temperatures.

In paper 2 some rough calculations on the moisture transport at Ringhals 4 and Forsmark 2 were presented. The calculations were made using equation 5 in average moisture

conditions at the 95th day at Forsmark 2 and the 100th at Ringhals 4. On these occasions the moisture and temperature distribution had stabilised.

For the calculations it was assumed that steady state moisture flux had been achieved and temperature effects were neglected.

The moisture transport coefficients that were used were taken from the measurements presented in (Hedenblad 1993). The measured moisture transport coefficients on concrete from Ringhals 4, as described in section 5.2.2, were not used in these calculations due to the uncertainty in small RH intervals. However, as stated in section 5.2.2, the measured moisture transport coefficient on concrete from Ringhals 4 was between 1/2 and 1/3 of the coefficient measured by Hedenblad. The corresponding moisture flows would therefore be between 1/2 and 1/3 of the calculated fluxes.

Only the inner cylinder wall located in the upper dry-well was included in the calculations for Forsmark 2, and the entire inner cylinder wall for Ringhals 4. At Forsmark 2 the wall contained ca 200 m3 concrete which stands for ca 10 % of the total amount of concrete in the RC. At Ringhals 4 the inner cylinder wall contains ca 2000 m3 concrete which is ca 25 % of all concrete in the RC.

The calculations presented in paper 2 showed that if the conditions that were assumed were constant over one year the total amount of moisture that would dry out was ca 750 kg at Ringhals 4 and 145 kg at Forsmark 2. This corresponds to ca 0.5 % of the total amount of evaporable water in the structure per year at Ringhals 4 and 0.8 % at Forsmark 2 or 85 % of the total moisture content in the RC at Forsmark 2 and 150 % at Ringhals 4 during operation.

However, if the effects from differences in moisture transport coefficients between Hedenblads measurements and those presented here are considered this would result in significantly lower total moisture fluxes.

7 Discussion of Results

This dissertation is divided into three parts. In the first part the concrete from Ringhals 4 was studied regarding moisture transport properties with a focus on variations over a structure depth. The measurements showed no clear evidence that the material properties varied depending if the concrete was collected close to the inner surface or on greater depth of the containment wall. Measurements of the amount of calcium hydroxide in the concrete also showed that there was no significant variation of degree of hydration over the depth. One reason is that the concrete cured for several years before the reactor was first started. This is an important knowledge especially when a model over the ongoing drying of the structures is designed. If there would have been a large divergence over the structure the model would require a material model that varied due to moisture content, temperature, age and depth. The measurements also showed that the moisture transport coefficient of the concrete from Ringhals 4 was between a third and a half of that of a similar concrete according to the measurements done by Hedenblad (Hedenblad 1993). One reason may be that the specimens were smaller then four times the biggest aggregates and thereby had too much or too small amount of aggregates in relation to cement paste. A higher amount of aggregates gives a smaller area of cement paste though which the moisture could be transported. However, the combined area of the three specimens should be enough to create a representative area and thereby the average value is true. A variation of the aggregate amount may however be the reason for the rather big spread from the measurements.

In the second part of this dissertation the actual climatic conditions inside nuclear reactor containments were studied. A surveillance method containing a measurements setup and data acquisition system was designed for measurements of relative humidity and temperature in concrete over time. The measurements setup was first evaluated in an accuracy evaluation with focus on leaktightness. The accuracy evaluation showed that on shallow depth tendencies of leakage was observed. However, together with results from monitoring campaigns on three nuclear power plants it was concluded that the setup worked on all depth but that extra attention on the installation has to be made when measuring on 50 mm depth or less. Supplementary tests of the setup will be performed on the leaktightness and the temperature dependency.

In the third part results from monitoring campaigns conducted on three Swedish nuclear power plants were presented. Two of which are boiling water reactors, Ringhals 1 and Forsmark 2, and the third, Ringhals 4, is a pressurized water reactor. The measurements

were conducted during one operational year from, 2012 to 2013. A fourth monitoring campaign on Forsmark 3 started in 2013 and will be presented at a later stage. In each campaign the relative humidity and temperature was monitored both in the reactor containment and in the concrete structures. Measurements in the concrete where done on different depth so that a moisture profile could be established and studied over time. The measurements on all three plants showed a clear moisture profile in the concrete structures which indicates that the structures are still drying after about 30 years of operation.

Some differences between the reactor containments could be found together with several similarities. The climatic conditions inside Forsmark 2 and Ringhals 4 was fairly similar, both regarding the conditions in the concrete and in the containment. Ringhals 1 showed the most differences compared to Forsmark 2 and Ringhals 4. In general the temperatures in Ringhals 1 were the highest and the relative humidity in the concrete the lowest. These findings show that there is no clear correlating due to design of the reactor containment and the conditions in the concrete. The main aspect affecting the concrete is instead the temperature in the containment.

No regulation regarding as-designed climatic conditions in the concrete or in the containments could be found. The only regulation was on concrete temperature. According to the ACI 349 (ACI 2001) the temperature in the concrete should not exceed 66 °C, however, temperatures up to 93 °C are accepted in small areas. The measurements show that the temperature in the concrete never reaches the 66 °C. The highest temperatures observed were at Ringhals 1 where temperatures around 55 °C were found in the inner cylinder wall, high in the upper dry-well. In the other plants and the other zones in Ringhals 1 the temperature was around 30–40 °C, with some exceptions.

From the measurements on Ringhals 4 and Forsmark 2 some rough calculations of the moisture contribution were done. In both plants the inner cylinder wall was studied. The calculations showed that in Ringhals 4 the inner cylinder wall, ca 2000 m^3 (ca 25 % of the total concrete amount inside the steel liner in the reactor containment), contributed with ca 750 kg water during one year. This is ca 0.5 %-points of the theoretical maximum amount of the evaporable water from the structure. The ambient climatic conditions measured at day 95 gave a total water vapour content of ca 500 kg in the reactor containment. The moisture addition due to the drying of the inner cylinder wall thereby corresponds to ca 1.5 times the water vapour in the reactor containment during operation. At Forsmark 2 the inner cylinder wall in the dry-well is about 200 m^3 and stands for ca 10 % of total amount of concrete inside the steel liner in the containment. The calculations showed that roughly 0.8 %-points, or ca 150 kg, of the evaporable water dried out of the concrete during one year. The total water vapour content in the reactor containment with the ambient climatic conditions measured at day 100 was ca 170 kg. Thereby the moisture addition from the inner cylinder wall in the upper dry-well corresponds to ca 85 % of the water vapour content in the reactor containment during operation. It should however be noted that these calculations are rough estimates e.g. the moisture transport coefficient used in these calculations was based on the measurements conducted by Hedenblad and, as stated previously, the moisture transport coefficient on the concrete from Ringhals 4 was

significantly lower. Apart from this the calculation was made based on the two deepest measurements and the flow was assumed to be in equilibrium over the structure. This estimation was not totally accurate hens the structure is drying. Due to this the moisture flow close to the concrete surface should be larger and thereby the total moisture contribution to the containment should be larger. This simplification was done due to the fact that the measurements on greater depth were more reliable and the temperature variations were lower.

In the forthcoming doctoral thesis the main focus will be on creating a model that can predict the total moisture contribution over time and predict past and future moisture conditions in the concrete.

8 Future Research

- Evaluate differences regarding climatic conditions inside the nuclear RCs and in the concrete structures.
- Evaluate differences between the NPPs regarding geographical location, seasonal climate and plant operation
- Evaluate long term effects on the concrete structures due to drying
- Further evaluate the measurement setup regarding temperature dependence, leakage and stability
- Develop a model that can predict past and future moisture and temperature conditions in different RCs and in the concrete structures

Appendix 1

Moisture contribution from wet-well through downcomers

The distance from the upper dry well down to the water level is close to twelve metres, both for Ringhals 1 and Forsmark 2. Assuming an isothermal condition of 20 °C the moisture contribution through one pipe with a diameter on 600 mm, as in Forsmark 2, can be calculated using Flick's first law; the equation is described in section 4.2.

The moisture transport coefficient of air at 20 °C is ca 25*10-6 m2/s and assuming the RH in the upper dry well to 60 % gives a moisture flux of ca 0.052 g/(m2×h) or 0.015 g/(pipe×h).

With a total of 40 downcomers, as in Forsmark 2, the total contribution in this scenario would be 0.6 g/h (ca 5 kg/year) which could be considered as a small contribution in relation to a total space volume of over 13000 m2. This scenario is valid when the reactor is shut down, during operation the temperature as well as the water vapour content would be significantly higher.

Appendix 2

Moisture transport

Diffusion is usually described by Fick's first law eq. (A1)

$$J = -D\frac{\partial c}{\partial x} \tag{A1}$$

Where J is the flux, D is the diffusivity, c is the concentration and x is the length. Flicks first law can then be rewritten to different driving potentials e.g. water vapour content eq. (A2) and water vapour pressure eq.(A3) (Claesson 1993)

$$J_v = -\delta_v \frac{\partial v}{\partial x} \tag{A2}$$

Where J is the moisture flux, [kg/(m^2×s)], v is the water vapour content [kg/m^3], x is the length [m] and δ_v is the vapour diffusion coefficient [m^2/s].

$$J_p = -\delta_p \frac{\partial p_v}{\partial x} \tag{A3}$$

Where p_v is the vapour pressure [Pa] and δ_p is the vapour diffusion coefficient [kg/(m×s×Pa)].

Liquid transport can be divided into viscous saturated flux and capillary transport. The viscous saturated flux is dependent on water pressure gradients and can be described with Darcy's law eq. (A4)

$$J = -\frac{k_p}{\eta}\frac{dP}{dx} \tag{A4}$$

J is the water flux [kg/(m^2×s)], k_p the permeability [kg/m^2], η is the dynamic viscosity [Pa×s], P is the pressure (Pa) and x is the length. However, if there is no pressure gradient, e.g. hydrostatic pressure, over the material this flux potential can be neglected.

The second liquid transport mechanism is capillary transport, which can be described using Darcy's law with the pore water pressure, P_l, as the driving potential (Janz 2000), eq. (A5)

$$J_l = -\frac{k_p}{\eta}\frac{\partial P_l}{\partial x} = -D_l\frac{\partial P_l}{\partial x} \quad \text{(A5)}$$

Where D_l [kg/(m×s×Pa)] is the transport coefficient, P_l the pore water pressure and x the length. The pore water pressure is defined as:

$$P_l = P_{atm} - s \quad \text{(A6)}$$

Where P_{atm} is the atmospheric pressure and s describes the suction according to Laplace equation:

$$s = \sigma\left(\frac{1}{r_1} + \frac{1}{r}\right) \quad \text{(A7)}$$

Where σ is the surface tension [N/m] and r_1 and r_2 is the radii of the meniscus.

Usually the atmospheric pressure, P_{atm}, is much smaller (ca 100 kPa) than the suction and can be neglected (Janz 2000) giving eq. (A8).

$$J_l = \frac{k_p}{\eta} * \frac{\partial s}{\partial x} = \lambda_m * \frac{\partial s}{\partial x} \quad \text{(A8)}$$

Where k_p is the permeability [kg/m^2] and η the dynamic viscosity [Pa×s] of the fluid which gives the moisture conductivity, λ_m (kg/(m×s×Pa)).

The pore water pressure can also be rewritten to:

$$-s \approx P_l = \frac{RT\rho_w}{M_w}\ln\left(\frac{v}{v_s}\right) \quad \text{(A9)}$$

Where R is the ideal gas constant [J/mol×K], T is temperature [K], ρ_w is the density of water [kg/m^3] and M_w the molar mass of water [kg/mol].

Due to the relation in equation 9 the pore water pressure, or suction, can be described with the water vapour content as in the model that describes the vapour diffusion.

The total flux can be described with eq. (A10) or (A11)

$$J_{tot} = J_v + J_l = -\delta_v \frac{\partial v}{\partial x} + \lambda_m \frac{\partial s}{\partial x} \quad \text{(A10)}$$

$$J_{tot} = J_p + J_l = -\delta_p \frac{\partial p}{\partial x} + \lambda_m \frac{\partial s}{\partial x} \quad \text{(A11)}$$

In equilibrium at an isothermal state it is possible to rewrite the total flux equation due to the relation between the pore water pressures, vapour pressure, water vapour content and similar to eq. A12 (Claesson 1993).

$$J = -\delta \frac{\partial \varphi}{\partial x} \quad (12)$$

Where δ is the moisture transport coefficient and φ can be either, pv, v, u, Φ, w or s. However if the system is not isothermal this simplification is not possible and the two fluxes have to be separated.

Appendix 3

Degree of capillary saturation

The degree of capillary saturation is a measured value that describes how much of the pores are water filled at a certain point. The method is suitable to use at high moisture levels when the RH is close to 100% or as an alternative to moisture ratio if the specimens do not have a representative size, 3–4 times the biggest aggregate in all sizes. Different methods have been described how to determine the capillary measured point e.g. by (Fagerlund 1977; Hedenblad and Nilsson 1985).The two methods differed somewhat, especially concerning the moisture content that represents capillary saturation. In both studies the measurements were made in a similar manner. The specimens were placed on a net in a plastic box and water was filled so that the net was just covered. A lid was placed over the box to prevent drying of the specimens. There after the specimens were weighed at certain intervals for several days. The weight increase (Hedenblad and Nilsson 1985) or the degree of saturation (Fagerlund 1977) was then plotted against the square root of the time. The water filling can then be identified as two stages. The first as a more rapid increase due to the filling of capillary pores and the second as a much slower one due to the filling of bigger pores. In ideal measurement these two stages change at a distinct point called the nick point (Fagerlund 1977). The nick point is thereby the point at which all the capillary pores are filled. To determine the point of capillary saturation two different methods were used by (Hedenblad and Nilsson 1985) and (Fagerlund 1977). In (Fagerlund 1977) the point of capillary saturation defined as the nick point was decided by plotting the linear regression of the two stages giving a nick point at their intersection. In (Hedenblad and Nilsson 1985) the moisture content corresponding to capillary saturation was decided by identifying when equilibrium was reached at the second stage. In Nordtest method NT BUILD 472, that is based on the work in (Hedenblad and Nilsson 1985), equilibrium is reached when the weight gain over 24 h is lower then 1% of total increase.

The degree of capillary saturation (S_{cap}) was decided using equation A13 (Hedenblad and Nilsson 1985):

$$S_{cap} = \frac{m_w - m_0}{m_{cap} - m_0} \qquad [A13]$$

Where mw is the weight of the specimen at the time it was extracted from the concrete, m0 is the weight after drying to equilibrium at 105 °C and m_{cap} the calculated weight of the specimen when capillary saturated.

The specimens used to determine the degree of capillary saturation were collected from a total of six concrete cylinders with a diameter of 300 mm. Two of the cylinders were 800 mm long and taken from the outer cylinder wall (S1 and S2) and four were 300 mm long from the inner cylinder wall (P1-4).

The concrete cylinders were core drilled with water used for cooling. The concrete was transported to the Building material laboratory at Lund University and within 24 h after the cylinders were collected. To avoid the influence of water from the cooling, the concrete specimens were collected from the centre of the cylinders. This gave a buffer of ca 100 mm of concrete to the zone where the specimens were collected.

The specimens were extracted from different depths in accordance with table A1. To reach the different depths the cylinders were first split using a 10 ton screw press and there after a specimen from the centre was separated using a jack hammer. Directly after a specimen was collected it was weighed (mw) and there after placed in plastic bags to lower the risk of carbonation. The weight of the specimen varied from ca 50–450 g with an average around 200 g.

Table A1. Specifications of specimens used for degree of capillary saturation profiles. Inner and outer represents the two parts of the cylinder wall

	Core Diameter [mm]	Specimen Depth [mm] (Inner)	(Outer)	Nr. Of specimens
Degree of capillary saturation	294	0-20	0-20	28
		40-60	40-60	
		140-160	100-120	
		240-260	140-160	
		-	290-310	
		-	440-460	
		-	590-610	
		-	740-760	

The specimens from the inner cylinder wall were capillary saturated one day after they had been collected. The specimens were placed on tissues that lay on a net on the bottom of a plastic box. Water was added so that the tissues were soaked. The specimens were weighed after 2, 4, 19, 43, 69, 76,101 and 122 hours. One specimen was weighed at a time and the remainder were left in the box with the lid on. This was done to minimise drying of the specimens. Figure A1 shows the weight increase in relation to the square root of time from one of the cylinders. Similar results were obtained from all cylinders. Only the two first

values were used to obtain the linearity in the first stage. In the second stage all values were used to obtain the linear regression.

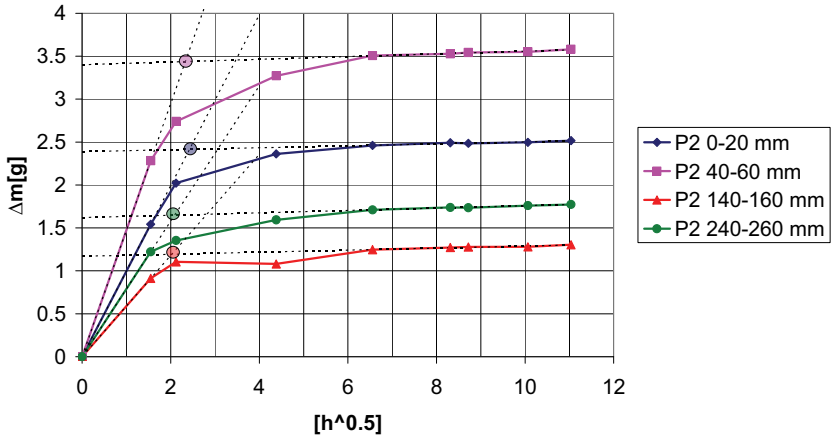

Figure A1. Obtained weight increase of four specimens from concrete sample 2 in relation to the square root of time. The nick points from the linear regressions show the weight gained at capillary saturation.

When the weight of the specimens at capillary saturation (m_{cap}) had been decided the specimens were dried at 105 °C until stable weight (m_0). Inserting these values together with mw in equation 28 the degree of capillary saturation was obtained.

In figure A2 the degree of capillary saturation over the depth of the inner cylinder wall from all four specimens is presented. No explanation why the results from P4 stood out has been found.

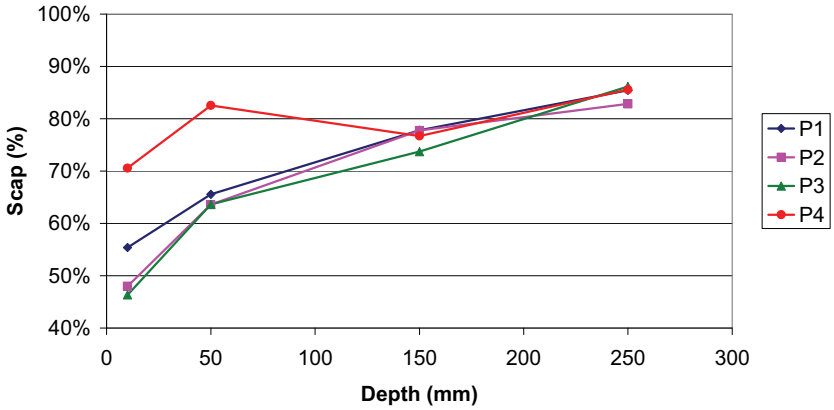

Figure A2. Measured degree of capillary saturation on concrete from the inner cylinder wall at Ringhals 4. The depth is measured from the inner surface. At 300 mm depth the steel liner is located

The measurements conducted on the specimens from the outer cylinder wall were first stored in sealed plastic bags for nearly one month before the specimens were capillary saturated. The same procedure as for the measurements on the inner wall was there after used.

The weight increase was measured after ca 1, 2, 3.5 4.5, 19 27, 54, and 93 hours. Unfortunately the measurements were stopped before all specimens had reached equilibrium in the second stage. The nick point of the specimens that had reached, or were close to, equilibrium was decided as for the measurements on concrete from the inner wall.

For the remainder, a total of five specimens, the nick point was assumed to be the last measured value. This assumption was however quite rough but with the accessible data it gave a plausible estimation.

Figure A3 shows the measured values for the five samples from cylinder 1 that had reached equilibrium. The sample named S1 590–610 only had two points on which the weight gain had an increase similar to the rest of the specimens. Only two values are however not enough to be certain that equilibrium in stage 2 had been achieved. The weight gain was however ca 1 % of the total weight increases per 24 h. In Nordtest NT build 472 this is the definition of equilibrium hence the specimens are assumed to have reached the equilibrium at this stage.

For at least three points which remain there is a linear relation between the weight increase and the square root of time, and it was therefore assumed that they had reached equilibrium. The samples from cylinder S2 showed similar results regarding weight gain and are therefore not presented.

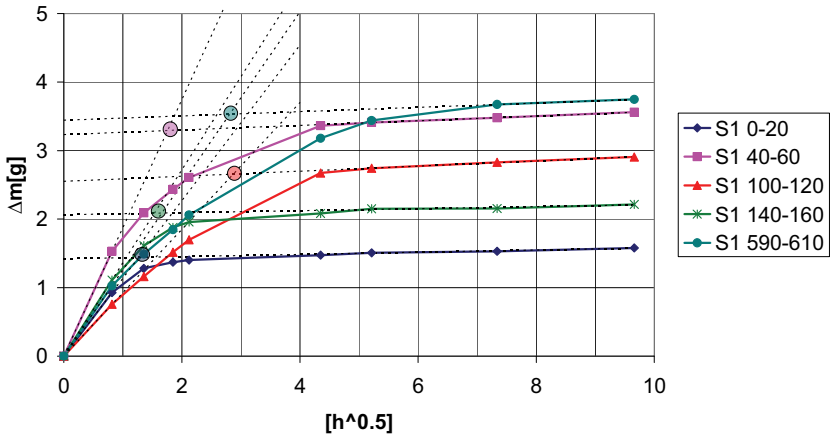

Figure A3. Obtained weight increase in five specimens from concrete cylinder 1 in relation to the square root of time. The nick points from the linear regressions show the weight gained at capillary saturation.

The five specimens that clearly not had reached equilibrium in stage 2 are presented in figure A4.

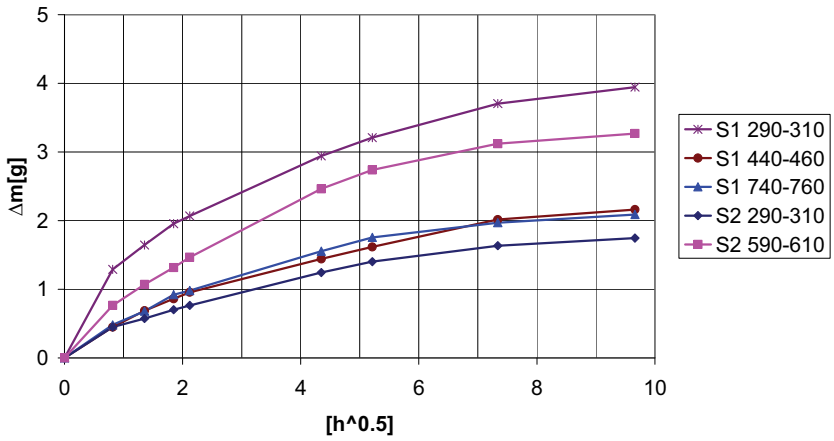

Figure A4. Obtained weight increase of five specimens from the concrete cylinders 1 and 2 in relation to square root of time.

All the curves in figure A4 show clear tendencies that weight gain rate in relation to the square root of time is decreasing. The weight gained per 24 h in relation to the total increase was between 2.7 and 4.4 %-points. The highest increase was measured in specimens S1 440–460 and the lowest in S2 590–610. It was however not possible to determine if equilibrium was reached directly after the last measured point or later.

The impacts of a 10 % error of m_{cap} dose, however, do not result in a 10% error in the degree of capillary saturation. Hence the impact depends on the starting weight, dry weight and cement content of the specimen. If a ±10 % error in m_{cap} on each specimen was assumed that error gave ca ±2 % error on S_{cap} on all five specimens. The error relation was linear with a 1/5 relation.

In figure A5 the S_{cap} profile of the outer cylinder wall is presented. On the five specimens that did not reach equilibrium in stage 2, error bars of ±4 % are included. A ±4 % error corresponds to a ±20 % on m_{cap}, which can be seen as a conservative estimation.

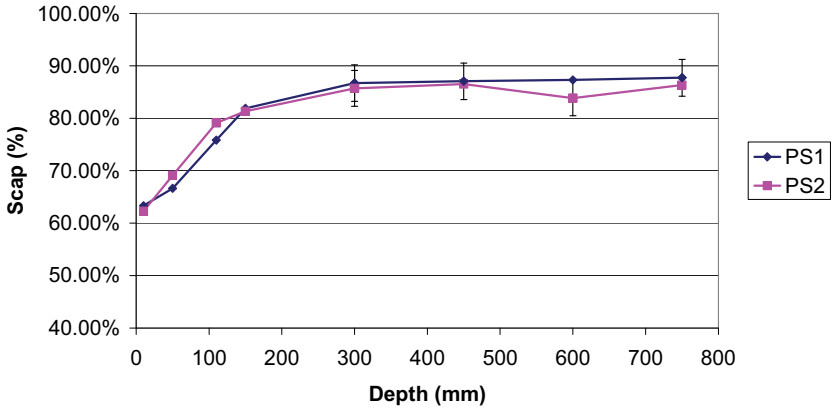

Figure A5. Measured degree of capillary saturation on concrete from the outer cylinder wall at Ringhals 4. The depth is measured from the outer surface. At 800 mm depth the steel liner is located. Error bars at five measurements represent a ±20 % error in estimation of m_{cap}.

Both the measurements from the inner and outer wall indicate that the concrete at great depth had not dried. Both measurements also show a moisture profile which indicates drying of the structure.

Reference

ACI-ASME (2001). Code for Concrete Reactor Vessels and Containments. ACI 359-01, American Society of Mechanical Engineers**:** 437-457.

ACI (2001). Code Requirements for Nuclear Safety Related Concrete Structures. (ACI 349-01), American Concrete Institute.

Ahlgren, L. (1972). Moisture fixation in porous building materials (In Swedish). Division of Building Materials. Lund, Sweden, Lund University. **PhD**.

Akkurt, I., H. Akyildirim, et al. (2010). "Gamma-ray shielding properties of concrete including barite at different energies." Progress in Nuclear Energy **52**: 620-623.

Alarcon-Ruiz, L., A. Ehrlacher, et al. (2005). "The use of thermal analysis in assessing the effect of temperature on a cement paste." Cement and Concrete Research **35**(3): 609-613.

Alhajali, S., B. Naoom, et al. (2009). "Estimation of the activation of local reactor shielding concretes." Progress in Nuclear Energy **51**(2): 374-377.

Anderberg, A. and L. Wadsö (2008). "Method for simultaneous determination of sorption isotherms and diffusivity of cement-based materials." Cement and Concrete Research **38**(1): 89-94.

Andrade, C., J. Sarrıa, et al. (1999). "Relative humidity in the interior of concrete exposed to natural and artificial weathering." Cement and Concrete Research **29**(8): 1249-1259.

Bažant, Z. P. (1969). Thermodynamic theory of concrete deformation at variable temperature and humidity. Berkeley, University of California.

Bažant, Z. P. (1970). "Delayed thermal dilatations of cement paste and concrete due to mass transport." Nuclear Engineering and Design **14**(2): 308-318.

Bhatty, J. I. and K. J. Reid (1985). "Use of thermal analysis in the hydration studies of a type 1 portland cement produced from mineral tailings." Thermochimica Acta **91**(C): 95-105.

Chang-Min, L., L. Yoon Hee, et al. (2007). "Cracking effect on gamma-ray shielding performance in concrete structure." Progress in Nuclear Energy **49**: 303-312.

Claesson, J. (1993). A few remarks on moisture flow potentials. TVBH-7163. Lund, Sweden, Lund University, Division of Building Physics.

El-Jazairi, B. and J. M. Illston (1977). "A simultaneous semi-isothermal method of thermogravimetry and derivative thermogravimetry, and its application to cement pastes." Cement and Concrete Research **7**(3): 247-257.

Fagerlund, G. (1972). Critical degree of saturation at freezing of porous and brittle materials. Division of Building Materials. Lund, Sweden, Lund University. **PhD**.

Fagerlund, G. (1977). "The critical degree of saturation method of assessing the freeze/thaw resistance of concrete." Matériaux et Constructions **10**(4): 217-229.

Fredlund, P. and L.-O. Nilsson (2009). Gas penetration in concrete reactor containments - Measurements and Modelling (In Swedish). Elforsk rapport 09:101. Lund, Sweden, Lund University, Division of Building Materials.

Fridh, K. (2005). Internal frost damage in concrete- Experimental studies of destruction mechanisms. Division of Building Materials. Lund, Sweden, Lund University. **PhD**.

Grasley, Z. and D. Lange (2007). "Thermal dilation and internal relative humidity of hardened cement paste." Materials and Structures **40**(3): 311-317.

Grasley, Z., D. Lange, et al. (2006). "Internal relative humidity and drying stress gradients in concrete." Materials and Structures **39**(9): 901-909.

Greenspan, L. (1977). "Humidity Fixed Points of Binary Saturated Aqueous Solutions." Journal of Research of the National Bureau of Standards. Section A: Physics and Chemistry **81A** (1): 89-96.

Hansen, T. (1986). "Physical structure of hardened cement paste. A classical approach." Materials and Structures **19**(6): 423-436.

Hedenblad, G. (1993). Moisture permeability of mature concrete, cement mortar and cement paste. Division of Building Materials. Lund, Sweden, Lund University. **PhD**.

Hedenblad, G. and L.-O. Nilsson (1985). Degree of Capillary Saturation - A tool for accurate determination of the moisture content in concrete. TVBM-3022. Lund, Sweden, Lund University, Division of Building Materials.

Hilsdorf, H. K. (1967). "A method to estimate the water content of concrete shields." Nuclear Engineering and Design **6**(3): 251-263.

Hjorslev Hansen, M. (1993). Estimation of transfer coefficients in models for coupled heat and moisture transfer in porous media. Building materials laboratory. Lyngby, Technical University of Denmark. **PhD**.

Hora, Z. and B. Patzák (2007). "Analysis of long-term behaviour of nuclear reactor containment." Nuclear Engineering and Design **237**(3): 253-259.

IAEA (1996). Defence in depth in nuclear safety: INSAG-10 INSAG series. Vienna, Austria, IAEA.

IAEA (1998). Assessment and management of ageing of major nuclear power plant components important to safety: Concrete containment building. IAEA-TECDOC Series. Vienna, Austria, IAEA.

IAEA (2004). Design of reactor containment systems for nuclear power plants. Safety standards series. Vienna, Austria, IAEA.

IAEA (2005). Assessment and management of ageing of major nuclear power plant components important to safety: BWR Pressure Vessels. IAEA-TECDOC Series. Vienna, Austria, IAEA.

IAEA (2007). Assessment and management of ageing of major nuclear power plant components important to safety: PWR Pressure Vessels. IAEA-TECDOC Series. Vienna, Austria, IAEA.

IAEA (2012). Operating experience with nuclear power stations in member states in 2011. Vienna, Austria, IAEA.

Janz, M. (2000). Moisture transport and fixation in porous materials at high moisture levels. Division of Building Materials. Lund, Sweden, Lund University. **PhD**.

Johansson, P. (2012). Drying of concrete - The laboratory study for TorkaS3 (In Swedish). Lund, Sweden, Lund University, Division of Building Materials.

Johansson, P. and L.-O. Nilsson (2007). Climatic conditions at the surfaces of concrete containments - examples for two BWR and PWR reactors. SMiRT 19. Toronto.

Kharita, M. H., M. AlNassar, et al. (2010). "The effect of the initial water to cement ratio on shielding properties of ordinary concrete." Progress in Nuclear Energy **52**(5): 491-493.

Kharita, M. H., M. Takeyeddin, et al. (2008). "Development of special radiation shielding concretes using natural local materials and evaluation of their shielding characteristics." Progress in Nuclear Energy **50**(1): 33-36.

Kharita, M. H., S. Yousef, et al. (2011). "Review on the addition of boron compounds to radiation shielding concrete." Progress in Nuclear Energy **53**(2): 207-211.

Korkut, T., H. Korkut, et al. (2011). "A new radiation shielding material: Amethyst ore." Annals of Nuclear Energy **38**(1): 56-59.

Midgley, H. G. (1979). "The determination of calcium hydroxide in set Portland cements." Cement and Concrete Research **9**(1): 77-82.

Nilsson, L.-O. (1980). Hygroscopic moisture in concrete - drying, measurements & related material properties. Division of Building Materials. Lund, Sweden, Lund University. **PhD**.

Nilsson, L.-O. (2007). Drying of reactor containment walls of concrete during past and future decades. SMiRT 19. Toronto, International association of structural mechanics in reactor technology.

Nilsson, L.-O. and P. Johansson (2009). Changes in reactor containments - The drying and climatic conditions in the concrete walls (In Swedish). Elforsk rapport 09:100. Lund, Sweden, Lund University, Division of Building Materials.

Ollivier, J. P., J. C. Maso, et al. (1995). "Interfacial transition zone in concrete." Advanced Cement Based Materials **2**(1): 30-38.

Pane, I. and W. Hansen (2005). "Investigation of blended cement hydration by isothermal calorimetry and thermal analysis." Cement and Concrete Research **35**(6): 1155-1164.

Picaut, J., J. Chataigner, et al. (2001). Nuclear containments. fib State-of-art report. Lausanne, Switzerland, International Federation for Structural Concrete (fib).

Powers, T. C. and T. L. Brownyard (1947). "Studies of the physical properties of hardened portland cement paste. Part 4." Journal of the American concrete institute **18**(5): 549-595.

Poyet, S. (2009). "Experimental investigation of the effect of temperature on the first desorption isotherm of concrete." Cement and Concrete Research **39**(11): 1052-1059.

Poyet, S. and S. Charles (2009). "Temperature dependence of the sorption isotherms of cement-based materials: Heat of sorption and Clausius-Clapeyron formula." Cement and Concrete Research **39**(11): 1060-1067.

Radjy, F., E. J. Sellevold, et al. (2003). Isosteric vapor pressure - Temperature data for water sorption in hardened cement paste: Enthalpy, entropy and sorption isothermal at different temperatures. Lyngby, Denmark, Technical University of Danmark.

Roth, T., J. Silfwerbrand, et al. (2002). Concrete reactor containments at Swedish Nuclear Power Plants (In Swedish). Stockholm, Sweden, KTH Royal Institute of Technology.

Ryu, D.-W., J.-W. Ko, et al. (2011). "Effects of simulated environmental conditions on the internal relative humidity and relative moisture content distribution of exposed concrete." Cement and Concrete Composites **33**(1): 142-153.

Schrefler, B. A., G. A. Khoury, et al. (2002). "Thermo-hydro-mechanical modelling of high performance concrete at high temperatures." Engineering Computations (Swansea, Wales) **19**(7-8): 787-819.

Sellevold, E. and Ø. Bjøntegaard (2006). "Coefficient of thermal expansion of cement paste and concrete: Mechanisms of moisture interaction." Materials and Structures **39**(9): 809-815.

Song, H.-W., S.-H. Kim, et al. (2002). "Creep prediction of concrete for reactor containment structures." Nuclear Engineering and Design **217**(3): 225-236.

Taylor, H. F. W. (1997). Cement chemistry. London, Thomas Telford Publishing.

Thorne, C. P. (1961). "Concrete properties relevant to rector shield behaviour." Journal of the American concrete institute **32**(11): 1491-1508.

VAISALA (2010). Vaisala HUMICAP - Humidity and Temperature probe HMP110. Ref. B210852EN-A.

Vodák, F., V. Vydra, et al. (2011). "Effect of gamma irradiation on properties of hardened cement paste." Materials and Structures/Materiaux et Constructions **44**(1): 101-107.

Wong, H. S. and N. R. Buenfeld (2009). "Determining the water-cement ratio, cement content, water content and degree of hydration of hardened cement paste: Method development and validation on paste samples." Cement and Concrete Research **39**(10): 957-965.

Åhs, M. (2011). Redistribution of moisture and ions in cement based materials. Division of Building Materials. Lund, Sweden, Lund University. **PhD**.